Ana Sofia Rações da Cruz

Dual-phase Inkjet Printed Electrochromic Layers based on PTA and WO_X/TiO_2 Nanoparticles for Electrochromic Applications

Monte de Caparica, 2010

Universidade Nova de Lisboa

Faculdade de Ciências e Tecnologia

Departamento de Ciências dos Materiais

Dual-phase Inkjet Printed Electrochromic Layers based on PTA and WO_X/TiO_2 Nanoparticles for Electrochromic Applications

By:

Ana Sofia Rações da Cruz

Thesis submitted in Faculdade de Ciências e Tecnologia da Universidade Nova de Lisboa for the degree of Master in Materials Engineering

Supervisor: Prof. Elvira Fortunato

Co-Supervisor: Eng. Pawel Wojcik

Monte de Caparica, 2010

Acknowledgments

This work was only possible thanks to several people, who during the whole semester helped me with their knowledge, kindness, support and friendship.

To Professor Elvira Fortunato, thank you for the availability to help and guide during this thesis. For the opportunity of doing my master thesis in such an interesting subject and for the interest shown in my work during the whole semester.

To Professor Rodrigo Martins and once more, to Professor Elvira Fortunato, thank you for giving me the possibility to make this work in facilities of excellence.

To Pawel Wojcik, without him this work was certainly not as interesting, challenging and fun as it was. Thank you for all your help and orientation during the whole work, for your patience, for being so available to all my questions, some of them really silly. Thank you for making the work of my master thesis very enjoyable and pleasant.

To Lidia Santos, thanks for all the availability to help, to discuss, to be bored and to laugh with me, during all those longs hours of measurements. This work would have been much harder without you.

To the entire MEO group, your kindness and availability allowed this work to be a very pleasant one, it almost didn't seem like work at all. A special thanks to Elamurugu Elangovan and Joana Vaz Pinto for the XRD measurements and to Tito Busani for the SEM images.

To my college colleagues and friends Adriana Nogueira, Joana Pereira and Ana Baptista for all the support, patient and friendship. You dealt with all my "pains" during this semester and it was your support which helped me to finish this important step of my academic life. I want to also thank to Gonçalo Pereira, for his constant and contagious good mood.

To all my friends, Ana Valério, André Duarte, Dalila Forte, Frederico Braga, Joana Viera, Sérgio Lopes, Ana Luz e Bruno Brás. Without you I can assure that I was not going to be the person that I am today. From this group I want to add a more special thanks to Dalila, for being so available in helping me with my English even though she was miles and miles away.

To Nuno Deusdado, thank you for all your love, friendship and support during this stage of my live. It was really important to me.

To all my family, for always believing in me and for always being present in my live.

To my parents, if I reached this achievement, it's owned to you both. Thank you for everything you did for me, for always being there with me and for making me the very happy girl that I am.

Thank you!

Abstract

The aim of the work was to develop flexible electrochromic windows via Inkjet Printing Technique based on amorphous Peroxotungstic Acid (PTA) and metal oxide nanocrystals. A unique selection of materials allows for a solution processed deposition of low temperature electrochromic layer which is compatible with flexible substrates such as PET, PEN and paper.

The use of Inkjet Printing Technique was motivated by the fact that it is a cost efficient method (mass production) which has a reduced consumption of materials and energy. It is also a non-contact, digital, no mask and no vacuum patterning method which greatly simplifies the technological process.

Developed devices were tested using optical, electrochemical, and structural characterization techniques, in order to find the optimum electrochromic layer composition which would guarantee desirable electrochromic behavior of the material.

Laboratory studies were supported by statistical techniques such as Design of Experiment (DOE) and Multiple Regression which leads to a fitting of mathematical model of the optical and electrical responses.

The dual-phase electrochromic layer consists in the combination of both amorphous and nanocrystalline phases significantly improve the electrochromic performance of the devices. The developed method of electrochromic windows manufacturing meets all the objectives at the beginning of the study.

Resumo

O objectivo deste trabalho consistiu no desenvolvimento de janelas electrocrómicas flexíveis com ácido peroxotungsténico amorfo (PTA) e nanocristais de óxidos metálicos. A tecnologia utilizada para a deposição destes materiais electrocrómicos foi a impressão a jacto de tinta, permitindo a deposição de soluções à temperatura ambiente, compatível com substratos flexíveis tais como PET, PEN e papel.

O baixo custo e o reduzido consumo de materiais e energia foi a motivação para a selecção da tecnologia de impressão por jacto de tinta como método de deposição. Aliado a estes factores, trata-se também de um método digital, sem contacto físico e sem necessidade da utilização de máscaras e vácuo, o que simplifica significativamente o processo.

Os dispositivos desenvolvidos foram testados recorrendo a técnicas de caracterização óptica, electroquímica e estructural, por forma a encontrar a composição óptima da camada electrocrómica que garanta o desempenho electrocrómico adequado do material.

Os estudos laboratoriais foram suportados por técnicas estatísticas, Desenho de Experiências (DOE) e Regressão Múltipla, que conduziram à adaptação das respostas ópticas e eléctricas obtidas a um modelo matemático.

A camada electrocrómica de duas fases consiste numa combinação de uma fase amorfa e outra nanocristalina, o que melhora significativamente o desempenho electrocrómico dos dispositivos. O método desenvolvido para a produção de janelas electrocrómicas foi de encontro a todos os objectivos propostos no início deste estudo.

List of Frequently Used Acronyms and Symbols

[BMIM][BF_4]	1-butyl-3-methylimidazolium tetrafluoroborate
[$EtNH_3$][NO_3]	Ethyl ammonium nitrate
A	Absorptance
CA	Chronoabsorptometry
CE	Coloration Efficiency
CQ	Chronocoulometry
CV	Cyclic Voltammetry
CVD	Chemical Vapor Deposition
d	Film Thickness
DOE	Design Of Experiments
EC	Electrochromic
FIB	Focuses Ion Beam
H_2O_2	Hydrogen Peroxide
In_2O_3:Sn	Indium Tin Oxide
i_{OX}	Oxidation peak max.
i_{RED}	Reduction peak max.
IrO_2	Iridium Dioxide
ITO	Indium Tin Oxide
IZO	Indium Zinc Oxide
LED	Light emitting diode
$LiClO_4$	Lithium perchlorate
Li_yWO_3	Tungsten Bronze
MnO_2	Manganese Dioxide

MoO_3	Molybdenum Trioxide
$NaClO_4$	Sodium perchlorate
NbO_5	Niobium Pentoxide
OAD	Oxalic Acid
PANI	Polyaniline
PEDOT	Poly(3,4-ethylenedioxythiophene)
PEO-PPO	Binary mixture of ethylene poly(oxide) and propylene poly(oxide)
PEN	Polyethylene naphthalate
PET	Polyethylene terephthalate
PC	Propylene carbonate
PMMA	Polymethacrylsauremethylester
PTA	Peroxotungstic Acid
Q_{ins}	Charge inserted to the device during coloration process
R	Reflection
RF	Radio Frequency
Rq	Film Roughness
SEM	Scanning Electron Microscopy
SrTiO3	Strontium Titanium Trioxide
T_{bl}	Transmittance in bleaching state
T_{col}	Transmittance in coloration state
TCO	Transparent Conductor Oxide
THF	Tetrahydrofuran
TiO_2	Titanium Dioxide
V_2O_5	Vanadium Pentoxide

W	Tungsten
WO_3	Tungsten Trioxide (*yellow*)
WO_X	Stoichiometry of tungsten oxide nanoparticles
$WO_{2.9}$	Tungsten Trioxide (*blue*)
XRD	X-Ray Diffraction
ΔOD	Change in Optical density
α	Optical absorption coefficient
θ	Contact angle
λ	Wavelength
τ_{col}	Coloration time
τ_{bl}	Bleaching time
ν	Ink viscosity
γ	Ink surface tension
ρ	Ink density

Contents

List of Figures

List of Tables

1. Introduction and objective

The overall objective of this work is to develop a complete solution processed and low temperature dual-phase electrochromic system based on PTA (Peroxotunstic Acid) precursor deposited via Inkjet Printing Technology. Whereby, the processability of precursors with nanocrystalline solid content via Inkjet Printing for smart windows applications is to be demonstrated. Applications related aims to include the optimization of the properties of the coating materials (composition, rheology, crystallinity, etc.) and the mechanical, optical and electrochemical characterization of the printed devices. In detail, developed electrochromic system which includes materials and deposition technique should satisfy the following conditions:

- low-temperature process compatible with flexible substrates, such as PET (Polyethylene terephthalate), PEN (Polyethylene naphthalate) or paper;
- non-contact, digital, additive, no mask and no vacuum patterning method;
- eco-friendly;
- coexistence of amorphous and nanocrystalline phases for better electrochromic performance;
- cost efficient in mass production;
- solution processed deposition;
- widely available materials;
- application of inorganic material, which provides a higher device stability;
- reduced consumption of materials and energy.

Although many research reports about the PTA precursor based depositions methods (dip-coating, spin-coating) for WO_3 (Tungsten Trioxide) thin film coating have been published, no attempt has yet been reported to prepare WO_3 coatings by Inkjet Printing. This study aims to synthesize amorphous WO_3 thin films containing TiO_2/WO_X nanocrystals (a-$WO_3/TiO_2/WO_X$) in a low temperature Inkjet Printing process.

As it is well known, fully crystalline WO_3 coating is not the best candidate for EC (Electrochromic) window application due to its slow diffusion rate and inferior coloration efficiencies. On the other hand, crystalline states have been shown to be able to withstand a

greater number of cycles. Several studies [1,2] have been made also on the TiO_2-doped WO_3 thin films using solution processed deposition techniques. The use of TiO_2 (Titanium Dioxide) as a doping material always resulted in improved electrochromic performance. It is shown that reversibility can be improved by adding TiO_2 to the WO_3 precursor and the lifetime of TiO_2/WO_3 thin films can be much longer that of pure WO_3 material [2]. As TiO_2 is hydrophilic it adsorbs water from air and this small amount of water accelerates the H^+ ion insertion/removal in to or from the TiO_2/WO_X thin films. In the present work TiO_2 doped *a*-WO_3/WO_X thin films were prepared by a simple and inexpensive way. The WO_3 sol was mixed with aqueous-alcohol TiO_2 nanoparticle dispersion resulting in a stable and printable ink.

It's intended to obtain an electrochromic window that has as main specifications high values of high coloration efficiency and change in optical density and a response time as small as possible. These specifications will allow the achievement of a device with a desirable electrochromic performance.

2. Fundamental

2.1 Electrochromism

Electrochromism is one of the several types of chromism. The word chromism stands for the ability of a substance to change its color in a reversible way in result of a process caused by some form of stimulus. Some types of chromism existing in a practical applications are listed bellow [3,4]:

- electrochromism – voltage application (Figure 2.1a);
- termochromism – temperature change (Figure 2.1b)
- photocromism – exposure to light radiation (Figure 2.1c);
- halochromism – change in pH of a solution;
- piezochromism – color change caused by mechanical grinding;
- solvatochromism – change of solvent polarity (Figure 2.1d);
- ionochromism – addition of ions.

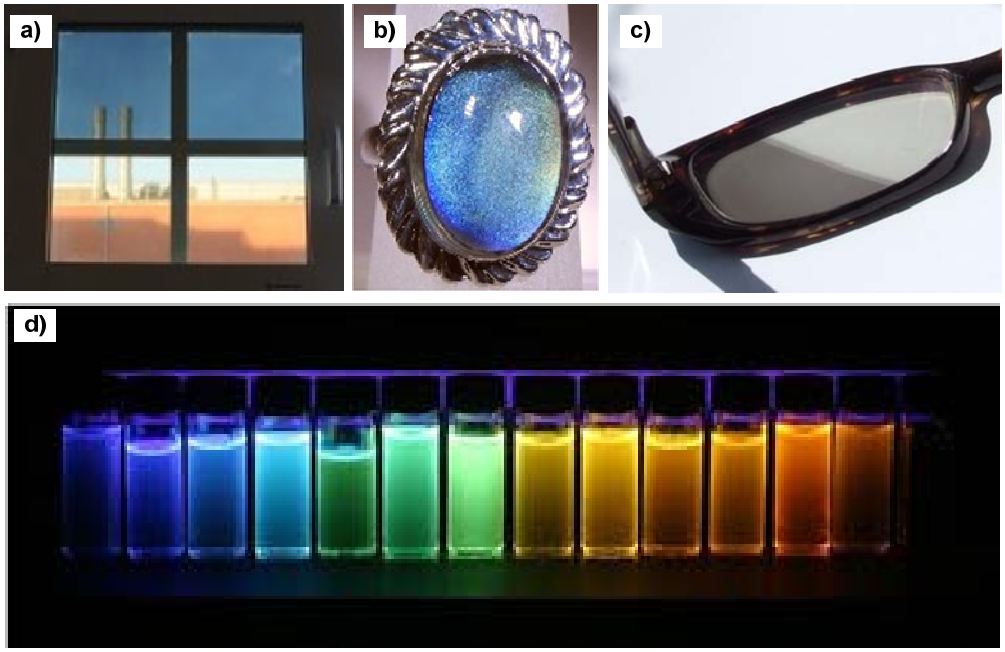

Figure 2.1 Chromism application examples: a) electrochromism for electrochromic window application [5], b) termochromism for ring application [6], c) photocromism for glasses application [7], d) the same organic compound dissolved in solvents with different polarity [8]

This thesis contains only a detailed exposure of one of the types of chromism which is electrochromism, since this is the scope of the conducted research. Electrochromism could be briefly defined as a persistent but reversible optical change produced electrochemically in selected thin films compounds, designated as electrochromic materials [9].

The Equation 2.1 represents the electrochromism phenomenon for amorphous WO_3 (the most typical and widely studied electrochromic material).

$$WO_3\,(s) + y\,(Li^+ + e^-) \rightarrow Li_yWO_3(s) \quad (2.1)$$

Amourphous WO_3 film in bleach state (transparent) can be switched reversibly to a colored state (dark blue) by both insertion of ions and electrons to form tungsten bronze (Li_yWO_3). The y value in Li_yWO_3 is the fractional number of sites of which are filled in the WO_3 lattice. For low y values the films have an intense blue [10,11]. The electrochromism history started in 1704, when Diesbach discovered the Prussian blue, an excellent dye which had also electrochromic properties. This material changes its state from dark blue to transparent when a voltage is applied. In 1815 the electrochromism of WO_3 was discovered, by Berzelius [12]. In fact, it was showed that pure WO_3 changed color on reduction when warmed under a flow of dry hydrogen gas. Later in 1824 Wohler effected a similar chemical reduction with sodium metal. Kobosew and Nekrasso in 1830, recorded that WO_3 powders could acquire the color blue by electrochemical reduction in an acid solution as it is represented in Equation 2.1. The first step towards an electrochromic device was taken in 1942 by Talmey, in studies on the coloration associated with electrolytic reduction of artificially produced particulate molybdenum and tungsten oxide layers. In 1953 Kraus made a very clear description of electrochromism in tungsten oxide films. As none of these studies attracted much attention, probably most current investigators attribute the first widely accepted suggestion of an electrochromic device to Deb, in 1969, with the tungsten oxide films, and after this point, there was a visible increase of the interest in electrochromism. In spite of the innovation on Deb's first electrochromic device it wasn't able to keep up with the fast development of liquid crystal devices [12,13]. In 1971, Blanc and Staebler produced an electrochromic effect superior to most of the previously published. They applied electrodes to the opposing faces of doped, crystalline $SrTiO_3$

(Strontium Titanium Trioxide) and observed an electrochromic color move into de crystal from the two electrodes. In 1972, Beegle developed a display having identical counter and working electrodes as the one from Blanc and Staebler, but made of WO_3 [12,13]. Nowadays, Deb's paper form 1973 is quoted as the work responsible for the true birth of electrochromic technology.

Nevertheless, electrochromism has remained an active area for basic and applied research, with large possibilities for applications in emerging technologies. The interest was boosted in the mid- 1980s with the awareness that electrochromism was of much interest as a mean to achieve energy efficiency in buildings, using smart windows. [14]

The smart windows and other electrochromic systems consist of two electrodes and an electrolyte. When applied voltage with appropriate polarity, charge in the cell drives in and out of the electrochromic material and an electrochemical redox reaction causes a corresponding color change. Therefore electrochromic materials are currently attracting much interest in industry for their commercial applications. [15]

Possible applications of electrochromic materials include, among others, electrochromic displays, cathode ray tubes, thermal-exposure indicator for frozen foodstuffs, electrochromic mirrors and windows. Electrochromic displays are an application where significant advances were made in the 1970s and 1980s with the development of watch and clock displays. However some of their biggest limitations were speed and lifetime. But for this kind of applications these limitations weren't critical because these areas do not require very rapid updating of display information. [16]

Electrochromic materials can also be used in cathode ray tubes with variable transmittance. An electrochromically darkening cathode ray tube screen employing oxides it's an alternative to the common *brilliance* adjustments of TV tubes, when room illumination alters. Electrochromic darkening is preferable to direct electrical control as color values are thereby better preserved. [17]

Another application can be a thermal-exposure indicator for frozen foodstuffs. In this case a thin electrochromic cell is attached as part of the labeling of frozen foodstuff. The composition of the cell is chosen so that it remains in the uncolored state when the foodstuff is frozen. The composition of the polymer electrolyte is chosen to have just the right temperature coefficient of conductivity so that, on warming, increased conductivity

allows electrochromism to set in, thus warning of the thermal deterioration of the goods. The higher the temperature and/or the longer the exposure, the more intense could the color become and show the deterioration level. It's also important to refer that after thermal exposure, re-freezing does not dispel the coloration. [17]

For the case of the electrochromic mirrors, the most common device is the car rear view mirror (Figure 2.2). This mirror changes its color to a dark blue-green color that allows only the outline of the usual dazzling headlights to appear. Here an optically absorbing electrochromic color is evoked over the reflecting surface, reducing reflection intensity and thereby alleviating driver discomfort. The back electrode is a reflective material allowing customary mirror reflection in the bleached state. [13,17]

Figure 2.2 Electrochromic car rear view mirror [18]

For electrochromic windows applications there's a coating of a transparent electrode, with electrochromic materials that allow the use of color change as shading of the substrate. This means that it is possible electronically to alter a window's transmission and reflection properties by use of electrochromic thin films. The electrochromic windows are commercially applied at present. Controlling the absorbance or reflectance properties of the glass using electrochromic cell is the core element of this application. [15]

Having in mind that modern man usually spends about 90% of his time inside buildings and vehicles, and that the quality of indoor environment is of greatest importance, the electrochromic windows represent a great advantage in terms of energy saving. In building equipped with smart windows (Figure 2.3), when the windows are colored there are reducing of the light that goes inside the room and consequently the air is fresher. With the decrease of the temperature inside the room there's no need to use air conditioner

leading to a big energy saving. It is important to note that the window maintains its primary function, which is allowing a constant visual contact between indoors and outdoors. [5,17]

Figure 2.3 Electrochromic window [19]

Besides the use of smart windows in energy efficient buildings, this device can also be used in automobiles and even aircrafts, with the same energy saving purpose. There are also other applications as well, for example motorcycle helmets (Figure 2.4) where the visors can be colored, during day and bleached at night, or before entering tunnels or other dark places. [5,13]

Figure 2.4 Motorcycle helmet with electrochromic visor [5]

Several applications of electrochomism, especially electrochromic windows, have five superimpose layers on one substrate, or positioned between two substrates in a laminate configuration [5]. The structure of an electrochromic window is showed in the Figure 2.5 and it's composed by two substrates covered with a transparent conductor oxide (TCO), next there's an ion storage film followed by an electrolyte and finally an electrochromic film.

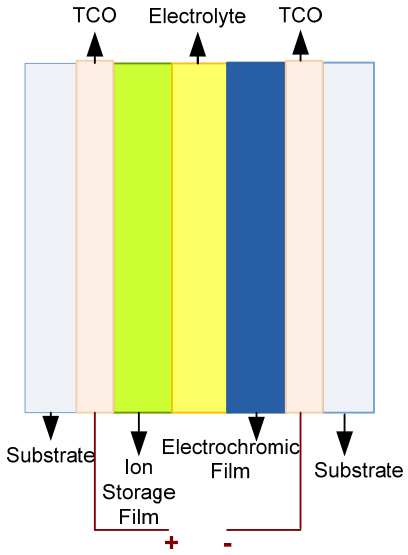

Figure 2.5 Basic design of an electrochromic window

There are basically three types of electrochromic materials that can be potentially used in application described above [12,20]:

- **type I** – Soluble in both the reduced and oxidized sates. A good example is aqueous methyl viologen (1,1´-dimethyl-4,4'-bipyridilium-II);
- **type II** – Soluble in one redox state but following electron transfer forms a solid film on one of the electrode surfaces. Organic examples of this type of electrochromic material are aqueous viologens systems such as heptyl or benzyl viologens, and inorganic example is the bismuth;
- **type III** – In this type of materials both redox states are solids. Most inorganic electrochromes are type III, like metal oxides.

For types II and III, once the redox state has been switched, no further charge injection is needed to retain the new electrochromic state and such systems are said to have *optical memory*. In contrast, for type I electrochromic materials, it is necessary to keep current flowing until the whole solution has been electrolyzed. The PTA precursor and WO_X nanoparticles used in studies described in this thesis belong to the type III group of electrochromic materials.

The electrochromic film is responsible for the change of the optical properties of the device, by switching between the oxidized and reduced form and by conducting electrons as well as ions. Darkening under ion insertion is referred as cathodic coloration, whereas darkening under ion extraction is referred as anodic coloration. The ion insertion and extraction are usually named as ion intercalation and deintercalation. Working electrode can be either organic, with conducting polymers such as PEDOT (Poly(3,4-ethylenedioxythiophene)), PANI (Polyaniline), viologens like salts of 4.4'-bipiridinum, or inorganic as it is in case of metal oxides. [13,14,21]

Table 2.1 contains examples of most popular electrochromic metal oxides, their coloration properties and typical deposition techniques.

Table 2.1 Examples of electrochromic metal oxides, their properties and typical deposition techniques [12,13]

Oxide	Coloration mechanism	Color	Full transparency	Deposition methods
WO_3	Cathodic	Intense Blue	Yes	Thermal Evaporation/RF Sputtering / Sol-gel
TiO_2	Cathodic	Blue	Yes	Thermal Evaporation/ RF Sputtering
IrO_2	Anodic	Blue/ Grey	Yes	Sputtering RF/Anodic Deposition
Nb_2O_5	Cathodic	Blue	Yes	Sol-gel/RF Sputtering
MnO_2	Anodic	Brown	No	Electrodeposition
V_2O_5	Cathodic/Anodic	Brown-Yellow	No	RF Sputtering
MoO_3	Cathodic	Intense Blue	Yes	Thermal Evaporation

There are many requirements for the electrochromic film. The optical modulation should be large enough for a practically realizable change in the electron density, in other words, the coloration efficiency should have high value. The conductivity for ions and electrons must be sufficient, so that the optical modulation is not excessively slow. It's

imperative that the electrochromic film has a structure that is permeable enough to permit easy intercalation and deintercalation of charges.

As it is shown in Figure 2.5, the electrochromic device is composed by two electrodes, separated with electrolyte, which can be any substance containing free ions that make the substance electrically conductive. The charge flow takes place from electrolyte to working electrode as well as from working electrode to electrolyte. The electrolyte, as a pure ion conductor must be ionically conductive, but electronically insulating. It must allow ions to be shuttled between an electrochromic film and an ion storage film (counter electrode) [13,14]. Typically, the electrolytes used in EC windows, as in any other electrochemical cell, belong to four main classes: aqueous electrolytes, organic liquid electrolytes, ionic liquids electrolytes and solid polymer electrolytes. [22]

The most common electrolytes are liquid (aqueous and organic), because they are easy to reproduce and very durable. On the other hand the probability of leakage and low chemical stability of the liquid electrolytes are inevitable drawbacks for electrochromic display applications. The aqueous liquids electrolytes encompass both acids and bases, while the group of organic liquid electrolytes include for example propylene carbonate (PC) or ethylene carbonate, with addition of lithium salts, such as lithium perchlorate ($LiClO_4$) or sodium perchlorate ($NaClO_4$)) in order to achieve improved electrochemical properties. The group of ionic liquid electrolytes is represented for example by ethyl ammonium nitrate ($[EtNH_3][NO_3]$) or 1-butyl-3-methylimidazolium tetrafluoroborate ($[BMIM][BF_4]$). Those room-temperature fluid salts consist of organic cations and inorganic anions, what results in improved lifetime and response speed of diverse types of electrochemical devices. [17,22,23]

Solid polymer electrolytes are usually a polymer or gel matrixes swollen with liquid electrolyte solutions, a single ion systems in which only one ionic species is mobile within a polymer matrix. Another common possibility is a solvent-free ion-coupled system consisting of ion-solvating polymers mixed with salts, so that cations and ions become mobile within the polymer network.

For EC windows applications gel electrolyte should be transparent, while for EC displays usually more suitable are opaque substances [17,22]. The measurements presented

in this thesis were performed using encapsulated EC windows filled with lithium perchlorate polymeric gel electrolyte.

Another layer of the EC device is the ion storage film, named also as counter electrode. This layer has the same demands on electronic and ionic conductivity as the working electrode. It should provide the same stability and durability to the device. If the ion storage film has electrochromic properties, it should be complementary to this of the electrochromic film. It means that when the electrochromic films darken upon ion intercalation the ion storage should darken upon ion deintercalation and vice versa. [13,14]

Finally the electrochomic device needs to have substrates to be built on. For windows applications, the electrochromic layer is deposited on a transparent substrate, typically glass or flexible polyester (PET) foil [3]. On the other hand, for display or mirrors applications, there's no need for both substrates to be transparent. For example, the substrates of an electrochromic watch can be glass and Graphite [16].

Both the targets are coated with electrically conducting transparent films, named Transparent Conductor Oxides (TCO). The TCO should have low electrical resistivity and high optical transparency. The best material in terms of optical and electrical properties are In_2O_3:Sn (Indium Tin Oxide, or ITO), IZO (Indium Zinc Oxide), PEDOT and more recently also carbon nanotubes. [3,14,21]

When a voltage is applied between the two electrodes, in the electrochromic film occurs a reaction of reduction that leads to the consumption of the electron, while in the counter electrode occurs reaction of oxidation that provides the departure of an ion that goes to the electrochromic layer. Consequently there's a drift of electrons through the external circuit from the counter electrode to the electrochromic layer, and to compensate this charge flow there's a passage of ions thought the electrolyte, which is located between the electrodes.

The Equation 2.2 represents the reaction mentioned above, where there's the need to provide electrons and ions to the WO_3 electrochromic layer.

$$WO_3(clear) + xe^- + xLi^+ \Rightarrow Li_xWO_3(deep\ blue) \qquad (2.2)$$

The presence of lithium ions in the electrochromic film leads to a variation of electron density and consequently a color change. The change of electric polarization or a short circuit brings back the original properties. The coloration can be stopped at any

intermediate level, and the device exhibits open-circuit memory so that the optical changes take place only when charge is in movement. [13,14]

2.2 Inkjet Printing Technique

Recently the thin films technology has grown world-wide. The importance of coatings and synthesis of new materials for the industry have also resulted in a tremendous increase of innovative thin films processing. Thin films consist of two dimensional materials created by the process of condensation and growth of atoms, molecules or ions. Regarding to its thickness there isn't any well defined value for it, but it should be much smaller regarding the other two directions.

Modern thin film technology has evolved into a sophisticated set of techniques used to fabricate many products. Applications include integrated circuits, electronic packaging, sensors and devices; optical films and devices; as well as protective and decorative coatings. Figure 2.6 presents short review of the thin film deposition techniques for electrochromic application. [24-26]

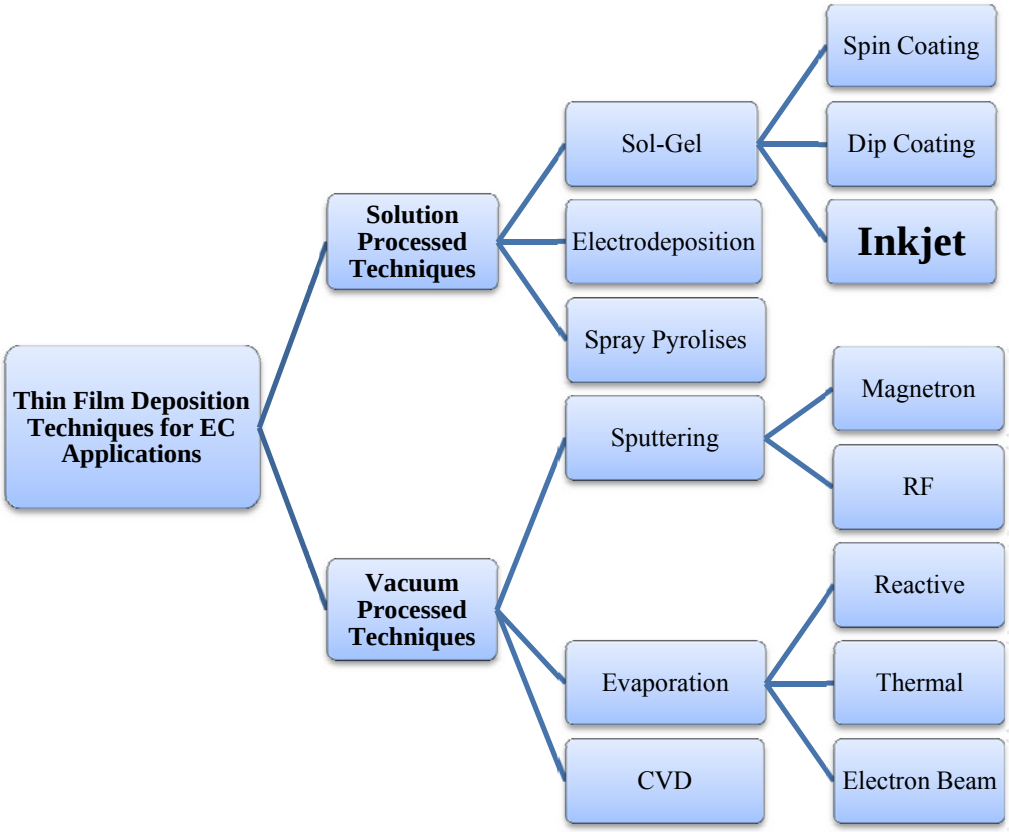

Figure 2.6 Thin Film Deposition Techniques for EC applications

The Inkjet Printing technique has been used successfully in the last few years as an alternative fabrication method of thin film technology for building electrical and photovoltaic devices, using organic as well as inorganic components, because it's an easy, low-cost and room temperature technology that allows the depositions of different kinds of materials.

Research presented in this thesis is based on Inkjet Printed Technology combined with sol-gel method for electrochromic window development. The use of this specific deposition technique is innovative and hasn't been reported before by any author. It is expected that combination of those two methods will not only make the process simpler but will also improve the overall EC device performance.

The Inkjet Printing technique is a non-contact, digital, additive, no mask and no vacuum patterning method, ideal for cost efficient mass production. The use of Inkjet Printing technique, not only simplifies a patterning process, but also reduces the consumption of materials and energy. [27]

In the other hand, the Inkjet Printing process is also very complicated, and the ink used must meet certain chemical and physicochemical requirements including those related to jetting performance, wetting and adhesion on various substrates. Furthermore, the ink must be formulated as a stable fluid and upon solidification on the substrate, the printed element must provide the properties required to the application. [28,29]

In terms of applications, the Inkjet Printing technique has been widely used in several laboratories as a way to develop alternative deposition methods. It has already been widely used for printing polymers, metal nanoparticles, carbon nanotubes, molten silver etc. The possibilities of this technique are vast since the printing can be done in all kinds of substrates including flexible ones. This allow to use of the Inkjet technology in electronics, to print on circuit boards, for flat panel displays printing light emitting polymers, producing organic thin film transistors, organic LEDs (Light emitting diode), sensors, organic solar cells, electrochromic and thermochromic devices. [28,29]

The typical Inkjet printer (Figure 2.7) is composed by the printing assembly tractor mechanism and paper tray. The printing assembly, constituted by the print head and the ink cartridges, it's the core of an Inkjet printer because it contains a series of nozzles that are used to spray drops of ink on the substrate. The tractor mechanism feeds the substrate through the printer in small jumps. The printer used in this studies it's a standard commercial desktop printer after small modifications.

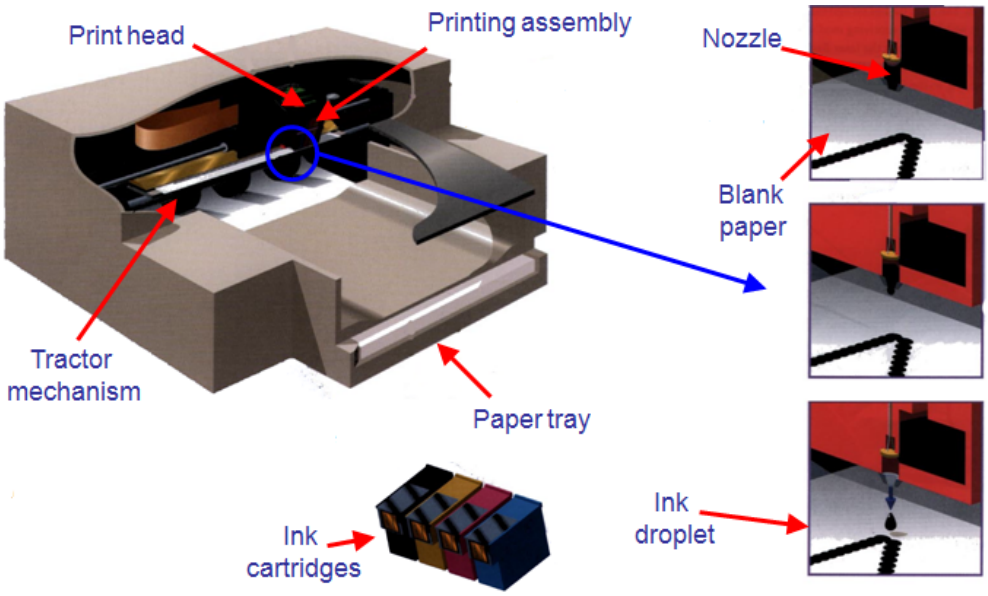

Figure 2.7 Typical construction of an office Inkjet printer [30]

Inkjet printing has been implemented in many different designs and has a wide range of potential applications. Figure 2.8 presents a basic map of the Inkjet technologies. Basically, the Inkjet Printing technique is divided in two main parts, the continuous and the drop-on-demand type.

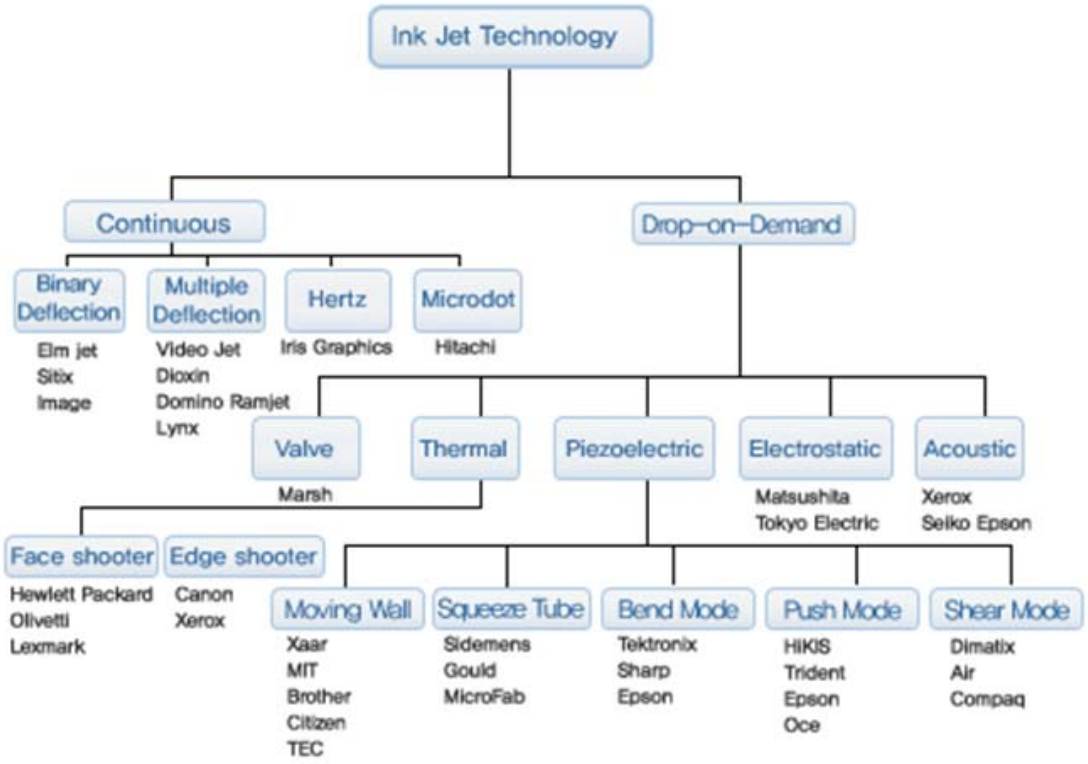

Figure 2.8 Inkjet Printing Technology map [30]

The continuous Inkjet printing is achieved using a device that applies an electric field to the droplets, charging them electrically. Those same droplets are diverted as they pass through the deflection plates, due to the applied magnetic field and are deposited on the substrate. Unused droplets are collected out of the printing area.

The Drop on Demand Inkjet printing it's a technique that only uses the droplets of ink needed to the printing of the pattern. Basically this technology uses cartridges with a series of chambers each containing a heater (thermoresistor). To eject a droplet from each chamber, a pulse of current is passed through the heating element causing a rapid vaporization of the ink in the chamber to form a bubble, which causes a large pressure increase, propelling a droplet of ink onto the substrate. The ink's surface tension as well as the condensation and thus contraction of vapor bubble, pulls a further charge of ink into the chamber through a narrow channel attached to an ink reservoir. This sequence of events is presented briefly on Figure 2.9. [27,30]

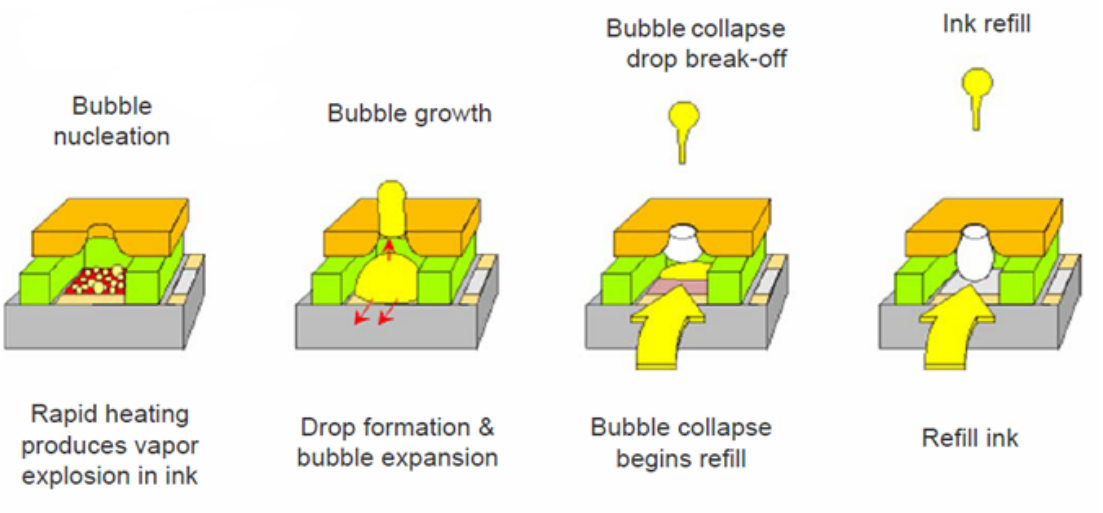

Figure 2.9 Thermal Inkjet printing: drop formation [30]

The most critical component of Inkjet printing is probably the ink. Ink chemistry and formulations not only dictate the quality of the printed image but they also determine the drop ejection characteristics and the reliability of the printing system. There are many different types of inks that have been developed and used for Inkjet Printing applications. The typical composition of Inkjet inks is presented on Figure 2.10.

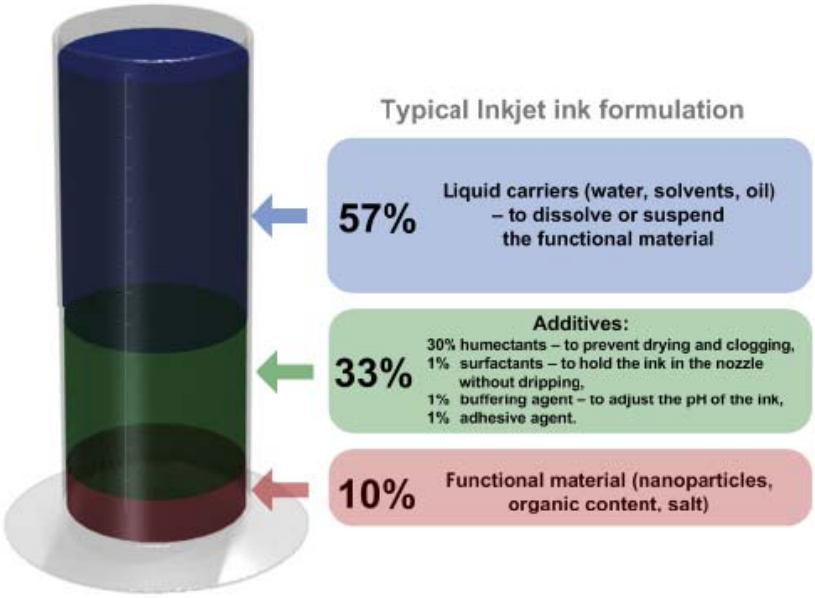

Figure 2.10 Typical inkjet ink formulation [28]

As it is shown in Figure 2.10 the main components are the liquid carriers, which are materials responsible for the dissolution or suspension of the functional material (57%). Around 33% of the ink is filled with additives. Generally around 30% of the additives placed on inks are humectants used to prevent drying and clogging. The rest of additives consist of surfactants, buffering agents and adhesive agents, used in much less quantity than humectants and their quantities are variable or even dispensable for some inks. Finally there's the functional material (10%), which is the one with less quantity but with more importance. [27,28]

The density, viscosity and surface tension are three the most important parameters, which characterize the inks. For a quality printing it is necessary to ensure that these parameters are in a certain range of values. The density of a substance is defined as its mass per unit volume. As known, different substances have different densities and the density is strongly dependent of the solid content. To have a quality printing, the printing suspension must be stable, implying that the solid content is low enough. The density also influences the drive force in the printing process, if the density is too high it will be the drive force in the process, contrarily to the correct way, where the process is driven by viscosity or capillary forces.

Viscosity is a measure of the resistance of a fluid which is being deformed by either shear or tensile stress. Basically the viscosity describes a fluid's internal resistance to flow. That is extremely important for the Inkjet printing because if an ink is too viscous it would clog the nozzles of the print head and if it's slightly viscous the ink will drip. Viscosity of water based Inkjet thermal inks vary from 1.7 to 2.0 cps.

The surface tension is a property of the surface of a liquid caused by cohesion of molecules. Since molecules on the surface of a liquid are not surrounded by molecules on all sides, they are more attracted to their neighbors on the surface. The surface tension for the thermal Inkjet printing is between 28 and 40 dyne/cm.

In the printhead the fluid properties are extremely important. For example, a low viscosity it's appropriate because it will allow a fast refill of the ink, a high viscosity allows damping and particle dispersion, a low surface tension it's used for an easy filling and uniform wetting, and a high surface tension for non-wetting. On the other hand, on the substrate the fluid properties are also important. On the substrate a high viscosity/surface

tension is relevant for the spot shape and size control, preventing a non-uniform spreading and low viscosity/surface tension will provide a rapid spreading.

In a field of electrochromic devices the Inkjet Printing Technology is extremely promising because it allows the production in series, at low-cost and at room temperature. The fact of operations and deposition in room temperature allows the production on flexible substrates.

The performance of printed electrochromic devices is expected to be different, and probably much better than the conventional ones. This difference it's due to the fact that deposited layers can have high porosities, the layer thickness can controlled much easier and the deposition process is much faster since the drying time is extremely low (the calcinations process is different than in other techniques). Briefly, when compare to the vacuum techniques, this is a simpler, cheaper, faster and probably a technique that can improve the electrochromic behavior of the printed devices. [31]

2.3 Sol-Gel Processing for Electrochromic Materials

Sols and gels are two forms of matter that have been known to exist naturally for a long time. They include various materials such as ink, clays and a number of other substances such as the blood and milk. A sol is a stable suspension of colloidal solid particles within a liquid. For a sol to exist, the solid particles, denser than the surrounding liquid, must be small enough for the forces responsible of dispersion to be greater than those of gravity. A gel is a porous 3-dimensionally interconnected solid network that expands in a stable fashion throughout a liquid medium and is only limited by the size of the container. If the solid network is made of colloidal sol particles the gel is said to be colloidal. If the solid network is made of sub-colloidal chemical units then the gel is polymeric.

A gel is formed when the homogenous dispersion present in the initial sol rigidifies. This process is called gelation and prevents the development of inhomogeneities within the material. A sol, or a solution, can be transformed into a colloidal (or polymeric) gel by

going through what is called a gel point. This is the point where the sol abruptly changes from a viscous liquid state to a solid phase called the gel. [32,33]

Sol-gel processing does not only designate a unique technique but a very broad type of procedures that centralizes around a single scheme as it is presented in Figure 2.11.

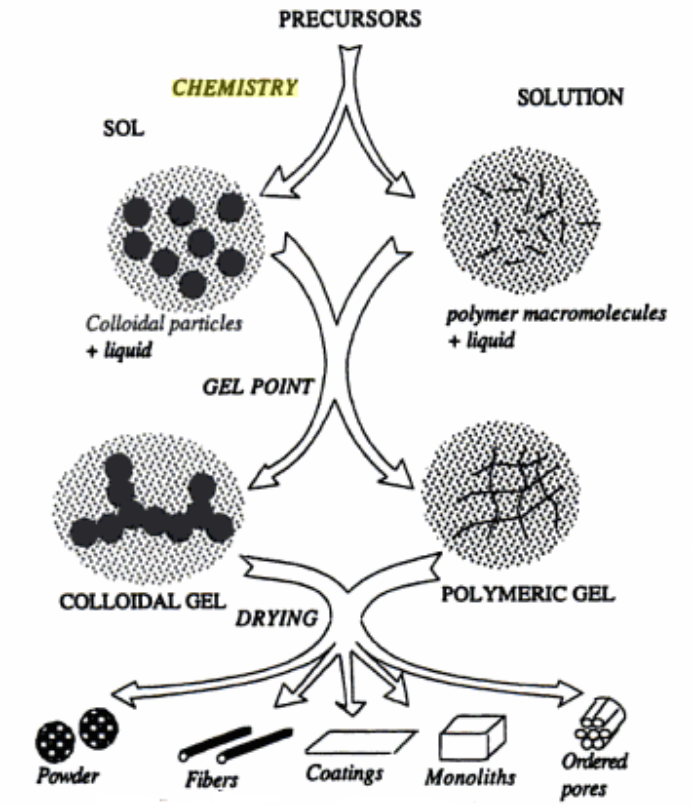

Figure 2.11 Sol-gel processes [32]

Sol-gel technology for deposition of thin films of electrochromic oxides has gained impetus in the last decade owing to the low capital cost of the technique and its adaptability towards large area deposition. Coatings can be deposited by techniques such as spin-coating, dip-coating, spray processes and recently also Inkjet printing. In sol-gel method the molecular precursors are transformed into an oxide network by hydrolysis and condensation reaction. Two routes are currently used depending on the nature or molecular precursors: metal alkoxides in organic solvents or metal salts in aqueous solutions. Ease of preparation of precursor sol makes metal alkoxides very popular as the starting reagents but their use is restricted by the fact that they are rather cumbersome to handle. The peroxo route offers the advantage of formation of pristine metal oxide films at a relatively low

temperature owing to the clean burn out properties of organic additives (with low carbon content) and other volatiles from the as-deposited film. [32,33]

The sol-gel processing has been widely used for deposition of WO_3 films. Besides of being cost-effective, this method has also good control over the microstructure and homogeneity of the coatings. Therefore this technique has also been used for development of electrochromic coating starting with the materials, either tungsten alkoxides $W(OR)_6$, tungsten oxyalkoxide $WO(OR)_4$ or $WO_2(OR)_2$. However, these precursors are not stable towards hydrolysis or condensation and consequently need some stabilizers. [34-36]

The best way to stabilize aqueous solutions of tungsten precursors is to use complexing reagents such as hydrogen peroxide (H_2O_2). With a proper concentration of H_2O_2, the product that appear at the end of the reaction is soluble in water Peroxotungstic Acid (PTA). The experimental formula of this crystal is:

$$WO_3 \cdot xH_2O_2 \cdot yH_2O \tag{2.3}$$

To obtain PTA, according to equation 2.3, the maximum value of x has to be 0.97 and y must be at least 1.1. When $1>x>0.53$ PTA is soluble in water and when $0.53>x>0$ is insoluble. Can be concluded that mixing W (tungsten) metallic powder and H_2O_2 gives crystalline PTA when $x=1$ or $x=0$, while for $1>x>0$ the result is amorphous PTA. In either case the acid suffers polymerization and dehydration during a heat treatment of the film at temperature between 100 and 200°C [37].

For the proposed objective, which is a large scale and low cost devices, the sol-gel method combined with Inkjet technology appears to be a versatile technology to deposit electrochromic tungsten oxide films. Due to the fact that is a non-contact, digital, room temperature and no vacuum patterning method, with the possibility to control the deposited layer thickness and porosity makes it ideal for cost efficient mass production.

To allow a correct quality analysis of the developed devices, it's necessary to compare the results with another technique. The deposition technique chosen as a reference is spin-coating, because it is a solution processed method with some similarities to the Inkjet technology.

Spin-coating has been used for several decades for the application of thin films. It's a simple process for rapidly depositing thin coatings onto relatively flat substrates. A typical process involves depositing a small quantity of a fluid onto the center of a substrate

that is held by some rotatable fixture and then spinning the substrate at high speed. Centripetal acceleration cause the fluid to spread to, and eventually off, the edge of the substrate leaving a uniform coating of the chosen material on the surface. Final film thickness and other properties will depend on the nature of the fluid (viscosity, drying rate, percent solids, surface tension, and so on) and the parameters chosen for the spin process. Factors such as final rotational speed and acceleration contribute to how the properties of coated films are defined. One of the most important factors in spin coating is repeatability. Subtle variations in the parameters that define the spin process can result in drastic variations in the coated film. [38]

The reason to use spin-coating as a reference technique is the fact that the substrates and materials in both methods are very similar. The solution prepared for Inkjet as an ink, can be directly deposited by spin-coating allowing an authoritative comparison and validation of the Inkjet printing as a deposition techniques in EC applications

3. Methods and Procedures

3.1 Experimental Design for Inkjet Electrochromic Devices

As described in Chapter 2, Inkjet Printing is a solution based technique in which the formulation of the inks is of great importance to the performance of printer and the final device performance as well.

The mixture components were selected based on literature review (sol-gel method for WO_3 films), Inkjet technique principles and using an experience of researchers in our group. Therefore, the chosen constituents are as follow:

1. The base solution (liquid carrier) is a simple mixture of water and isopropyl alcohol with a weight fraction of 0.7 and 0.3 respectively.
2. The functional materials are:
   - PTA;
   - WO_X nanoparticle dispersion;
   - TiO_2 nanoparticle dispersion;
3. The additive used as a dispersant is, the oxalic acid (OAD).

The PTA as a WO_3 precursor has been obtained by a sol-gel method in which 6g of tungsten monocrystalline powder, (99.9%, Aldrich, Japan) was carefully added to 50ml mixture (50:50) of distilled water (Milipore S.A, France) and hydrogen peroxide (30% by weight, Sigma-Aldrich, Germany). Since the reaction is strongly exothermic, as icy ambient was employed and the solution was kept slowly stirring for 24 hours. The excess of tungsten powder was then removed by filtration (0.45 μm syringe filter, Roth, Germany) leading to a transparent solution. In order to remove the excess of hydrogen peroxide the solution was dried at 65º C and washed several times with distilled water. After drying the final result is a water soluble orange crystal powder (PTA). The formation of PTA mainly depends on the degree of excess decomposed H_2O_2 in the solution, the atmospheric humidity during the condensation and the condensation rate [36,39]. Variations of those parameters lead to emergence of a white powder in a product during condensation which

should be removed by subsequent washing with distilled water and drying at the same temperature till the yellow crystals are obtained.

The solution processed PTA is the functional material which as-deposited forms amorphous phase causing high optical modulation of the layer when electrical potential is applied. Considering the fluid properties of aqueous-alcohol PTA solution, the use of this material for printing seems to be reasonable. The quantity of PTA used in experiments is in the range from 0.01 to 0.2 w/w because that's the standard PTA concentration used in other sol-gel deposition techniques, like dip coating. [39]

According to *C.M. White et al* [40], the crystalline structure of the material influences the diffusion coefficient inside the electrochromic layer and the length of the diffusion path. It is therefore obvious that the varied, dual-phase microstructure would significantly improve the electrochromic performance. The creation of the crystalline phase in a low temperature, deposition process has so far been possible only using electrodeposition [41]. Here it's proposed a new approach which allows for the incorporation of the crystalline phase into the layer using Inkjet Printing. This innovative method is based on dispersions of nanocrystals used as components of the printable ink. It's expected that this will allow for simultaneous use of the advantages of both phases without necessity of using high energetic depositions methods or annealing.

The two types of commercially available WO_X nanoparticles were used as a source of crystalline phase, WO_3 hereinafter called *yellow* (Sigma Aldrich Chemistry, USA) and $WO_{2.9}$ hereinafter called *blue* (99.99% pure WO_3 ceramic oxide target, Super Conductor Materials, USA). The suggested designation of those materials is thin film deposition using PVD techniques. Here, however it serves as a solid content in liquid dispersions. These liquid dispersions are aqueous alcohol dispersions with a solid content of around 0.01% and base solution of isopropyl alcohol and water in a constant proportion 0.3/0.7. The different colors of the WO_X nanoparticles are due to their stoichiometry.

Figure 3.1 and 3.2 shows the SEM (Scanning Electron Microscopy) micrographs of the *yellow* and *blue* WO_X nanoparticles, respectively. The *yellow* tungsten oxide exhibits grains of about 85 nm in diameter, while *blue* tungsten oxide has grains of 70 nm in diameter. For convenience, shall refer to those powders as *blue* and *yellow* respectively.

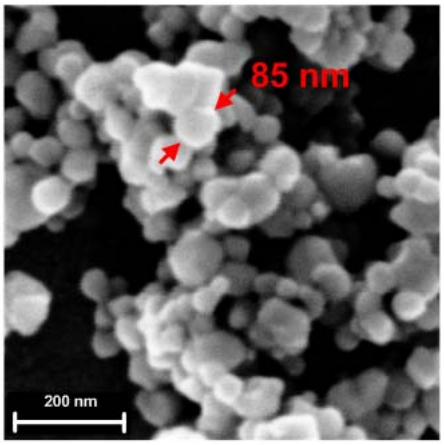

Figure 3.1 WO_3 *yellow* nanopowder SEM micrograph

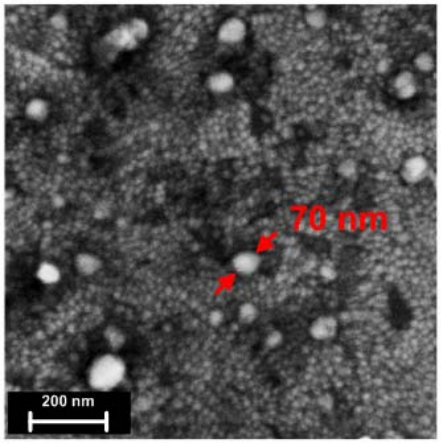

Figure 3.2 $WO_{2.9}$ *blue* nanopowder SEM micrograph

The TiO_2 nanopowder in aqueous alcohol dispersion has a solid content of nanoparticles of around 0.01% and the same proportion of isopropyl alcohol and water, as the WO_X dispersions. The presence of titanium dioxide has the objective of increasing the electrochromic behavior, because this material tends to increase the contact surface area of the electrochromic material. According to *P.S. Patil et al* the presence of TiO_2 nanoparticles modifies the electrochromic layer structure leading to greater electrochromic reversibility, stability and coloration efficiency of the devices. The presence of titanium dioxide also helps the intercalation and deintercalation process due to formation of open channels resulting in an increase of the surface area of the layer [1]. In this research, was decided to examine the impact of this factor using TiO_2 nanopowder (T20/SC, 3% by weight, Solaronix). A TiO_2 nanopowder SEM micrograph represented in Figure 3.3 indicates that the grain size is much smaller (30 nm) than the WO_X nanoparticles.

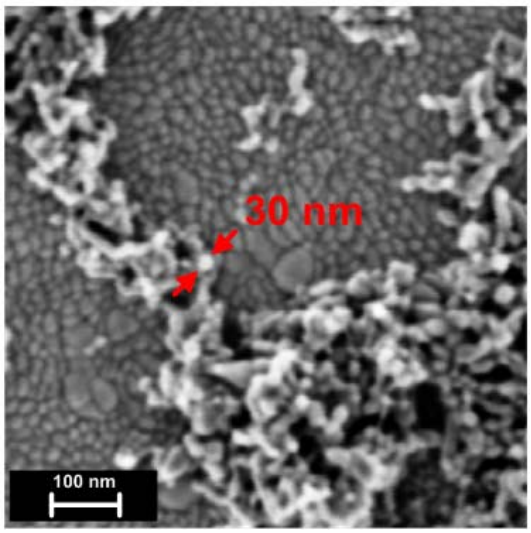

Figure 3.3 TiO_2 nanopowder SEM image

The Oxalic Acid (OAD dihydrate, Merck, Germany) with chemical formula $(COOH)_2*2H_2O$ is a white powder working as a drying control and a dispersant for the inks. The addition of this material is known to prevent coagulation of particles in dispersion [42]. According to *Deepa et al* [43] the presence of OAD in the precursor controls also the microstructure of WO_3 annealed in elevated temperature and consequently affects the electrochromic performance. In present studies OAD serves as a dispersant in the ink and potential impact of this component on electrochromic performance is going to be exanimate.

Resuming, the ink components described above were used in appropriate concentrations in order to study their impact on mechanical, electrical and optical performance of Inkjet Printed electrochromic layers. All nanoparticles have been incorporated to the ink as aqueous alcohol dispersion with a solid content of around 0.01% of total dispersion mass.

The scope of research is to find the best combination of factors (components of the mixture) to obtain the EC window with the best performance. The optimum electrochromic device is characterized by high coloration efficiency, short response time, high transparency in a bleach state, and high optical modulation.

In order to design the mixture composition and perform statistical analysis of results a statistical method called design of experiments (DOE) have been used. This method

allows several factors to be analyzed at the same time in order to know which one has the greatest impact on the final result.

Design of experiment is the design of any information gathering exercises where variation is present, whether under the full control of the experiment or not. The purpose of this method is to characterize, predict, and then cost-effectively improve the behavior of any system or process [44]. Basically it's a method to increase productivity and improve quality of a process.

There are several kinds of Design of Experiments, such as the Factorial Design (full or fractionated), Taguchi Design, Optimal Design for Regression Models, among others.

For this work was used the Optimal Design for Regression Models. The fact that, Optimal Designs reduce the costs of experimentations by allowing statistical models to be estimated with fewer experimental runs and the fact that, it can accommodate multiple types of factors, such as process, mixture and discrete factors is an advantage of this kind of design. Specifically, was used the D-Optimal Design, which is most appropriate for screening experiments because the optimality criterion focuses on precise estimates of the coefficients.[44]

The software used in this work is JMP® Statistical Discovery Software, which is a statistical tool that allows the interaction with data, the creation of relations between important factors and it provides more specific information about the areas that interest the most in a certain study.

This software allows the choice of several designs. After choosing a specific design it's imperative to introduce the responses and factors of the experiment. Afterwards, with the collected information the program will create a design, which provides the recipes for the formulation of the sufficient inks to obtain a reliable study. In order to evaluate the created design, the program will make a table with the ink formulation values and where the results of measurements and calculations performed to obtain the responses values must be insert.

When the table is filled the program can finally create a model. In the model specification, if the effect leverage is chosen then the program will provide the whole model for each response, the leverage plots for each factor and factors interactions, the summary of fit table, the parameter estimates and the effects test table, among other

statistical information. On the other hand if the effect screening is chosen the program will provide some similar information to the effect leverage, with the addition of the sorted parameters estimates plot, and some other statistical information. In the effect screening is also possible to obtain mixture profiles where, with the data inserted in the table, is possible to create surface response prediction plots of every response. These plots are important for this study because they allow the observer to see the behavior of the devices when the quantity of nanoparticles changes.

With all the information obtained from the program it is possible to analyze if the model created is or isn't reliable, it is also possible to know the significance of the effects and it's possible to obtain a prediction study of the behavior of the devices.

More detailed information about the JMP® Statistical Discovery Software is available in [44].

Figure 3.4 presents step by step all the important phases of the design of experiments process for this experiment.

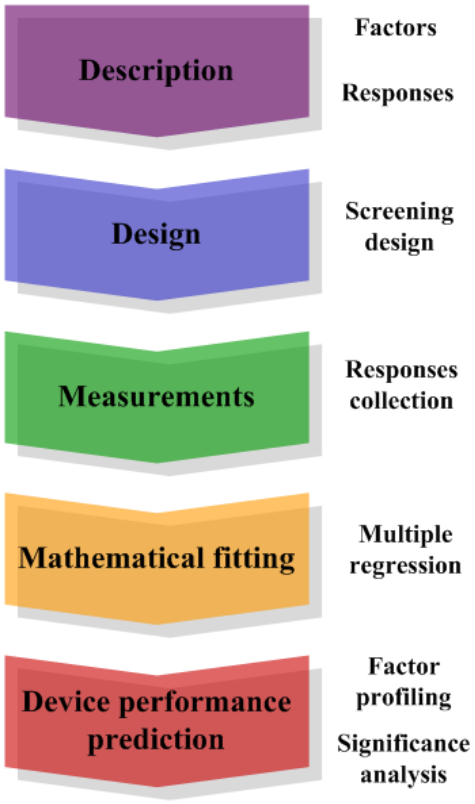

Figure 3.4 Design of Experiment phases[44],[45]

The *description* step is where the factors and responses are identified. Factors can be either continuous concentrations of mixture components and categorical types of components. The responses are all the results of measurements and calculations that can be helpful in analysis of electrochromic device performance. Table 3.1 contains all factors for this specific design of experiments. All factors except WO_X *stoichiometry* are continuous in defined range, while the exception has only two categorical values *yellow* and *blue* which stand for WO_X nanoparticle stoichiometry.

All factors were coded using abbreviations in order to simplify the nomenclature, and from now on will be referred as following:

- $w_{iso/water}$ - base solution content;
- w_{PTA} - Peroxotungstic Acid content;
- w_{OAD} - Oxalic Acid content;
- w_{TiO2} - amount of TiO_2 nanoparticle dispersion;
- w_{WOX} - amount of WO_X nanoparticle dispersion;
- WO_X - stoichiometry of tungsten oxide nanoparticles.

Table 3.1 Factors to be examined, its role and range

Factor	Role	Value
Base solution (aqueous alcohol)	Mixture component	0 to 0.99
PTA	Mixture component	0.01 to 0.2
OAD	Mixture component	0 to 0.5
TiO_2 nanopowder in aqueous alcohol dispersion	Mixture component	0 to 0.99
WO_X nanopowder in aqueous alcohol dispersion	Mixture component	0 to 0.99
WO_X stoichiometry	Categorical	*yellow* or *blue*

Table 3.2 Defined responses and their goals

Response Name	Goal
Roughness	None
Coloration Time	Minimize
Bleaching Time	Minimize
Change in Optical Density	Maximize
Coloration Efficiency	Maximize
Oxidation Peak Max	None
Reduction Peak Max	None
Transmittance (bleaching)	None
Transmittance (coloring)	None
Inserted Charge Density	None
Optical Absorption Coefficient	None
Density	None
Viscosity	None
Surface Tension	None
Contact Angle	None

The responses shown in Table 3.2 concern the measurements performed on printed electrochromic devices developed according to the DOE recipes. The results of the measurements were divided in five groups, and coded as following:

1. Mechanical parameters
   - d - film thickness;
   - R_q - film roughness;
2. Optical parameters defined for $\lambda=900nm$
   - τ_{col} - coloration time;
   - τ_{bl} - bleaching time;
   - ΔOD - change in optical density;
   - T_{col} - transmittance in coloration state;
   - T_{bl} - transmittance in bleaching state;
   - α – optical absorption coefficient;
3. Electrical parameters
   - i_{RED} - reduction peak max.
   - i_{OX} - oxidation peak max.
   - Q_{ins} - Charge inserted to the device during coloration process
4. Fluid parameters of the ink
   - ν - ink viscosity;

- γ - ink surface tension;
- θ - ink contact angle on ITO PET substrate;
- ρ - ink density;

5. Overall performance defined for λ=*900nm*
   - *CE* - coloration efficiency

In *design* step the determination of mixture formulations is performed, using the *screening design* method. The choice of the screening design occurs because it has the ability of examine many factors, with fewer experimental runs, to see which have the greatest effect on examined responses. In addition to the influence of the main components of the mixture, the screening design allows also to indicate the relevant correlations between factors. In *measurements* step all the responses defined in Table 3.2 are physically collected for all printed devices. The *mathematical fitting* is a mathematical procedure for finding the best fitting curve of a given set of points, in order to analyze the data collected during measurements step. Finally in *device performance prediction* phase the performance of any possible device can be predicted based on mathematical model. This phase allow also to perform analysis of significance in order to classify the factors and extract information about their interactions.

3.2 Electrochromic ink formulation

The ink used in thermal Inkjet printers should meet certain physical properties compatible with a wide range of ejecting conditions, i.e., driving voltages and pulse, and the shape and size of the nozzle. The exact choice of ink components depends upon the specific application and performance requirements of the printhead from which they are jetted. Thermal printhead requires ink compositions with a certain set of physical properties in order to achieve reliable and accurate jetting of the ink, as is well known in the art of Inkjet printing. Acceptable viscosities are typically no greater than 3 cP, and preferably in the range of about 1.5 to 2.5 cP.

The Inkjet inks applied to non-absorbing substrates should have a surface tension in the range of about 20 dynes/cm to about 40 dynes/cm and, more preferably, in the range 25 dynes/cm to about 35 dynes/cm. Control of surface tensions in aqueous inks is usually accomplished by additions of small amounts of surfactants or low viscosity alcohols.

Using the *screening design*, the program provides a set of recipes for formulation of 30 inks, which are sufficient for obtain the good statistical study. Table 3.3 shows the formulation of each ink with total weight of 5g.

Table 3.3 Ink Recipes

Ink	**Base solution (aqueous alcohol)**		***PTA***		***OAD***		***TiO_2* dispersion**		***WO_X* dispersion**		***WO_X* Stoichiometry**
No.	**w/w**	**[g]**	**w/w**	**[g]**	**w/w**	**[g]**	**w/w**	**[g]**	**w/w**	**[g]**	**Code name**
1	0.54	2.69	0.01	0.05	0	0	0	0	0.45	2.25	*yellow*
2	0	0	0.2	1	0	0	0	0	0.8	4	*blue*
3	0	0	0.11	0.56	0.05	0.25	0.84	4.19	0	0	*blue*
4	0	0	0.2	1	0	0	0.8	4	0	0	*yellow*
5	0.8	4	0.2	1	0	0	0	0	0	0	*yellow*
6	0.57	2.87	0.01	0.05	0	0	0.42	2.08	0	0	*yellow*
7	0	0	0.01	0.05	0.05	0.25	0	0	0.94	4.7	*blue*
8	0	0	0.01	0.05	0.05	0.25	0.94	4.7	0	0	*yellow*
9	0	0	0.01	0.05	0	0	0.50	2.49	0.49	2.46	*blue*
10	0.94	4.7	0.01	0.05	0.05	0.25	0	0	0	0	*yellow*
11	0	0	0.01	0.05	0	0	0	0	0.99	4.95	*yellow*
12	0	0	0.2	1	0.05	0.25	0	0	0.75	3.75	*blue*
13	0	0	0.01	0.05	0	0	0	0	0.99	4.95	*blue*
14	0	0	0.01	0.05	0	0	0.99	4.95	0	0	*yellow*
15	0	0	0.2	1	0	0	0	0	0.8	4	*yellow*
16	0.46	2.33	0.01	0.05	0.02	0.13	0	0	0.49	2.49	*blue*
17	0.94	4.7	0.01	0.05	0.05	0.25	0	0	0	0	*blue*
18	0.8	4	0.2	1	0	0	0	0	0	0	*blue*
19	0.87	4.33	0.11	0.54	0.02	0.12	0	0	0	0	*yellow*
20	0.44	2.20	0.01	0.05	0.03	0.13	0.52	2.61	0	0	*blue*
21	0	0	0.08	0.40	0.02	0.12	0.44	2.22	0.45	2.25	*yellow*
22	0	0	0.01	0.05	0	0	0.99	4.95	0	0	*blue*
23	0	0	0.2	1	0.02	0.12	0.77	3.88	0	0	*blue*
24	0	0	0.2	1	0.05	0.25	0.75	3.75	0	0	*yellow*
25	0.99	4.95	0.01	0.05	0	0	0	0	0	0	*blue*
26	0	0	0.01	0.05	0.05	0.25	0.94	4.7	0	0	*blue*
27	0.35	1.75	0.2	1	0.05	0.25	0	0	0.40	2.00	*yellow*
28	0	0	0.01	0.05	0.05	0.25	0	0	0.94	4.7	*yellow*
29	0.40	2.00	0.11	0.54	0	0	0.49	2.46	0	0	*blue*
30	0.75	3.75	0.2	1	0.05	0.25	0	0	0	0	*blue*

The ink preparation is followed by magnet stirring for a few minutes till all the soluble components are completely dissolved. The obtained mixtures are ready to use as an electrochromic ink in a printer and they are stable for couple of hours.

The surface tension of poor water is higher than acceptable value for Inkjet while the viscosity is under the lower limit. Rheological parameters of the base solution can be adjusted by appropriate amount of alcohol. Taking under account rheological properties of common alcohols, the best candidate seems to be isopropyl alcohol. It is a good choice also due to the low boiling point which promotes solvent evaporation form the layer. In order to study the influence of isopropyl alcohol content in aqueous solution on surface tension and viscosity parameters, series of tests were performed.

The presence of isopropyl alcohol in aqueous solution decreases the value of surface tension of the mixture. Isopropyl weight fractions higher than 0.2 keep the surface tension value on the same level below 30 dyne/cm which is acceptable for Inkjet.

The value of viscosity of isopropyl alcohol aqueous solution increase with the alcohol concentration reaching 2.6 cP in 50:50 mixture. Further increasing in alcohol concentration leads the viscosity value to decrease.

Concluding, the most suitable concentration of isopropyl alcohol in water is 0.3/0.7 which keeps the surface tension below 30 dyne/cm and viscosity on level of 2 cP.

In order to develop a printable ink which satisfies all rheological conditions, series of measurement have been performed. The most important parameters from the ink formulation point of view are density, surface tension, viscosity and contact angle.

The density of the ink was calculated by measuring the weight of the ink (2ml in volume) using a digital balance (OHAUS, ANALYTICAL Plus) and using following equation:

$$\rho = \frac{m}{V} \tag{3.1}$$

where, m is weight in [g] and V the volume in [ml].

The viscosity of inks and their individual liquid components were measured using simple *custom made* viscometer based on laminar flow in a capillary.

The Poiseuille Equation (3.2) describes a physical law that gives the pressure drop in a fluid flowing through a long cylindrical pipe. The assumptions of the equation are that

the flow is a laminar viscous and incompressible and is through a constant circular cross section that is considerably longer than its diameter.

$$\frac{V}{t} = \pi r^2 \bar{v} \tag{3.2}$$

Where, V is the volume between levels a and b from Figure 3.5, r is the capillary radius, $\bar{v}$ the average speed of laminar flow and t is the flow time.

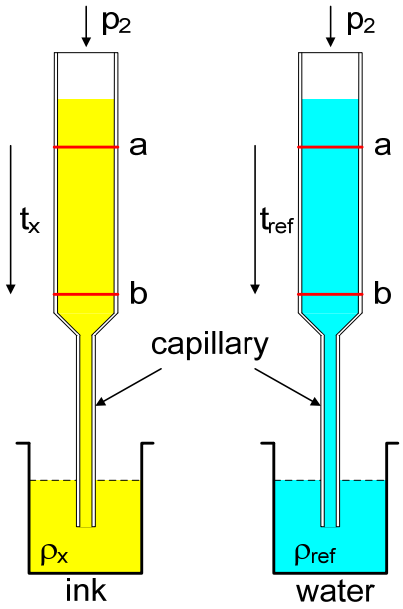

Figure 3.5 The principle of *custom made* viscometer based on laminar flow

Equation 3.2 adapted to the viscometer has the following form:

$$V = \frac{\pi r^4 \Delta p}{8 \eta d} t \tag{3.3}$$

where, d is the capillary length, Δp is the difference of pressures, $\Delta p = p_1 - p_2$, shown in Figure 3.6, and η is the viscosity.

Figure 3.6 shows the laminar flow of a fluid. The cross section of a cylindrical pipe, confirms that the pressure is different between the end of the pipes and, the bigger the pressure difference, the faster will be the flow.

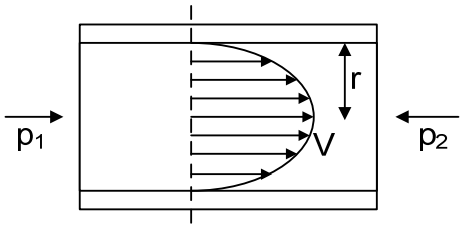

Figure 3.6 Laminar flow representation

The change in pressures through the capillary applied to the Equation 3.3 gives the final formula for relative viscosity:

$$\eta_x = \eta_{ref} \frac{\rho_x t_x}{\rho_{ref} t_{ref}} \tag{3.4}$$

where, η_{ref} is the viscosity of the water, ρ_x and ρ_{ref} are the density of ink and water, t_x and t_{ref} are the flow time of ink and water respectively.

The final value of ink viscosity taking under account temperature fluctuation is then calculated using following formula:

$$\eta_x(T) = \eta_{ref}(T) \frac{\rho_x(T) T_x(T)}{\rho_{ref}(T) T_{ref}(T)} \tag{3.5}$$

The ink surface tension and the contact angle on ITO PET substrate were obtained using Contact Angle Measurement System (OCA 15, DataPhysics, Germany). For the static contact angle measurements, the sessile drop method is the standard method. For that a sessile drop is illuminated from one side with a diffuse light source and from the other side the contour of the drop is observed. [46]

The contact angle, θ, is a quantitative measure of the wetting of a solid substrate by a liquid ink. It is defined geometrically as the angle formed by a liquid at the three phase boundary where a liquid, gas and solid intersect. Low values of θ indicate that the liquid spreads, or wets well, while high values indicate poor wetting. If the contact angle is bigger than 90º the substrate is hydrophobic, and consequently there isn't a good adhesion between the surfaces form the materials in contact. On the other hand if the angle is less the 90º, the substrate is hydrophilic and the materials adhesion is favored. A zero contact angle represents complete wetting. [47,48]

Surface tension was measured using a pendant drop shape analysis. The shape of a drop of a liquid hanging from a syringe tip is determined from the balance forces which include the surface tension of a liquid. The surface or interfacial tension at the liquid interface can be related to the drop shape through the following equation:

$$\gamma = \Delta\rho \times g \times \frac{R_0^2}{\beta} \tag{3.6}$$

where, γ is the surface tension, $\Delta\rho$ the difference in density between fluids at interface, g is the gravitational constant, R_0 the radius of drop curvature at apex and β is the shape factor. The shape factor can be defined trough the Young-Laplace equation expressed as 3 dimensionless first order equations:

$$\frac{dx}{ds} = \cos\phi \tag{3.7}$$

$$\frac{dz}{ds} = \sin(\phi) \tag{3.8}$$

$$\frac{d\phi}{ds} = 2 + \beta x - \frac{sin\phi}{x} \tag{3.9}$$

3.3 Electrolyte Preparation

The gel electrolyte which contains a lithium salt, a polymeric matrix and an organic solvent or a mixture of organic solvents was used as ion conductor layer between counter and working electrodes. The polymeric matrix in this specific electrolyte is a mixture of PMMA/PEO/PPO with PC as solvent and plasticizer, which allows the ionic ($LiClO_4$) conduction. [49]

The materials used in the electrolyte preparation were polymethacryl-sauremethyleste-PMMA (Fluka, Germany), PEO-PPO (Zeon Chemicals, Spain), which is a binary mixture of ethylene poly(oxide) and propylene poly(oxide), lithium perchlorate (Fluka, Germany), propylene carbonate (99%, Fluka, Germany) and tetrahydrofuran-THF (99.9% THF, Sigma-Aldrich, Germany).

In order to obtain 3g of electrolyte, 0.36g of PMMA, 0.21g of PEO-PPO, 0.33g of $LiClO_4$ and 1.75 PC were mixed with 4ml of THF and followed by stirring for about 4 hours until a transparent uniform lightly viscous gel were obtained [49].

3.4 Processes

Since the main purpose of this work is to develop a flexible EC window, a transparent ITO PET foils (Indium Thin Oxide coated polyethylene terephthalate, Aldrich Chemistry, 100Ω/sq) have been chosen as a device substrate (see section 2.1). Preliminary tests carried out at the beginning of the research scope identification, have demonstrated that PET foil is compatible with all materials and technological steps performed in this studies.

For research purposes, the Inkjet deposition of working electrode was carried out simultaneously on multiple ITO PET, ITO glass and uncoated glass substrates depending of the layer assignment which are as follow:

- substrate 1 and 2 – 25x25mm ITO PET for device electrode (100Ω/sq, Aldrich Chemistry, Germany);
- substrate 3 – 25x25mm ITO glass for SEM measurements (15Ω/sq, Blazers, Germany);
- substrate 4 and 5 – 25x25mm uncoated glass for XRD measurements (Ref: 1523100091, Marienfeld, Germany);
- substrate 6 – 75x25mm uncoated glass for mechanical properties measurements (microscope slides, Carl Roth, Germany).

The conductive surface of the ITO PET targets was originally sealed using protection foil. Despite this, just before deposition process, the top (conductive) surface was cleaned using isopropyl alcohol. The same procedure was applied also for the rest of the substrates. The substrates were transferred to the printer using modified Canon CD tray which serves as target holder during deposition. The individual layers were printed in a sufficiently long time intervals to ensure adequate drying. This time period depending on the ink composition ranged from several to tens of seconds. The round shape deposited area was equal to 1 cm^2. A modified commercially available Canon PIXMA IP4500 desktop printer (Canon Virginia, Inc., Newport News, USA) shown in Figure 3.7, with a resolution of 9600×2400 dpi was used as the printing device. This thermal-type printing unit allows deposition of the material as a digital printing process, where the ink/material is ejected directly onto a substrate from 1536 nozzles driven by an electronic signal. The

fabrication of the active layer by Inkjet Printing was performed at room temperature and atmosphere pressure.

In case of spin-coating, the solution was spun onto ITO PET substrate (Aldrich Chemistry, 100Ω/sq) of 25x25mm dimensions at 200 rpm for 100 s using spinner (Braive Instruments, Belgium). The deposition area was limited to 1 cm^2 using kapton tape (3M,USA).

When inkjet/spin-coating deposition process was completed, the samples were left to dry in a room temperature and 49 % humidity for 24 hours. Drying process was followed by annealing for 1h in a 120 deg C using laboratory furnace (EHRET, TK4067, Germany).

Figure 3.7 Inkjet Canon PIXMA iP4500 printer

Figure 3.8 shows a modified CANON printhead (QY6-0075-000, Canon Fine Technology, Japan) in which access to one of five channels is provided by a plastic tube placed in an adequate carriage (in this case Magenta channel). The ink is supplied in small quantities using a pipette.

Figure 3.8 Modified Canon cartridges

The shapes and positions of patterns on the substrates were designed using Microsoft Visio 2010 vector graphics software and Canon Inkjet iP4500 series driver working in a high quality mode.

The counter electrode was deposited on the same ITO PET substrates (Aldrich Chemistry, 100Ω/sq) by brushing. The solution used as a counter electrode material is an alcohol based paint containing a chemical platinum precursor (Platisol T, Solaronix, Switzeland). The deposition was followed by annealing for 1h at 120 deg C using laboratory furnace (EHRET, TK4067, Germany) in order to activate a platinum layer. This temperature is lower than recommended by the manufacturer, due to the use of flexible, temperature sensitive substrate. The result is a layer with inferior properties, but still fulfilling the task.

3.5 Device structure and encapsulation

The performance and operating characteristics of electrochromic devices strongly depend on encapsulation process. The method used in this work enables to make a small lab-test EC window that consists of an electrochromic layer, electrolyte and counter electrode sandwiched between two flexible ITO PET targets. As both targets are made from transparent plastic foil, the window can be seen clearly through it when active layer is

bleached. The active area of the device changes from one color to another when stimulated by an electric current applied to electrodes. All technological steps of proposed encapsulation method for EC windows are shown in Figure 3.9. On the beginning of the encapsulation process, the tape spacer (1mm thick, Ceys, Spain) is placed on the bottom substrate which is partially covered with dried and annealed electrochromic layer. The main task of using a double site tape as a spacer is to limit the volume of electrolyte and to establish a constant thickness of the device. In the next step, both substrates are combined together in a sandwich structure, and the connection is reinforced using thermoplastic glue (iTools Thermoplastic Gun). The volume inside the device contains one small hole placed in the corner necessary to introduce gel electrolyte. Prepared structure is ready for filling with electrolyte which is performed using syringe with a needle. In order to finalize encapsulation the device is sealed by the same thermoplastic glue. The use of conductive tape in order to improve the electrical contact is optional. It is important that the volume of electrolyte inside the device should not contain air bubbles, because their presence may interfere with measurements.

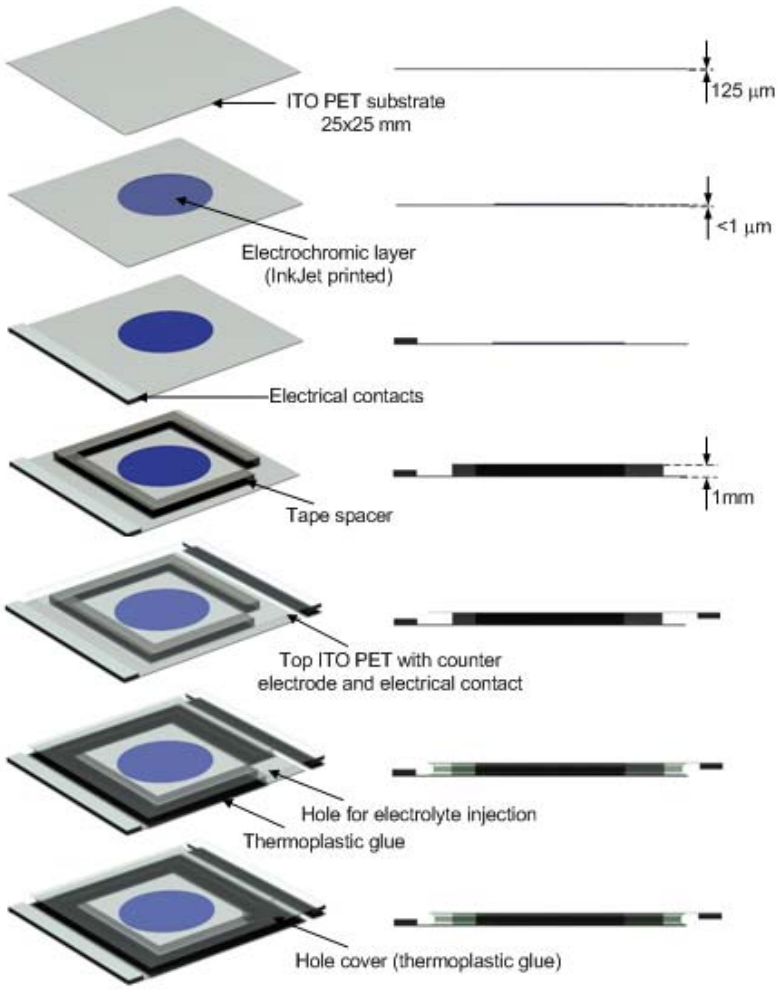

Figure 3.9 Lab-test device encapsulation method

Just before measurements, both sides of the device were cleaned using isopropyl alcohol in order to remove all contaminations and thermoplastic glue residue.

Coloring and bleaching states of the lab-test device picked-up from the series are shown in Figure 3.10.

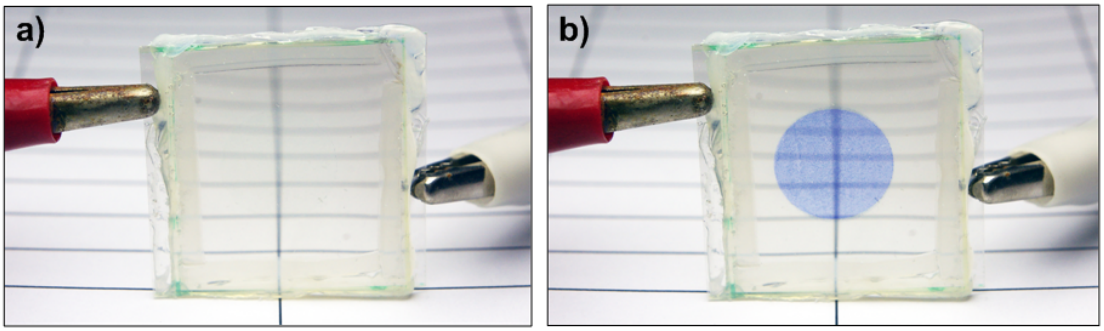

Figure 3.10 Prototype of Inkjet printed lab-test EC window in a) bleached and b) colored state

3.6 Device Characterization

In order to examine the structure and composition of printed electrochromic layers, the profilometry, X-ray diffraction (XRD) and Scanning Electron Microscopy (SEM) measurements have been performed. The use of these techniques aims to perform phase identification and confirm of the presence of different mixture components (structures and phases) in the printed layer, as well as to determine its thickness and roughness. It is expected that all these information will help to understand the dependence between the active layer structure and its electrochromic behavior.

The roughness of the films printed on uncoated glass was measured using mechanical profilometry technique (Ambios XP-200 Profilometer, USA). In this technique, a very precise stylus tip scans the surface at a programmable speed while the information on its different positions is sampled at small and regular intervals. The fact that this is a very precise stylus allows the detection of the smallest surface variation to the level of Angstroms, obtaining the profile of the deposited layers. The data is then processed by the application software to extract useful information such as step height and surface roughness [50]. The surface of the sample was scanned by a stylus through the 5mm wide printed area from one edge to another in a distance of 7mm. The stylus registers the vertical motion at the edges and thereby allows determining the roughness and thickness of the coatings for parameters presented in Table 3.4. For this specific measurement the active layer was deposited on a glass substrate as the rigid substrates facilitate accurate measurement.

Table 3.4 Profilometry parameters

Parameters	Value
Speed	0.20 mm/s
Length	7 mm
Range	100 μm
Stylus Force	0.5 mg

X-ray diffraction (XPert PRO, PANalytical, Netherlands) is usually used in electrochemistry to identify a material and give information about the phase, lattice stress, texture orientation and grain size. It is based on the constructive interference between x-rays reflected at different atomic planes. By varying the angle between the incident and diffracted beam and recording the diffracted radiation, a chart with material and phase specific peaks is achieved. In this work the XRD method has been used to determine the electrochromic layer crystalline structure.

The X-ray diffraction occurs when a beam focuses on a material, causing a vibration and which consequence is the emission of a wave with the same length as the focused beam. If the atoms are periodically organized, forming plans and if the wavelength of the radiation is in the range of inter atomic spaces, like in X radiation, may occur constructive or destructive interferences. This effect is described by Bragg's law represented by the following equation [51]:

$$n_i \times \lambda = d_{hkl} \times sen\theta \tag{3.10}$$

where, θ is a certain angle of the radiation when it hits the surface of the sample, the constructive interferences occur to multiple (n_i) of the wavelength (λ), related to the space between atomic plans (d_{hkl}). The θ angle is also known as Bragg angle, being 2θ, the diffraction angle. The phase and components identification is achieved by comparing the X-Ray diffraction patterns obtained from the sample with an internationally recognized database containing reference patterns.

The structural analysis of printed active layers was supported by SEM measurements (Auriga SEM-FIB, Zeiss, USA). This method enables to study the

morphology of the surface and cross section (possible on the edges of the fracture) due to its ability to produce 3D images.

The SEM analysis consists on an electron beam (primary electrons) that makes the scan of the samples' surface. When electrons hit the solid state matter they cause the emission of electrons from the surface (secondary electrons). These electrons are emitted in every direction and in bigger number according to the proximity of the incident beam. If the primary electrons beam hits perpendicularly the sample, the activated region and consequently the secondary emission, is symmetric around that axis. If the primary incident beam changes, the activated area changes position and the distance traveled by the secondary electrons changes, changing also the signal generated on the detector. That way it is possible to obtain a 3D image of the sample surface, with possible amplification up to 500 000 times, where the brightest points represent the highest points of the surface. [51]

The electrochemical measurements which include Chronocoulometry (CQ) and Cyclic Voltammetry (CV) were performed using galvanostatic method (Gamry Reference 600 Potentiostat, Gamry Instruments, USA). The CQ which involves the measurement of charge inserted to the device as a function of time is a controlled-potential technique with a potential step wave form. According to Table 3.5, voltage level of -4V is applied and due to the reduction reaction the device changes is color to blue. Then, stepping the potential to a second value (4V), another electrochemical reaction occurs (oxidation) and the device come back to its bleached state. This test provides the value of Charge Density, which is the amount of electric charge per unit area.

Table 3.5 CQ parameters

Parameters	Value
Step 1 Voltage (V)	-4
Step 1 Time (s)	30
Step 2 Voltage (V)	4
Step 2 Time (s)	30
Sample Period (s)	0.001
PF Corr. (ohm)	50
Equil. Time (s)	5
Conditioning Time (s)	120
Conditioning E (V)	-4

The CV measurements were preformed in order to examine existence of electrochemical reactions and the kinetics of electron transfer in the oxidation-reduction reactions. During CV measurements a voltage is applied to the electrodes and the corresponding current that flows through the device is monitored. This technique allows the scanning of the potential in both directions for a finite number of cycles. This fact gives the possibility of studying the reversibility and the stability of chemical reactions giving also information about reduction and oxidation current. The reactions detection is possible due to the approximation of the difference of the voltage to the necessary value to a certain reaction to occur, taking to an increase of the magnitude in the current. The current is then limited for the decrease of the reagents forming a peak of current. [52] In a total reversible reaction, an oxidized component during part of the cycle returns to its reduced state during the reverse scanning, being possible to oxidize again in a new cycle. This is a very important measurement for electrochromic applications because it allows the study of the reversibility and stability of reaction represented in Equation 2.1, Chapter 2, while the device is in the bleach and in the colored state. The set of parameters used in CV measurements is shown in Table 3.6.

Table 3.6 CV parameters

Parameters	Value
Initial voltage (V)	4
Scan Limit 1 (V)	-4
Scan Limit 2 (V)	4
Final voltage (V)	4
Scan Rate (mV/s)	50
Step Size (mV)	10
Cycles	2
Initial Delay Time (s)	0.25
Initial Delay Stab. (mV/s)	0
Conditioning Time (s)	120
Conditioning voltage (V)	4

Optical measurements were performed using a spectrometer set-up (Figure 3.11) consist of following elements:

- KEITHLEY 238 High Current Source Measure Unit,
- Halogen Light Source HL-2000-FHSA (Mikropack),

- HR4000 High-Resolution Spectrometer (Ocean Optics),
- spectrometer holder (Micropack Holder),
- lab made acrylic glass sample holder,
- QP600-2-SR/BX optical fibers (type – SR, core diameter - 600 µm, connector – QSMA, jacketing – BX).

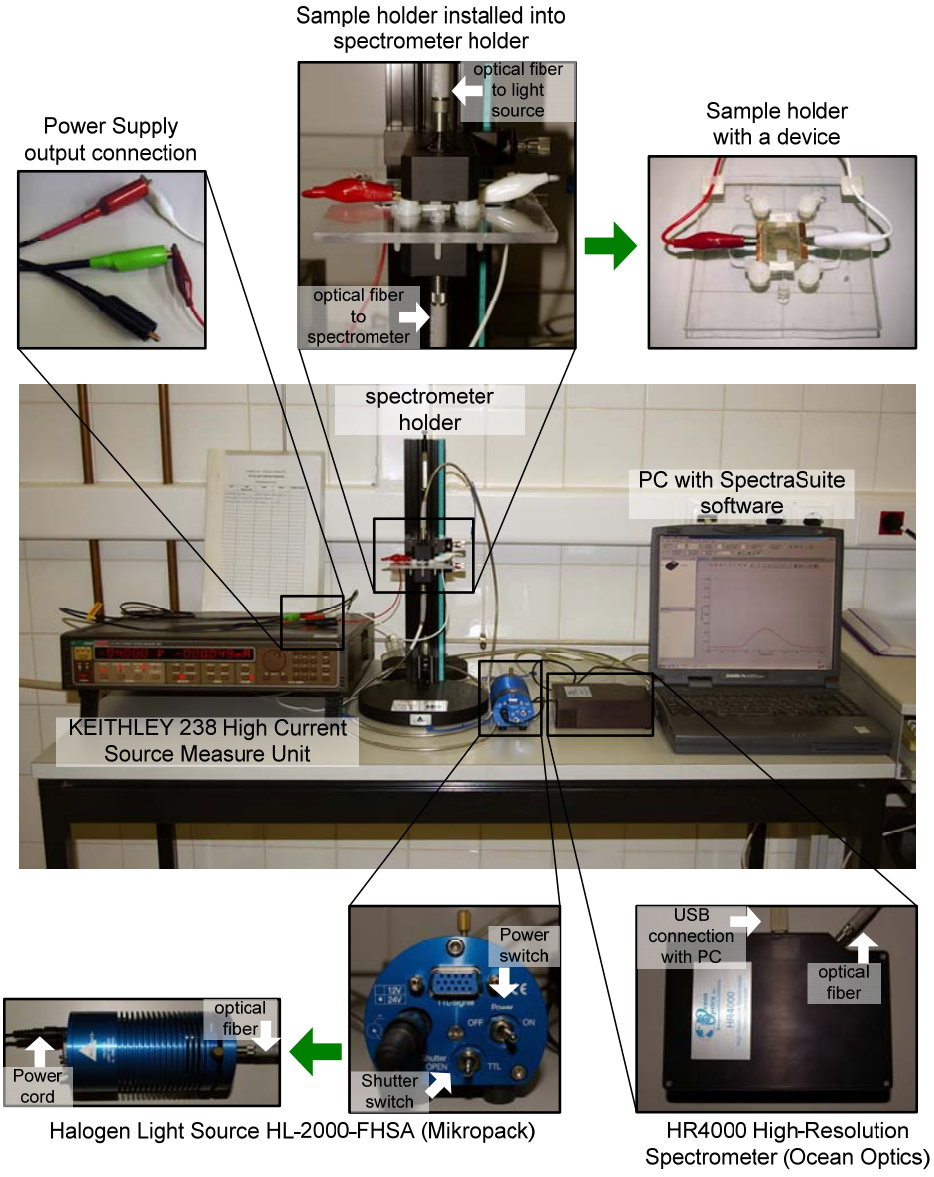

Figure 3.11 Optical measurements set-up [53]

The spectral response: transmittance (*T*), reflectance (*R*) and absorptance (*A*) were measured in a wide range of wavelength (400 to 900nm) for the films colored and bleached after a constant time period (1min) at operating voltage values of 4 and -4V respectively.

The spectral response measurements provide the following information:

- Change in optical density (*ΔOD*) - indicates how much the transmittance of the electrochromic layer reduces during the coloring process. The change in optical density is calculated using following equation [1,9]:

$$\Delta OD = ln\left(\frac{T(t_1,\lambda)}{T(t_2,\lambda)}\right) \tag{3.11}$$

  where $T(t_1,\lambda)$ and $T(t_2,\lambda)$ are transmission of the films at λ=900 nm before (t_1) and after (t_2) the coloration process, respectively.

- Coloration efficiency (*CE*) - the amount of electrochromic color formed by the charge consumed indicates the overall device performance. The *CE* value depends on the wavelength chosen for study and its represented by the following equation [1,12]:

$$CE = \frac{\Delta OD}{Q_{INS}} \tag{3.12}$$

  where *ΔOD* is the change in optical density for λ=900nm and Q_{INS} is the charge density inserted to the device.

- The optical absorption coefficient (α) - determines the amount of absorbed optical energy and it's given by the following equation [54,55] :

$$\alpha = \frac{\Delta OD}{d} \tag{3.13}$$

  where *ΔOD* is the change in optical density for λ= 900nm and *d* is the thickness of the layer. In this work thickness value is an average thickness of the printed pattern.

Optical measurements also include Chronoabsorptometry (CA) technique which is a square-wave potential step method coupled with optical spectroscopy used to probe switching times and contrast of the film. The electrochromic testing was processed within an appropriate voltage range (-4V to 4V) so as to avoid electrolyte oxidation and (eventual) ITO reduction [9].

Chronoabsorptometry measurements are divided in two procedures, pulse wave and linear stair pulse. The pulse wave procedure it's a test where a positive and negative voltages are applied with constant time periods so that the transmittance change can be measured. The resulting plot shows the difference between the coloration and bleaching states of the device. In the linear stair pulse measurement different voltages are applied in a sequence. In steps of 30 seconds, the lower voltage is always -4V while the upper value raises of 0.5V every step until it reaches the 4V level.

The CA measurements provide following information:

- Coloration time (τ_{col}) – is the time required for an electrochromic device to change from its bleached to colored state [55]. The coloration time is defined in these studies as the requisite time for reduction of the device's transmittance to 80% of the final reduction.
- Bleaching time (τ_{bl}) – is the time required for an electrochromic device to change from its colored to bleached state [55]. The bleaching time is defined in these studies as the requisite time for change of the device's transmittance to 80% of the final bleach level.
- Switching stability with long-term cycles - double potential step used to evaluate the long-term switching stability of films during 5 cycles.

4. Results and Discussion

4.1 Selection of relevant deposition parameters

The selection of relevant deposition parameters is a fundamental procedure before starting deposition of materials via Inkjet Printing. It brings a lot of useful information about relation between electrochromic parameters and number of passes. The tests were performed using ink with simple composition of 0.75g of PTA, 7.5g of the base solution (mixture of isopropyl alcohol and water) and 0.45 g of OAD. Developed test devices were printed 1, 3 and 5 times, annealed at 120 deg C and encapsulated in the same way like the rest of the devices in this work.

Figure 4.1 represents results of mechanical measurements of thickness as a function of number of passes. Results of linear fitting show that every successive printing causes the layer grow of about 23 nm.

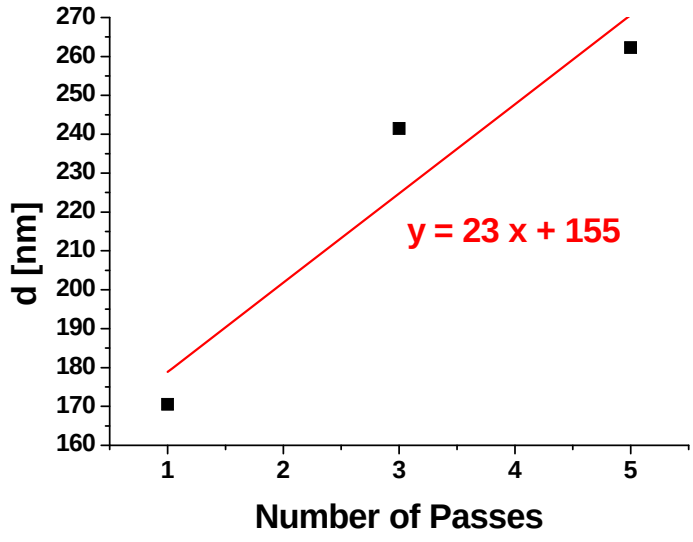

Figure 4.1 The thickness of printed test layers vs. number of passes

Figure 4.2 shows the optical measurements results in spectral response and coloration-bleaching characteristic of each device. Change in optical density increase with layer thickness while the fastest optical response was measured in device printed 3 times.

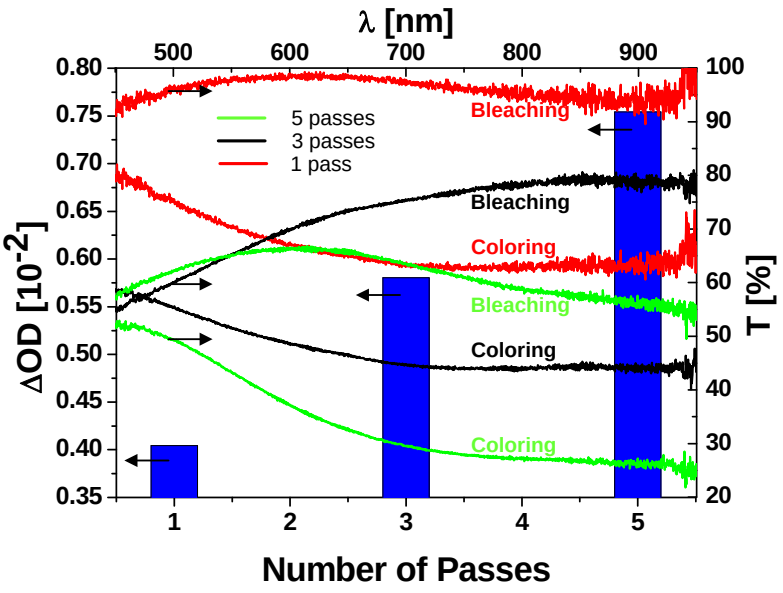

Figure 4.2 The change in optical density (bottom and left axis) for layers printed with different number of passes and spectral transmittance (top and right axis)

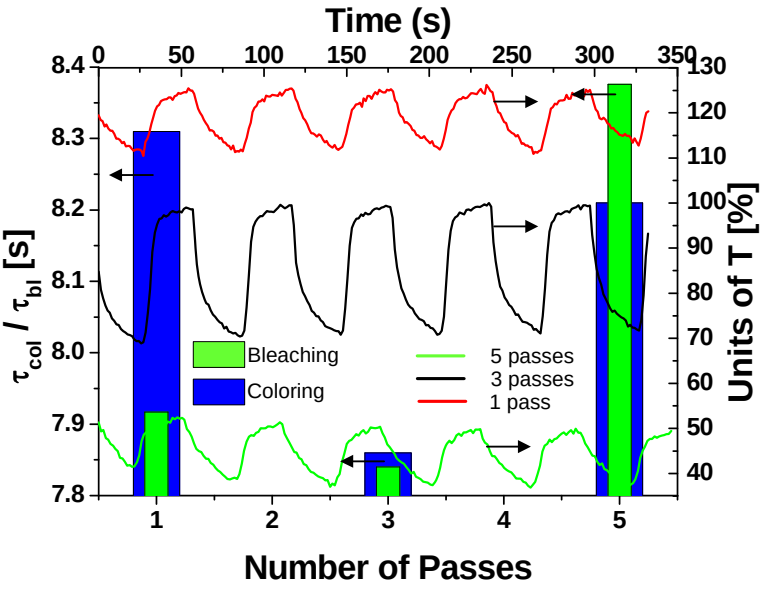

Figure 4.3 The coloring and bleaching time responses (bottom and left axis) of printed layers vs. number of passes and coloration-bleaching characteristic (top and right axis)

During the pulse wave test a positive and negative voltage is applied with constant time periods so that the transmittance change can be measured. High variation of transmittance form transparent to blue state implies good overall electrochromic

performance described by coloration efficiency. Figure 4.3 shows that the device with a layer printed 3 times is the one with a higher transmittance variation for the colored and the bleached state. Device printed 3 times is characterized by medium value (70-80%) of transmittance in a bleach state what makes it almost completely transparent. It is also clear in Figure 4.3, that the device printed 3 times is the one with the lowest coloration and bleaching time, which is a desirable characteristic for the EC windows.

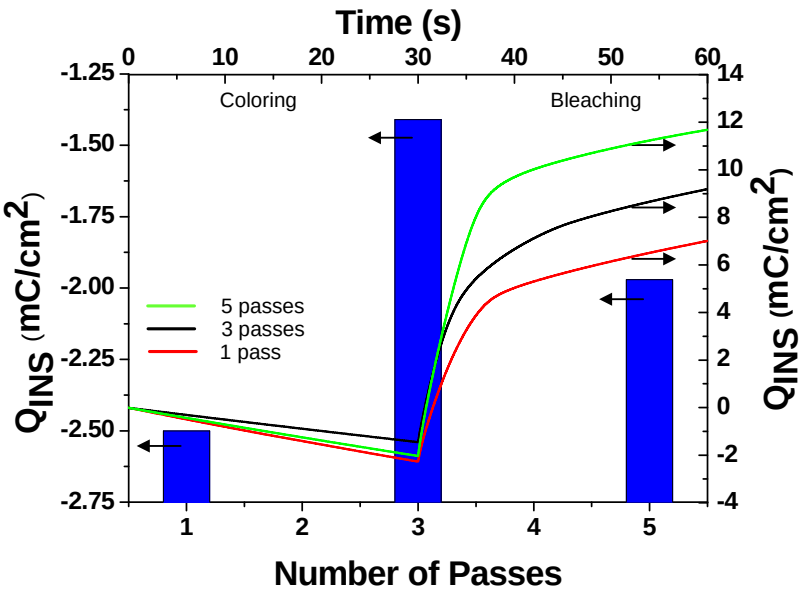

Figure 4.4 The charge inserted density for printed layers vs. number of passes (bottom and left axis); chronocoulometric curves for printed layers (top and right axis)

Device printed 3 consumes the smallest amount of charges during coloration and medium value for bleaching (Figure 4.4).

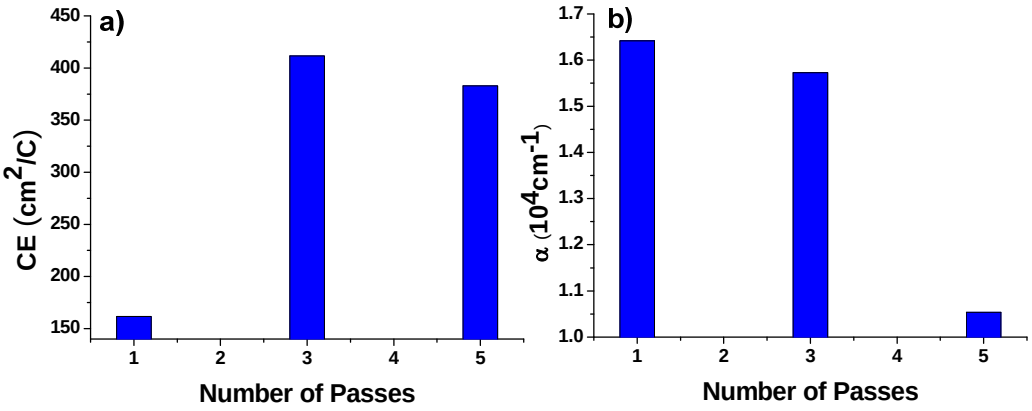

Figure 4.5 The a) coloration efficiency and b) optical absorption coefficient of printed layers vs. number of passes

The highest coloration efficiency was calculated for device with a layer printed 3 times (Figure 4.5.a), and this film is also characterized by medium optical absorption coefficient (Figure 4.5.b). The optical absorption coefficient tends to decrease with the thickness and it varies within the range of 10^4 to $1.7x10^4$ cm^{-1}. The device printed 5 times is the one with the lowest absorption coefficient, which means that it absorbs the smallest quantity of optical energy.

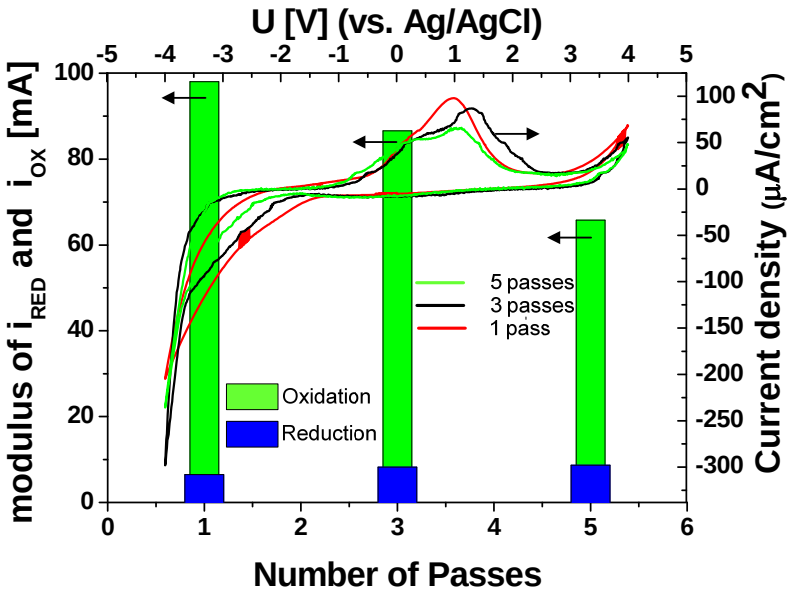

Figure 4.6 The reduction (blue) and oxidation (green) peak maximum for printed layers vs. number of passes (bottom and left axis); cyclic voltammograms of printed layers (top and right axis)

Cyclic voltammograms of test printed devices show that layer printed 3 times is characterized by medium values of reduction and oxidation current peaks (Figure 4.6).

The main finding of performed thickness tests is that the best electrochromic performance was achieved in device based on layer printed 3 times. This value, which represents the main deposition parameter in Inkjet printing, is therefore considered to be optimal for a set of used materials.

4.2 Statistical Analysis of significance

All experimental work and data analysis performed in these studies have been supported by JMP® Statistical Discovery Software, a powerful, interactive, data visualization and statistical analysis tool. This program was selected from among many because of wide functionality in Design of Experiment, statistical analyses and modeling. It characterizes, predicts and reduces the time of the series of experiments which is the most important in such a complex studies. The resulting statistical analysis involves fitting of

mathematical equations to the experimental results to get the entire estimation of response surface, and testing of all individual effect (factors) in a model for significance.

One of the basic tools in this scientific investigation is the regression analysis since it enables the identification of functional relationship between independent and dependent variables. In case of classical regression analysis both the variables are given as real numbers, but for multiple regressions the purpose is to know more about the relationship between several independent variables and a dependent variable. [56,57] In this case the fitting principle is the same as the classical linear regression but the fit is five dimensions.

Table 4.1 and 4.2 list the composition of all mixtures designed using DOE for 30 devices. The marked rows represent devices excluded from the analysis due to low measurement accuracy. The results of the measurements were divided for a five groups as presented in section 3.1.

All ink compositions are presented using weight fractions (see also section 3.2):

- $w_{iso/water}$ - base solution content;
- w_{PTA} - Peroxotungstic Acid content;
- w_{OAD} - Oxalic Acid content;
- w_{TiO2} - amount of TiO_2 nanoparticle dispersion;
- w_{WOX} - amount of WO_X nanoparticle dispersion;
- WO_X - stoichiometry of tungsten oxide nanoparticles.

Table 4.1 A tabular summary of factors and responses for all tested devices (part1). Devices extracted from the analysis due to low accuracy of measurements were marked (•)

	The composition of the mixture						**Mechanical Parameters**		**Optical Parameters**					
Ink	$w_{iso/water}$ (w/w)	w_{PTA} (w/w)	w_{OAD} (w/w)	w_{TiO2} (w/w)	w_{WOX} (w/w)	WO_X	d [nm]	R_q [nm]	τ_{col} [s]	τ_{bl} [s]	ΔOD [10^{-2}]	T_{col} [%]	T_{bl} [%]	α [10^3 cm^{-1}]
1	0.54	0.01	0	0	0.45	*yellow*	161	283	14	9	36.18	61.55	88.38	12.78
•2	0	0.2	0	0	0.8	*blue*	168.7	556.7	5	3	2.69	55.23	56.74	0.48
•3	0	0.11	0.05	0.84	0	*blue*	352.3	563.8	3	4	97.71	23.88	63.43	17.33
4	0	0.2	0	0.8	0	*yellow*	965	888	2	3	4.25	63.61	66.38	0.48
5	0.8	0.2	0	0	0	*yellow*	176.7	242.7	3	4	11.5	58.32	65.43	4.74
6	0.57	0.01	0	0.42	0	*yellow*	253	174	4	5	46.05	51.57	81.73	26.46
7	0	0.01	0.05	0	0.94	*blue*	66.6	153.8	9	4	8.25	78.06	84.77	5.36
8	0	0.01	0.05	0.94	0	*yellow*	49.8	65.4	4	4	3.84	80.73	83.89	5.87
9	0	0.01	0	0.50	0.49	*blue*	110	71.5	10	7	37.73	64.39	93.9	52.77
10	0.94	0.01	0.05	0	0	*yellow*	65.8	74.1	4	3	10.23	79.43	87.98	13.81
11	0	0.01	0	0	0.99	*yellow*	170.3	131.7	4	2	23.31	65.04	82.11	17.7
12	0	0.2	0.05	0	0.75	*blue*	87.1	86.8	11	9	38.72	59.44	87.54	44.61
13	0	0.01	0	0	0.99	*blue*	112	171	10	7	26.85	61.24	80.1	15.7
14	0	0.01	0	0.99	0	*yellow*	138	87	3	3	50.98	54.24	90.31	58.6
•15	0	0.2	0	0	0.8	*yellow*	82	311	2	2	4.24	51.29	53.51	1.36
16	0.46	0.01	0.02	0	0.49	*blue*	42.9	100.6	8	6	4.5	84.11	87.98	4.47
•17	0.94	0.01	0.05	0	0	*blue*	18.8	144.1	30	30	3.88	91.47	95.09	2.69
18	0.8	0.2	0	0	0	*blue*	193	536	6	2	1.36	65.67	66.57	0.25
19	0.87	0.11	0.02	0	0	*yellow*	589.6	501	4	8	75.3	42.28	89.78	15.03
20	0.44	0.01	0.03	0.52	0	*blue*	79.8	61.4	2	4	6.95	91.81	98.42	11.32
21	0	0.08	0.02	0.44	0.45	*yellow*	220.7	204.6	14	12	82.64	36.81	84.12	40.39
22	0	0.01	0	0.99	0	*blue*	115	87	4	5	46.44	45.14	71.82	53.38
23	0	0.2	0.02	0.77	0	*blue*	85.2	95.5	4	2	20.72	71.51	87.98	21.7
24	0	0.2	0.05	0.75	0	*yellow*	23.4	36.4	5	5	18.21	65.1	78.1	50.02
25	0.99	0.01	0	0	0	*blue*	57	237	3	2	17.56	63.03	75.13	7.41
26	0	0.01	0.05	0.94	0	*blue*	49.1	103.1	8	5	9.39	75.4	82.82	9.11
•27	0.35	0.2	0.05	0	0.40	*yellow*	351.7	401.2	30	30	130.93	23.45	86.83	32.63
28	0	0.01	0.05	0	0.94	*yellow*	58.5	107.3	9	2	13.12	80.01	91.22	12.22
•29	0.40	0.11	0	0.49	0	*blue*	754	804	7	7	5.72	53.38	56.53	0.71
30	0.75	0.2	0.05	0	0	*blue*	361.3	399.5	5	6	55.93	48.88	85.51	14

Table 4.2 A tabular summary of the factors and responses for all tested devices (part2). Devices extracted from the analysis due to low accuracy of measurements were marked (•)

	The composition of the mixture						**Electrical Parameters**			**Fluid Parameters**				**Overall Performance**
Ink	$w_{iso/water}$ (w/w)	w_{PTA} (w/w)	w_{OAD} (w/w)	w_{TiO2} (w/w)	w_{WOX} (w/w)	WO_X	i_{OX} [μA]	i_{RED} [μA]	Q_{ins} [mC/cm^2]	ν [cP]	γ [mN/m]	θ [deg]	ρ [g/cm^3]	CE [cm^2/C]
1	0.54	0.01	0	0	0.45	*yellow*	118	- 23.4	1.92	1.63	40.87	41.6	0.95	188.42
•2	0	0.2	0	0	0.8	*blue*	51.7	- 14.9	2.89	1.99	31.79	37.3	1.11	9.3
•3	0	0.11	0.05	0.84	0	*blue*	148	- 16.7	1.78	1.85	32.8	44.2	1.05	548.95
4	0	0.2	0	0.8	0	*yellow*	43.8	- 16.6	1.46	2.01	34.8	34.5	1.11	29.13
5	0.8	0.2	0	0	0	*yellow*	97	- 45.3	1.37	1.88	31.45	37.7	1.11	83.95
6	0.57	0.01	0	0.42	0	*yellow*	91.1	- 15.2	2.04	1.66	38.32	35.7	0.95	225.72
7	0	0.01	0.05	0	0.94	*blue*	10.5	- 12.5	1.17	1.64	37.44	41.1	0.96	70.51
8	0	0.01	0.05	0.94	0	*yellow*	9.23	- 11.8	1.1	1.67	36.92	40.6	0.96	34.87
9	0	0.01	0	0.50	0.49	*blue*	23.8	- 8.3	0.79	1.55	37.25	43.5	0.94	474.01
10	0.94	0.01	0.05	0	0	*yellow*	16.4	- 13.9	1.39	1.61	37.22	58.3	0.96	73.6
11	0	0.01	0	0	0.99	*yellow*	36.8	- 15.5	1.24	1.54	39.61	43.3	0.95	187.99
12	0	0.2	0.05	0	0.75	*blue*	102	- 18.5	2.21	1.9	33.45	47.1	1.13	175.2
13	0	0.01	0	0	0.99	*blue*	129	- 24	3.32	1.52	40.81	42.9	0.94	80.88
14	0	0.01	0	0.99	0	*yellow*	59.4	- 12.5	1.33	1.72	40.66	43.6	0.95	383.31
•15	0	0.2	0	0	0.8	*yellow*	76	- 17.8	1.91	1.89	33.99	40.2	1.11	22.22
16	0.46	0.01	0.02	0	0.49	*blue*	33.5	- 14.1	2.94	1.56	41.02	45.8	0.95	15.29
•17	0.94	0.01	0.05	0	0	*blue*	13.2	- 8.07	1.87	1.54	40.46	42.5	0.96	20.74
18	0.8	0.2	0	0	0	*blue*	71	- 8.65	4.79	1.88	32.38	38.1	1.11	2.84
19	0.87	0.11	0.02	0	0	*yellow*	138	- 18.7	1.86	1.69	37.28	37.2	1.03	404.82
20	0.44	0.01	0.03	0.52	0	*blue*	9.5	- 10.9	1.59	1.58	38.39	36.1	0.95	43.72
21	0	0.08	0.02	0.44	0.45	*yellow*	114	- 32	1.82	1.62	34.12	40.1	1.01	454.09
22	0	0.01	0	0.99	0	*blue*	105	- 23.1	1.52	1.57	39.03	44.2	0.94	305.56
23	0	0.2	0.02	0.77	0	*blue*	46.3	- 15.9	1.04	1.98	34.1	39.2	1.12	199.22
24	0	0.2	0.05	0.75	0	*yellow*	51.9	- 38.6	1.4	2.05	33.53	44.3	1.13	130.05
25	0.99	0.01	0	0	0	*blue*	46.7	- 12	1.91	1.6	36.31	32.7	1.89	91.96
26	0	0.01	0.05	0.94	0	*blue*	32.8	- 16.5	2.02	1.7	40.02	31.5	0.96	46.48
•27	0.35	0.2	0.05	0	0.40	*yellow*	304	- 77.3	2.41	1.96	34.18	38.8	1.14	534.27
28	0	0.01	0.05	0	0.94	*yellow*	31.4	- 18.4	2.73	1.56	37.88	40.1	0.96	48.04
•29	0.40	0.11	0	0.49	0	*blue*	0.00	0.0	2.71	1.69	37.98	38.4	1.02	21.12
30	0.75	0.2	0.05	0	0	*blue*	84.5	- 14.6	1.74	1.99	35.66	42	1.13	321.43

Detailed statistical analysis of significance have been presented only on four of the most important parameters of electrochromic device which are coloration time τ_{col}, bleaching time τ_{bl}, change in optical density ΔOD and coloration efficiency CE. Those parameters describe optical and electrical performance of the devices. At the same time it is assumed that coloration and bleaching time should be as short as possible while optical density and coloration efficiency should be as high as possible, which describes the most desirable performance of the electrochromic device. Preliminary models of τ_{col}, τ_{bl}, ΔOD and CE responses are shown below on Figure 4.7, 4.8, 4.9 and 4.10 respectively. Fitting was performed based on responses measured on 29 of 30 designed devices. Devices number *29* was extruded form the analysis because some of the responses were in this case not measurable.

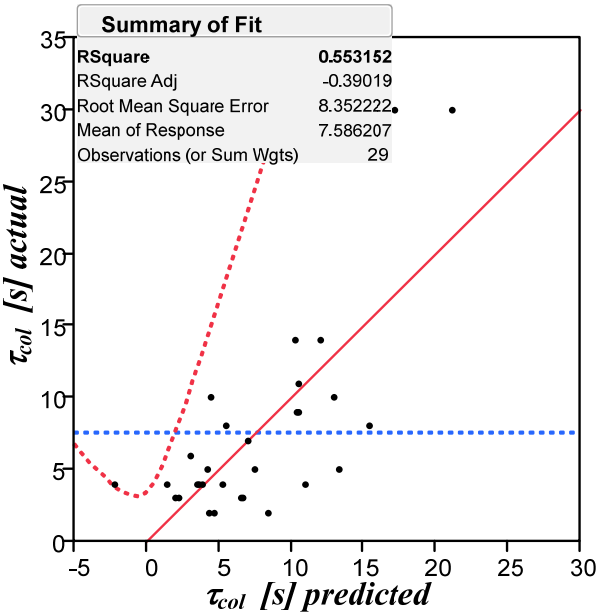

Figure 4.7 Initial whole multiple regression model with the numeric summaries for coloration time responses

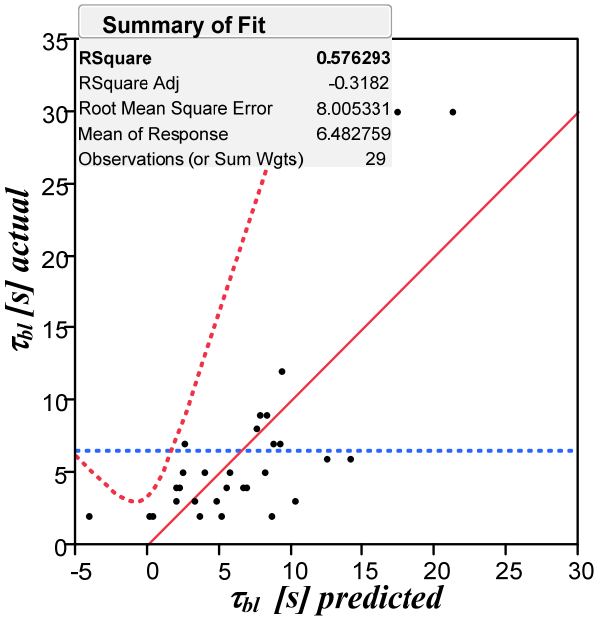

Figure 4.8 Initial whole multiple regression model with the numeric summaries for bleaching time responses

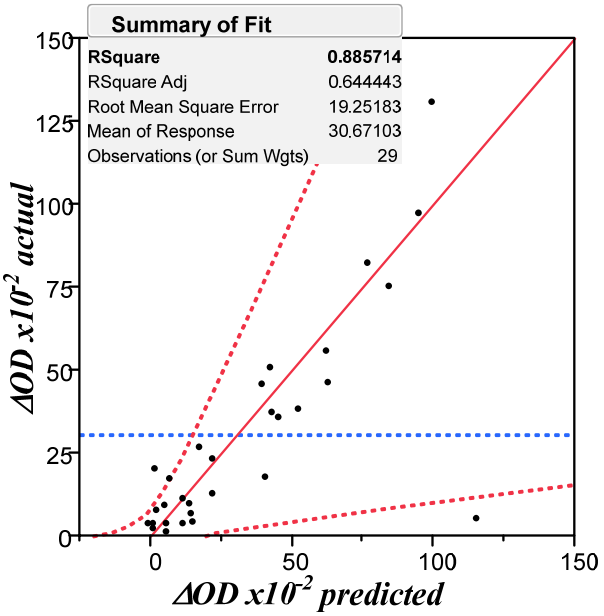

Figure 4.9 Initial whole multiple regression model with the numeric summaries for optical modulation responses

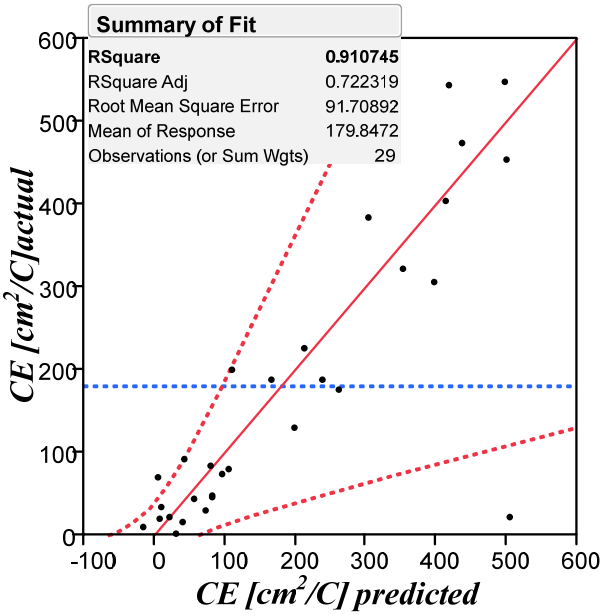

Figure 2.10 Initial whole multiple regression model with the numeric summaries for coloration efficiency responses

The Whole-Model is a statistical process where the model fits as a whole. Information obtained from this analysis is contained in several tables generated by JMP software, such as *Analysis of Variance*, *Lack of Fit*, *Parameter Estimates*, *Effect Tests* and *Summary of Fit.* The *Analysis of Variance* table shows the calculations for a linear model; the *Lack of Fit* table shows a special diagnostic test and appears only when the data and the model provide the opportunity; the *Parameter Estimates* table shows the estimates of the parameters in the linear model; the *Effects Tests* check the null hypothesis which says that the variable has no effect on the probability of success; the *Summary Fit* table shows the numeric summaries of the response for the multiple regression model.

The whole-models for selected responses shown in Figure 4.7, 4.8, 4.9 and 4.10 are the plots of the actual response versus the predicted response. Points lying on the continuous red line are those that are perfectly predicted and when this occurs it means that the model created by the program is reliable for future analyses.

Numeric summaries the model in a *Summary Fit* table shown in upper left corner of every whole-model brings direct information about quality of the fitting using specific statistical parameters. The *Rsquare* parameter often called the coefficient of determination is defined as the ratio of the *Sum of Squares* explained by a regression model and the *Total Sum of Squares* around the mean. The *RSquare Adj* parameter

adjusts *Rsquare* in order to make it more comparable over models with different numbers of parameters. The *Root Mean Square Error* estimates the standard deviation of the random error. The *Mean of Response* is the overall mean of the response values. It is especially important as a base model for prediction because all other models are compared to this value. Finally the *Observations* (or *Sum of Weights*) are the number of observations used in the fit. Since in this case the device number *29* is excluded, there are 29 observations taken under account.

The *RSquare* parameter which shows the correlation between the actual and predicted response of τ_{col}, τ_{bl}, ΔOD and *CE* is *0.55*, *0.57*, *0.88* and *0.91* respectively (*RSquare =1* when there is a perfect fit, the errors are all zero). That suggests that all those models would be more accurate if the points lying far from the correlation line were excluded from analysis. It is also important to note the presence of negative values for *RSquare Adj* of Figure 4.7 and 4.8, this can occur when there are few observations and a lot of regressors, so there will be some useless regressors in the model that will influence the parameter value.

In order to obtain more reliable and precise results it's imperative to exclude more points, than just device number *29*. To obtain a better fit, the points extremely distant from the line and from any other close point should be ignored, because they don't truly represent the model for these devices. When a point is excluded it means that its data row is not taken under account for any analysis, but the point will still appear in plots.

As can be seen in Figures 4.11 to 4.14, the most distant points (observations) from the line of fit are *2*, *3*, *15*, *17*, and *27* therefore they are (including also device number *29*) excluded from further analysis. This operation provides significant improvement in correlation between actual and predicted values of τ_{col}, τ_{bl}, ΔOD and *CE* which have from now on the values of *0.91*, *0.95*, *0.97* and *0.99* respectively.

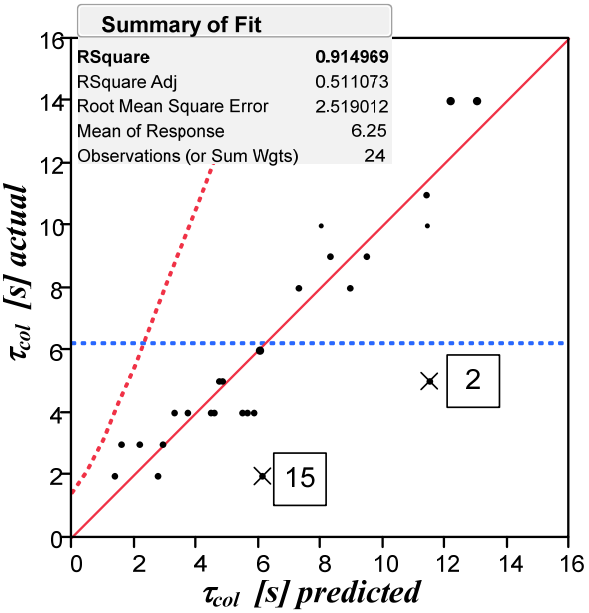

Figure 4.11 Final whole multiple regression model with the numeric summaries for coloration time responses after excluding the most distant observations

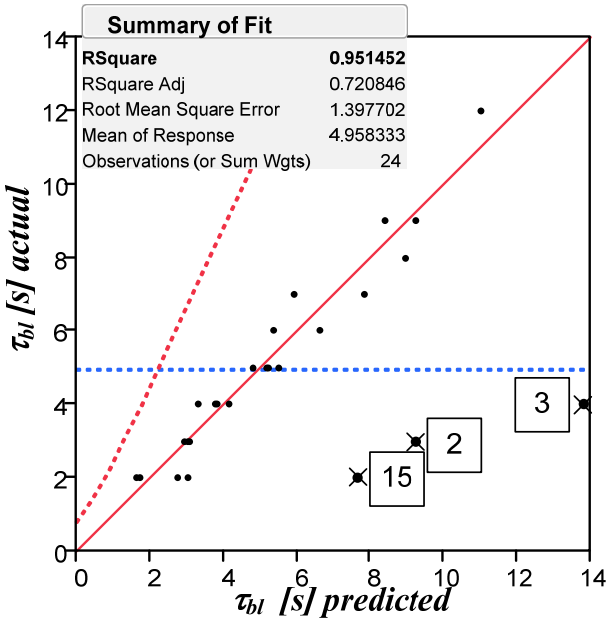

Figure 4.12 Final whole multiple regression model with the numeric summaries for bleaching time responses after excluding the most distant observations

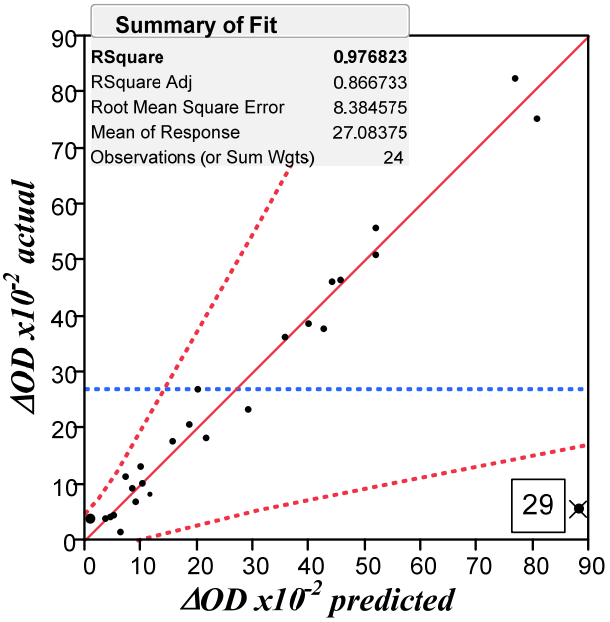

Figure 4.13 Final whole multiple regression model with the numeric summaries for change in optical density after excluding the most distant observations

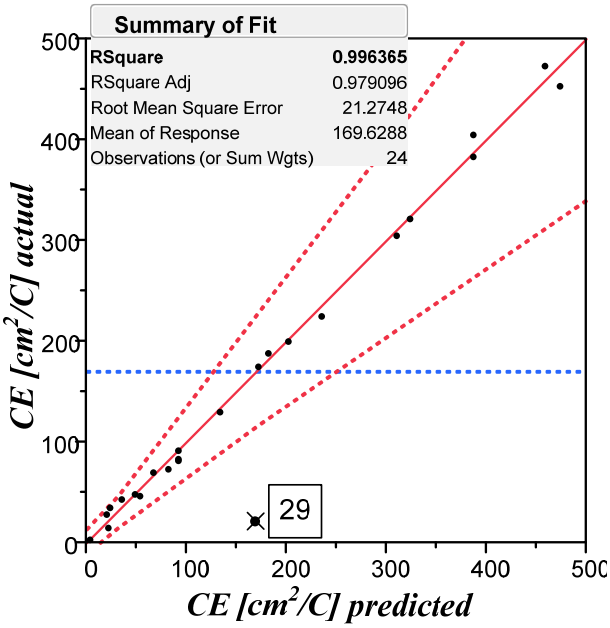

Figure 4.14 Final whole multiple regression model with the numeric summaries for coloration efficiency responses after excluding the most distant observations

In a field of statistics, a result is called statistically significant if it is unlikely to have occurred by chance. In other words, all results obtained by statistical methods suffer from the disadvantage that they might have been caused by pure statistical accident. The level of statistical significance is determined by the probability that this

has not, in fact, happened. A usual level of significance is 5%, which means that there is 5 % chance that the result was accidental (or not true) and 95% of being true. [58] It is then important to perform analysis of significance in case of these studies, because this method provides the information, of whether a test is reliable, because if the level of significant is above 5% than the chance of the results have been caused by accident is high.

To graphically view the significance of the model or focus attention on whether an effect is significant, the data should be displayed by focusing the hypothesis for that effect. The effect in a model is tested for significance by comparing the *sum of squared residuals* to the *sum of squared residuals* to the model with the effect removed. The graphical display of an effect's significance test is called a *leverage plot*. The significance of all factors and their interactions in a model of τ_{col}, τ_{bl}, ΔOD and CE responses are represented graphically by the *leverage plots* shown on Figure 4.15, 4.16, 4.17 and 4.18. The points on a leverage plot for simple regression are actual data coordinates, the slanted red solid line is the fitted model without constraint, and the horizontal blue dotted line is the sample mean of the response. The main idea of leverage plots is to see if the line of fit on the effect's leverage plot carries the points significantly better than does the horizontal line. Each observation is positioned as a point in the plot such that the vertical distance from that point to the slanted line is the unconstrained residual and the distance from the point to the horizontal line is the residual constrained by the hypothesis.[59] It's important to clarify that residuals are fitting errors. For each response, the residual is the difference between the real response and the estimated function value. The confidence curves are also showed in the *leverage plots* as dotted red lines. These indicate whether the test is significant at the 5% level by showing a confidence region for the line of fit. If the confidence region between the curves contains the horizontal dotted blue line, then the effect is not significant. On the other hand, if the curves cross this line, the effect is significant.

The significance of all factors and their interactions in a model of τ_{col} response are represented graphically by the *leverage plots* shown on Figure 4.15.

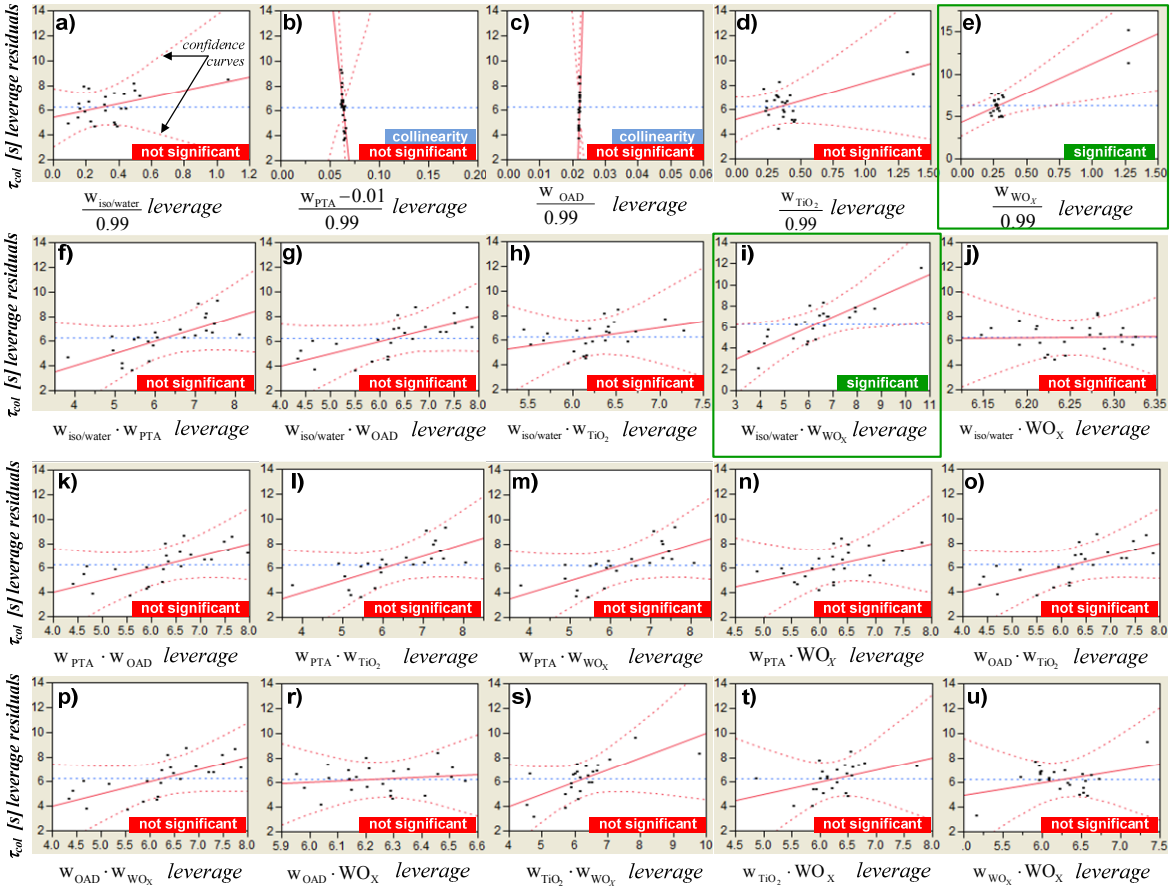

Figure 4.15 Leverage plots of main effects and factors correlations for τ_{col} response

Analysis of all leverage plots for τ_{col} response regression leads to the conclusion that the significant factor for this response is w_{WOX} (Figure 4.15e) and interaction between $w_{iso/water}$ and w_{WOX} (Figure 4.15i);

The factor shrinkage on leverage plot measures how collinear the particular factor is with the other factors. The factor shrinkage is obtained in Figure 4.15b and 4.15c what means that weight fraction of PTA and OAD are not linearly orthogonal to the other factors. Those two factors shrink almost completely and have no independent variation to support fitting τ_{col} response variation. It means that the weight fractions of PTA and OAD are an exact linear function of other factors. The shrinkage along the x axis in a leverage plots makes an especially compelling picture, since it also portrays the instability of the line of fit due to the collinearity. This phenomenon may translate into high standard errors for the parameter estimates, because a small random error in the narrow direction can have a huge effect on the slope of the correspondent fitting plane [57].

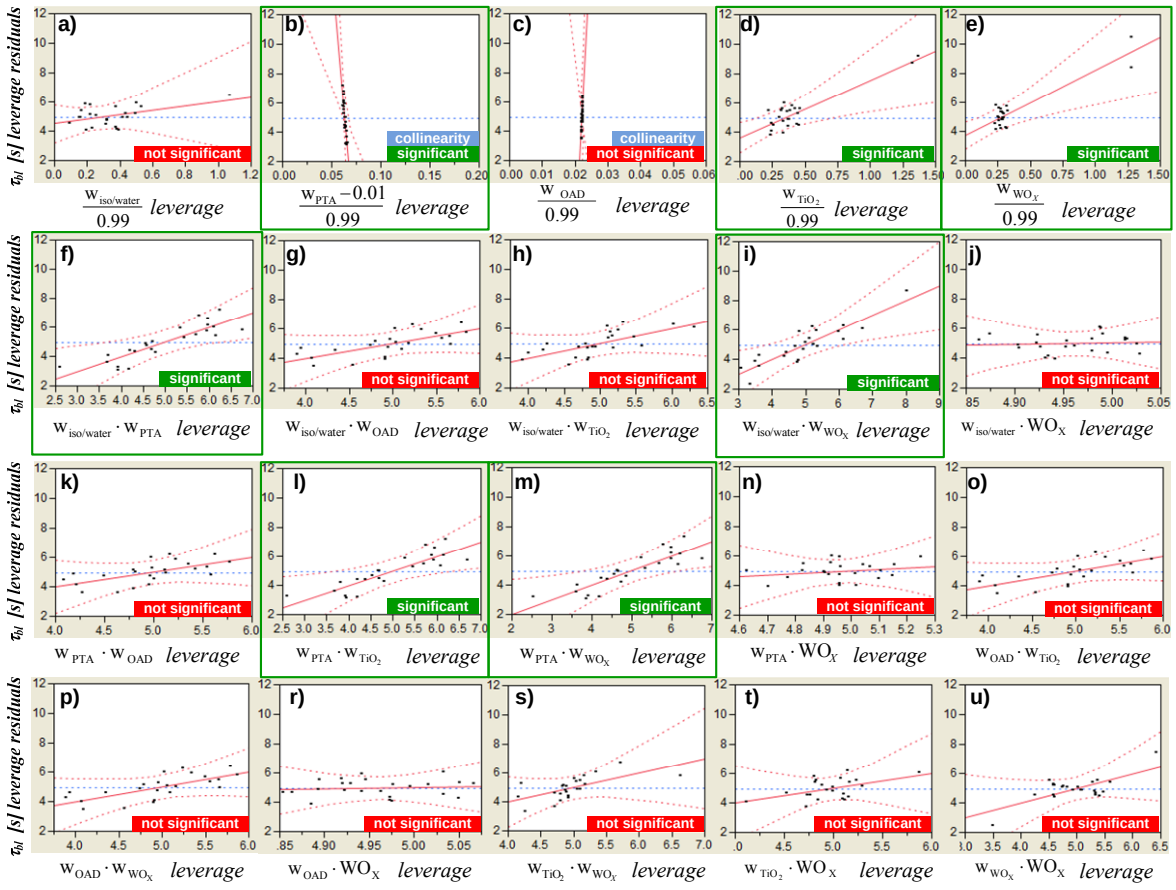

Figure 4.16 Leverage plots of main effects and factors correlations for τ_{bl} responses

Analysis of all leverage plots for τ_{bl} response regression leads to the conclusion that the significant factors for this response are w_{PTA} (Figure 4.16b), w_{TiO2} (Figure 4.16d), w_{WOX} (Figure 4.16e) and interactions between $w_{iso/water}$ and w_{PTA} (Figure 4.16f), $w_{iso/water}$ and w_{WOX} (Figure 4.16i), w_{PTA} and w_{TiO2} (Figure 4.16l), w_{PTA} and w_{WOX} (Figure 4.16m). The factor shrinkage is obtained in Figure 4.16b and 4.16c what means that weight fraction of PTA and OAD are not linearly orthogonal to the other factors like it was also in case of τ_{col} response.

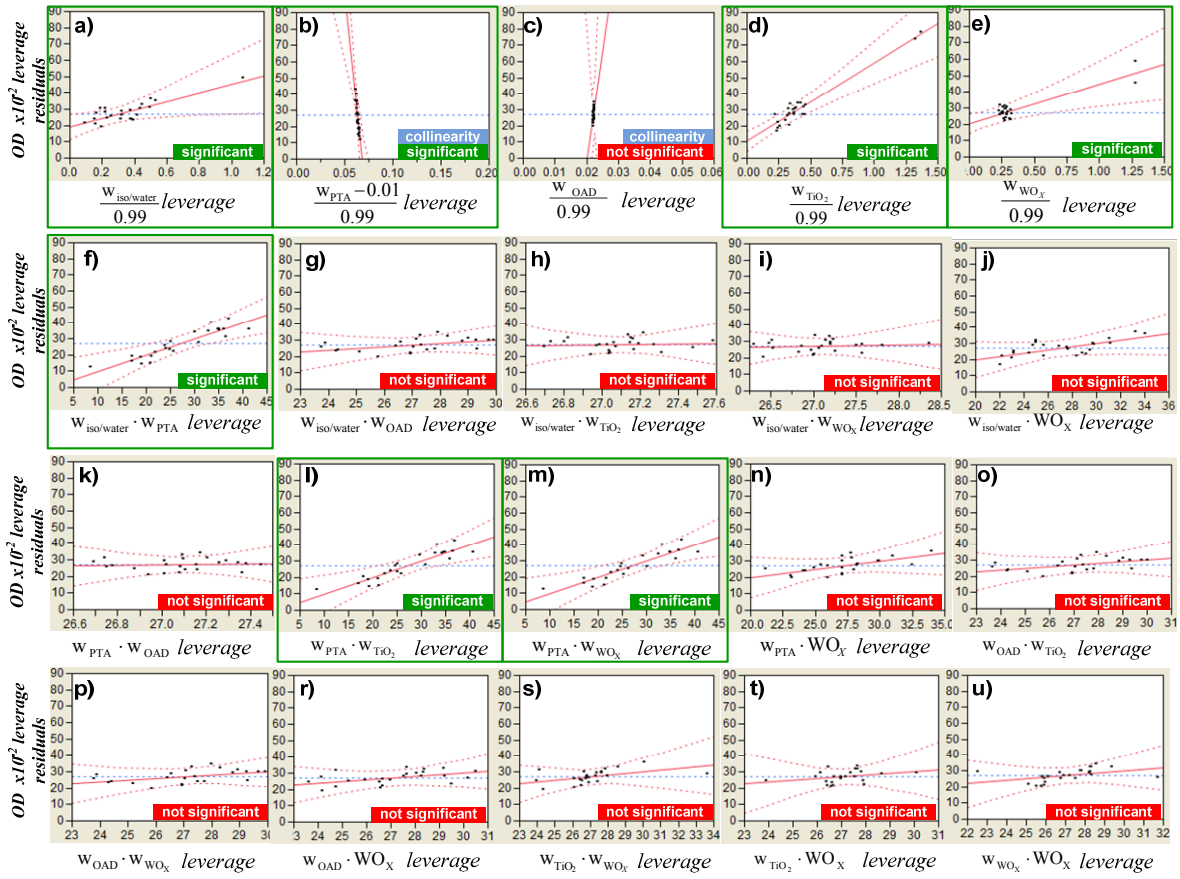

Figure 4.17 Leverage plots of main effects and factors correlations for *ΔOD* responses

Analysis of all leverage plots for *ΔOD* response regression leads to the conclusion that the significant factors for this response are $w_{iso/water}$ (Figure 4.17a), w_{PTA} (Figure 4.17b), w_{TiO2} (Figure 4.17d), w_{WOX} (Figure 4.17e) and interactions between $w_{iso/water}$ and w_{PTA} (Figure 4.17f), w_{PTA} and w_{TiO2} (Figure 4.17l), w_{PTA} and w_{WOX} (Figure 4.17m). The factor shrinkage is obtained in Figure 4.17b and 4.17c what means that weight fraction of PTA and OAD are not linearly orthogonal to the other factors like it was also in case of τ_{col} and τ_{bl}.

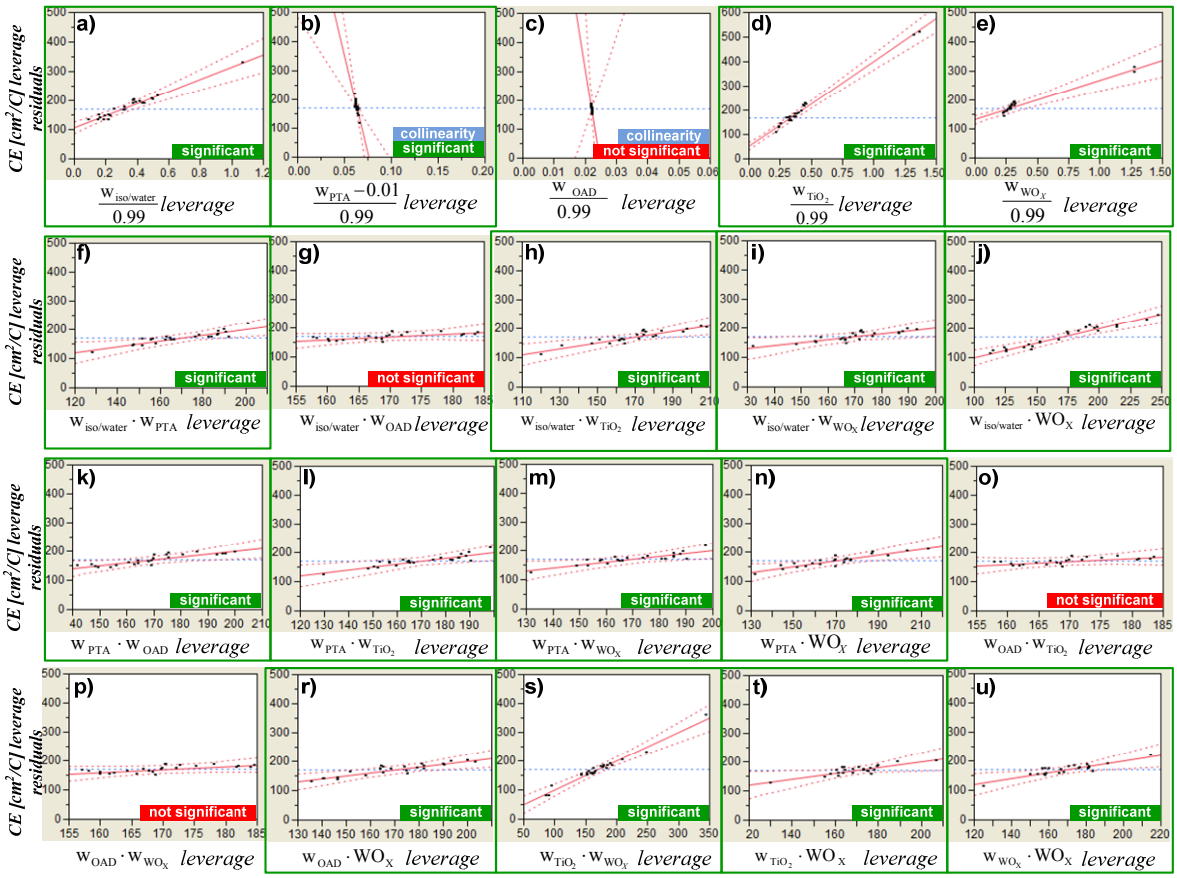

Figure 4.18 Leverage plots of main effects and factors correlations for *CE* responses

Analysis of all leverage plots for *CE* response regression leads to the conclusion that almost all of the factors and their interactions are significant. Unique factor that does not count is w_{OAD} (Figure 4.18c) and interaction between $w_{iso/water}$ and w_{OAD} (Figure 4.18g), w_{OAD} and w_{TiO2} (Figure 4.18o), w_{OAD} and w_{WOx} (Figure 4.18p). The factor shrinkage is obtained in Figure 4.18b and 4.18c what means that weight fraction of PTA and OAD are not linearly orthogonal to the other factors like it was also in case of τ_{col}, τ_{bl} and ΔOD.

The graphical analysis of significance based on leverage plots was confirm by computational method using estimates of a linear model and a *t*-test for the hypothesis that each parameter is zero (*Parameter Estimate*, Table 4.3, 4.4, 4.5 and 4.6). The individual columns of these tables stand for:

- *Term* – contain names of the estimated parameters;
- *Estimate* – lists the parameter estimates for each term;
- *Std Error* – contain standard errors, which are a standard deviation estimates of the distribution of the parameter estimate;

- *t Ratio* – is a statistic that tests whether the true parameter is zero; more precisely, it is the ratio of the estimate to its standard error;
- *Prob* > |*t*| - is a probability of getting an even greater *t*-statistic (in absolute value), given the hypothesis that the parameter is zero. It is also important to notice that probabilities less than 0.05 are often considered as significant evidence that the parameter is not zero.

Table 4.3 The *Parameter Estimates* and *Effect Test* table for τ_{col} parameter (*indication of significance)

Term/Source	**Parameter Estimates**				**Effect Test**				
Term	*Estimate*	*Std Error*	*T Ratio*	*Prob>|t|*	*Nparm*	*DF*	*Sum of Squares*	*F Ratio*	*Prob>F*
$(w_{iso/water})/0.99$	2.76	2.60	1.06	0.35	1	1	7.19	1.13	0.35
$(w_{PTA} - 0.01)/0.99$	-753.42	370.04	-2.04	0.11	1	1	26.30	4.14	0.11
$(w_{OAD})/0.99$	8203.79	4124.5	1.99	0.1176	1	1	25.10	3.96	0.12
$(w_{TiO_2})/0.99$	3.04	1.73	1.76	0.15	1	1	19.60	3.09	0.15
$(w_{WO_X})/0.99$	6.94	1.77	3.91	0.02*	1	1	97.14	15.31	0.02*
$w_{iso/water} \cdot w_{PTA}$	944.68	460.42	2.05	0.11	1	1	26.71	4.21	0.11
$w_{iso/water} \cdot w_{OAD}$	-8632.02	4316.76	-2.00	0.12	1	1	25.37	4.00	0.12
$w_{iso/water} \cdot w_{TiO_2}$	9.89	11.93	0.83	0.45	1	1	4.36	0.69	0.45
$w_{iso/water} \cdot w_{WO_X}$	36.18	11.71	3.09	0.04*	1	1	60.58	9.55	0.04*
$w_{iso/water} \cdot WO_{X\ [yellow]}$	-0.15	1.60	-0.10	0.93	1	1	0.06	0.01	0.93
$w_{PTA} \cdot w_{OAD}$	-7800.91	4103.37	-1.90	0.13	1	1	22.93	3.61	0.13
$w_{PTA} \cdot w_{TiO_2}$	953.50	467.22	2.04	0.11	1	1	26.43	4.16	0.11
$w_{PTA} \cdot w_{WO_X}$	953.02	461.00	2.07	0.11	1	1	27.12	4.27	0.11
$w_{PTA} \cdot WO_{X\ [yellow]}$	-9.49	7.28	-1.30	0.26	1	1	10.78	1.70	0.26
$w_{OAD} \cdot w_{TiO_2}$	-8566.85	4336.46	-1.98	0.12	1	1	24.76	3.90	0.12
$w_{OAD} \cdot w_{WO_X}$	-8591.79	4340.64	-1.98	0.12	1	1	24.86	3.92	0.12
$w_{OAD} \cdot WO_{X\ [yellow]}$	9.15	28.03	0.33	0.76	1	1	0.68	0.11	0.76
$w_{TiO_2} \cdot w_{WO_X}$	20.80	10.43	1.99	0.12	1	1	25.22	3.97	0.12
$w_{TiO_2} \cdot WO_{X\ [yellow]}$	-1.43	1.44	-0.99	0.38	1	1	6.21	0.98	0.38
$w_{WO_X} \cdot WO_{X\ [yellow]}$	-1.09	1.36	-0.80	0.47	1	1	4.07	0.64	0.47

The Tables 4.3, 4.4, 4.5 and 4.6 contain also part called *Effect Test* which represent the results of joint tests where all the parameters for an individual effect are zero. The *Effect Test* table section contains the following information:

- *Source* - provides the list of all names of the effects in the model;
- *Nparm* - is the number of parameters associated with the effect;
- *DF* - is the degrees of freedom for the effect test and usually *DF* and *Nparm* have the same value;
- *Sum of Squares* - is the sum of squares for the hypothesis that the listed effect is zero;

- *F ratio* - is the *F-statistic* for testing that the effect is zero; value obtained by the ratio of the *Mean Square* for the effect divided by the *Means Square for Error*; the *Mean Square* for the effects is the *Sum of Squares* for the effect divided by its *DF* value;
- *Prob>F* - is the significance probability for the *F ratio*, it is the probability that if the null hypothesis is true; it is also important to note that values less than 0.0005 appears as <0.0001, which is a conceptually zero.

Table 4.4 The *Parameter Estimates* and *Effect Test* table for τ_{bl} parameter (*indication of significance)

Term/Source	**Parameter Estimates**				**Effect Test**				
Term	*Estimate*	*Std Error*	*T Ratio*	*Prob>|t|*	*Nparm*	*DF*	*Sum of Squares*	*F Ratio*	*Prob> F*
$(w_{iso/water})/0.99$	1.51	1.44	1.05	0.35	1	1	2.15	1.10	0.35
$(w_{PTA} - 0.01)/0.99$	-733.92	205.32	-3.57	0.02*	1	1	24.96	12.78	0.02*
$(w_{OAD})/0.99$	4550.29	2288.52	1.99	0.12	1	1	7.72	3.95	0.12
$(w_{TiO_2})/0.99$	3.93	0.96	4.10	0.01*	1	1	32.78	16.78	0.01*
$(w_{WO_X})/0.99$	4.48	0.98	4.55	0.01*	1	1	40.37	20.66	0.01*
$w_{iso/water} \cdot w_{PTA}$	919.88	255.47	3.60	0.02*	1	1	25.33	12.96	0.02*
$w_{iso/water} \cdot w_{OAD}$	-4761.39	2395.20	-1.99	0.12	1	1	7.72	3.95	0.12
$w_{iso/water} \cdot w_{TiO_2}$	12.90	6.62	1.95	0.12	1	1	7.42	3.80	0.12
$w_{iso/water} \cdot w_{WO_X}$	25.27	6.50	3.89	0.02*	1	1	29.54	15.12	0.02*
$w_{iso/water} \cdot WO_X$ [yellow]	-0.14	0.89	-0.16	0.88	1	1	0.05	0.03	0.88
$w_{PTA} \cdot w_{OAD}$	-3699.59	2276.8	-1.62	0.18	1	1	5.16	2.64	0.18
$w_{PTA} \cdot w_{TiO_2}$	909.76	259.54	3.51	0.02*	1	1	24.06	12.32	0.02*
$w_{PTA} \cdot w_{WO_X}$	939.38	255.79	3.67	0.02*	1	1	26.35	13.49	0.02*
$w_{PTA} \cdot WO_X$ [yellow]	2.00	4.04	0.50	0.64	1	1	0.48	0.25	0.64
$w_{OAD} \cdot w_{TiO_2}$	-4776.23	2406.13	-1.99	0.12	1	1	7.70	3.94	0.12
$w_{OAD} \cdot w_{WO_X}$	-4819.89	2408.45	-2.00	0.12	1	1	7.82	4.00	0.12
$w_{OAD} \cdot WO_X$ [yellow]	3.24	15.55	0.21	0.84	1	1	0.08	0.04	0.84
$w_{TiO_2} \cdot w_{WO_X}$	9.78	5.79	1.69	0.17	1	1	5.58	2.85	0.17
$w_{TiO_2} \cdot WO_X$ [yellow]	-0.88	0.80	-1.10	0.33	1	1	2.35	1.20	0.33
$w_{WO_X} \cdot WO_X$ [yellow]	-1.46	0.75	-1.94	0.12	1	1	7.38	3.78	0.12

Table 4.5 The *Parameter Estimates* and *Effect Test* table for *ΔOD* parameter (*indication of significance)

Term/Source	**Parameter Estimates**				**Effect Test**				
Term	*Estimate*	*Std Error*	*T Ratio*	*Prob>|t|*	*Nparm*	*DF*	*Sum of Squares*	*F Ratio*	*Prob>F*
$(w_{iso/water})/0.99$	25.92	8.64	3.00	0.04*	1	1	632.47	9.00	0.04*
$(w_{PTA} - 0.01)/0.99$	-5918.35	1231.69	-4.81	0.009*	1	1	1623.14	23.09	0.009*
$(w_{OAD})/0.99$	13941.51	13728.47	1.02	0.37	1	1	72.50	1.03	0.37
$(w_{TiO_2})/0.99$	48.76	5.76	8.46	0.001*	1	1	5037.4	71.66	0.001*
$(w_{WO_X})/0.99$	24.63	5.90	4.17	0.01*	1	1	1222.96	17.40	0.01*
$w_{iso/water} \cdot w_{PTA}$	7232.68	15.32.50	4.72	0.009*	1	1	1565.87	22.27	0.009*
$w_{iso/water} \cdot w_{OAD}$	-15078.34	14368.41	-1.05	0.3532	1	1	77.42	1.10	0.35
$w_{iso/water} \cdot w_{TiO_2}$	4.78	39.70	0.12	0.91	1	1	1.02	0.01	0.91
$w_{iso/water} \cdot w_{WO_X}$	10.48	38.98	0.27	0.80	1	1	5.08	0.07	0.80
$w_{iso/water} \cdot WO_{X\ [yellow]}$	10.46	5.33	1.96	0.12	1	1	270.47	3.85	0.12
$w_{PTA} \cdot w_{OAD}$	-1648.99	13658.15	-0.12	0.91	1	1	1.02	0.01	0.91
$w_{PTA} \cdot w_{TiO_2}$	7133.58	1555.14	4.59	0.01*	1	1	1479.24	21.04	0.01*
$w_{PTA} \cdot w_{WO_X}$	7092.39	1534.43	4.62	0.01*	1	1	1501.94	21.36	0.01*
$w_{PTA} \cdot WO_{X\ [yellow]}$	-41.45	24.23	-1.71	0.16	1	1	205.75	2.93	0.16
$w_{OAD} \cdot w_{TiO_2}$	-15522.57	14433.97	-1.08	0.34	1	1	81.30	1.16	0.34
$w_{OAD} \cdot w_{WO_X}$	-14946.3	14447.9	-1.03	0.36	1	1	75.24	1.07	0.36
$w_{OAD} \cdot WO_{X\ [yellow]}$	-104.53	93.30	-1.12	0.32	1	1	88.25	1.26	0.32
$w_{TiO_2} \cdot w_{WO_X}$	38.19	34.73	1.10	0.33	1	1	85.03	1.21	0.33
$w_{TiO_2} \cdot WO_{X\ [yellow]}$	3.09	4.81	0.64	0.55	1	1	29.18	0.41	0.55
$w_{WO_X} \cdot WO_{X\ [yellow]}$	4.61	4.52	1.02	0.36	1	1	73.00	1.04	0.36

Table 4.6 The *Parameter Estimates* and *Effect Test* table for *CE* parameter (*indication of significance)

Term/Source	**Parameter Estimates**				**Effect Test**				
Term	*Estimate*	*Std Error*	*T Ratio*	*Prob>|t|*	*Nparm*	*DF*	*Sum of Squares*	*F Ratio*	*Prob>F*
$(w_{iso/water})/0.99$	207.71	21.93	9.47	0.0007*	1	1	40601.43	89.70	0.0007*
$(w_{PTA} - 0.01)/0.99$	-13640	3125.27	-4.36	0.01*	1	1	8622.75	19.05	0.01*
$(w_{OAD})/0.99$	-64741.6	34834.27	-1.86	0.14	1	1	1563.45	3.45	0.14
$(w_{TiO_2})/0.99$	348.56	14.61	23.85	<0.0001*	1	1	257454.28	568.81	<0.0001*
$(w_{WO_X})/0.99$	136.66	14.99	9.12	0.0008*	1	1	37639.01	83.16	0.0008*
$w_{iso/water} \cdot w_{PTA}$	16106.59	3888.54	4.14	0.01*	1	1	7765.44	17.16	0.01*
$w_{iso/water} \cdot w_{OAD}$	64547.42	36458.04	1.77	0.15	1	1	1418.74	3.13	0.15
$w_{iso/water} \cdot w_{TiO_2}$	-474.81	100.73	-4.71	0.009*	1	1	10056.90	22.22	0.009*
$w_{iso/water} \cdot w_{WO_X}$	-310.70	98.90	-3.14	0.04*	1	1	4466.61	9.87	0.04*
$w_{iso/water} \cdot WO_{X\ [yellow]}$	116.52	13.53	8.61	0.001*	1	1	33574.34	74.18	0.001*
$w_{PTA} \cdot w_{OAD}$	126644.62	34655.84	3.65	0.02*	1	1	6044.38	13.35	0.02*
$w_{PTA} \cdot w_{TiO_2}$	15320.17	3945.98	3.88	0.02*	1	1	6822.60	15.07	0.02*
$w_{PTA} \cdot w_{WO_X}$	14497.24	3893.43	3.72	0.02*	1	1	6275.35	13.86	0.02*
$w_{PTA} \cdot WO_{X\ [yellow]}$	-262.60	61.48	-4.27	0.01*	1	1	8256.53	18.24	0.01*
$w_{OAD} \cdot w_{TiO_2}$	62081.31	36624.38	1.70	0.16	1	1	1300.51	2.87	0.16
$w_{OAD} \cdot w_{WO_X}$	66686.80	36659.72	1.82	0.14	1	1	1497.73	3.31	0.14
$w_{OAD} \cdot WO_{X\ [yellow]}$	-1028.30	236.73	-4.34	0.01*	1	1	8539.82	18.87	0.01*
$w_{TiO_2} \cdot w_{WO_X}$	1028.15	88.12	11.67	0.0003*	1	1	61613.79	136.13	0.0003*
$w_{TiO_2} \cdot WO_{X\ [yellow]}$	38.42	12.20	3.15	0.03*	1	1	4491.88	9.92	0.03*
$w_{WO_X} \cdot WO_{X\ [yellow]}$	44.96	11.47	3.92	0.02*	1	1	6954.30	15.36	0.02*

Values in tables above fully confirm the results of graphical leverage plots analysis indicating the significance of same factors and the same factor interactions.

The *Sorted Parameter Estimates* plots presented in Figure 4.19 and 4.20 show all the effects sorted by the absolute value of the *t Ratio*, where the most significant effects starting from the top. The vertical blue lines represent the 0.05 significance level or in other words, the *t-ratio*.

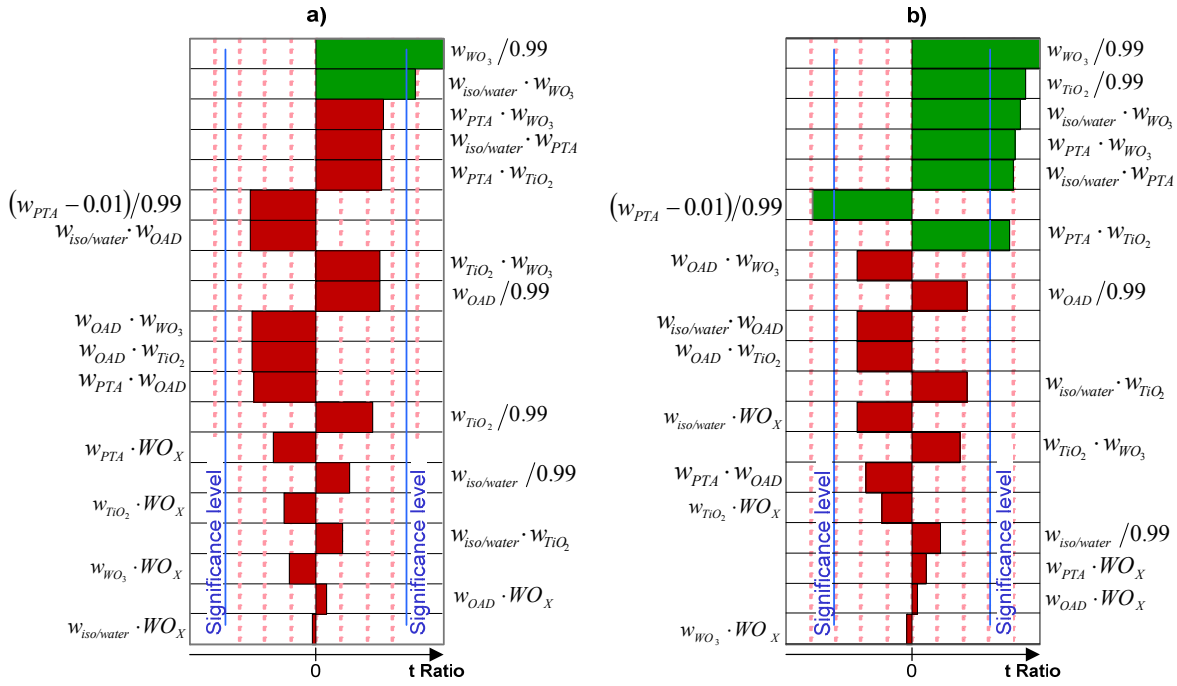

Figure 4.19 *Sorted Parameter Estimates* plot for a) τ_{col} and b) τ_{bl} response

The significance analysis allows drawing a conclusion that the coloration time (τ_{col}) depends mainly on the quantity of WO_X nanocrystals in electrochromic layer. The bleaching time (τ_{bl}) is influenced by the quantity of WO_X and TiO_2 nanocrystals and also depends of WO_3 amorphous content formed from PTA precursor.

The change in optical density (*ΔOD)* which describes the optical contrast between colored and bleached states mainly depends on quantity of TiO_2 nanocrystals and WO_3 amorphous content. Less important, but still significant is amount of WO_X nanocrystals and their stoichiometry.

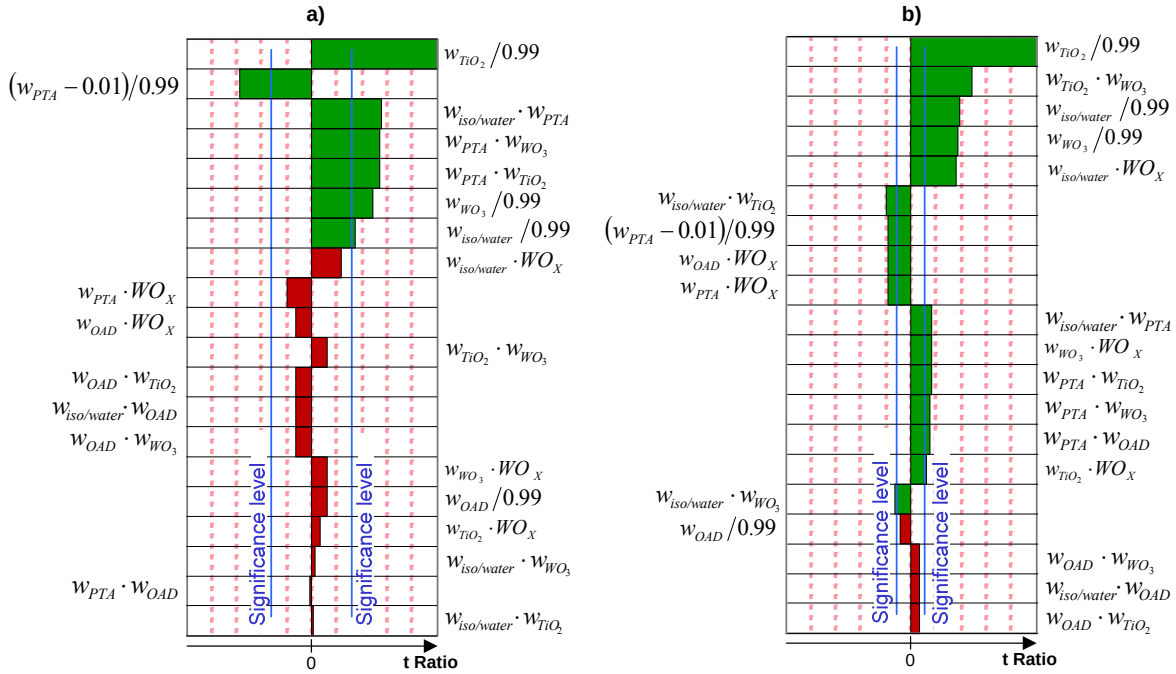

Figure 4.20 *Sorted Parameter Estimates* plot for a) *ΔOD* and b) *CE* response

The coloration efficiency (*CE*) depends to a greater or lesser extent on all the mixture components. The most important are TiO_2 and WO_X crystalline nanoparticles, while amount of amorphous WO_3 and OAD have a secondary impact on overall EC performance.

It may be also deduced that the most synergistic interaction for τ_{col}, τ_{bl}, and *ΔOD* responses is that manifested between amorphous WO_3 and crystalline WO_X, while the most synergistic interaction for *CE* response is associated with the proportion between TiO_2 and WO_X nanocrystals.

The exact impact of all mixture components on electrochromic performance and physical description of the phenomena occurring in the film will be presented later in this chapter.

The main task of desirability optimization (see section 3.1) is to maximize *CE* and *ΔOD* while the response time values of τ_{col} and τ_{bl} are as small as possible. The statistical program provided the information that the result of optimization calculated for maximum desirability, indicates that EC device with the best performance would have following concentration:

- $w_{iso/water}=0;$
- $w_{PTA}=0.01;$
- $w_{OAD}=0;$

- w_{TiO2}=0.83;
- w_{WOX}=0.16;
- WO_X stoichiometry: yellow.

4.3 Analysis of electrochromic performance – surface response estimation

The control of surface morphology is of crucial importance in the synthesis of electrochromic coatings. In particular, a developed pore system facilitates ion transport and, hence, intercalation/deintercalation of protons or alkali metal cations, which considerably enhances the electrochromic performance of a material. [60]

The porosity of the films not only increases the surface area and ion-insertion kinetics, but also reduces the overall material cost, leading to an inexpensive, large-area EC material.

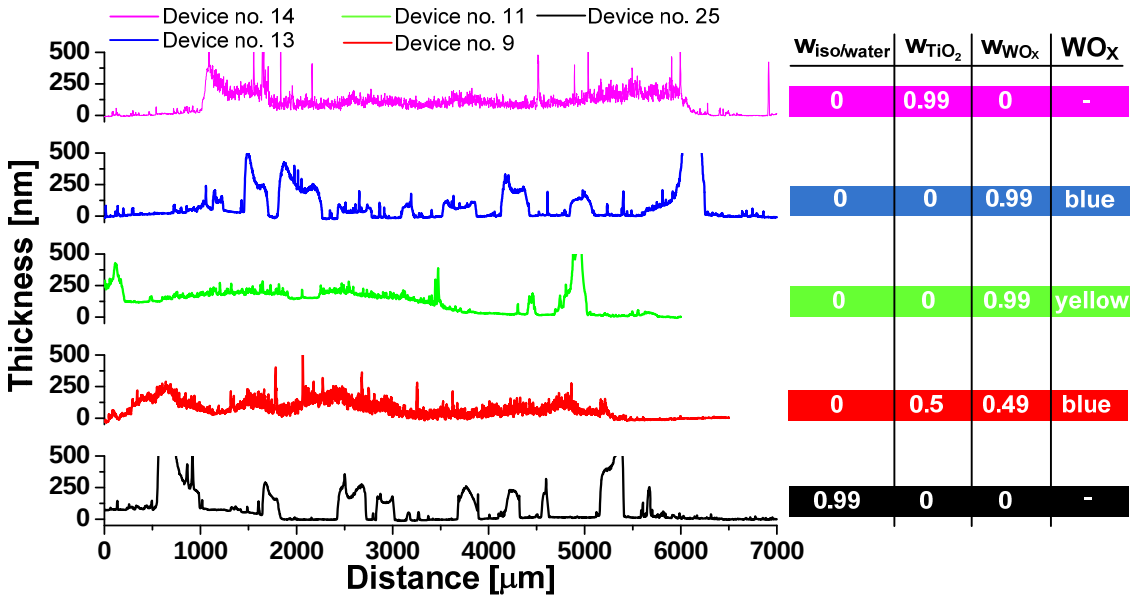

Figure 4.21 Profiles of several *a*-$WO_3/TiO_2/WO_X$ samples for different compositions

Profiles shown in Figure 4.21 indicate different morphologies depending on film composition. In order to investigate those variations, the topography of selected samples was measured using Scanning Electron Microscopy, and changes occurring on the surface of printed *a*-$WO_3/TiO_2/WO_X$ films for different compositions are illustrated by a series of micrographs in Figures 4.22 to 4.25.

Annealing process induced fast removal rates of the organic species from the film generate stresses, which, in turn, cause cracking. All films irrespective of

compositions contain those cracks. The perpendicular and parallel cracks probably impede conductivity between ITO layer and electrochromic film affecting electrochromic performance.

The film based only on *a*-WO_3 has a smooth surface and no grains were observed even at a magnification. The absence of a distinct granular morphology, points towards amorphous nature of this film. It is noteworthy that layers which do not contain any nanoparticles form smooth and continuous film with local cracks scattered throughout the area.

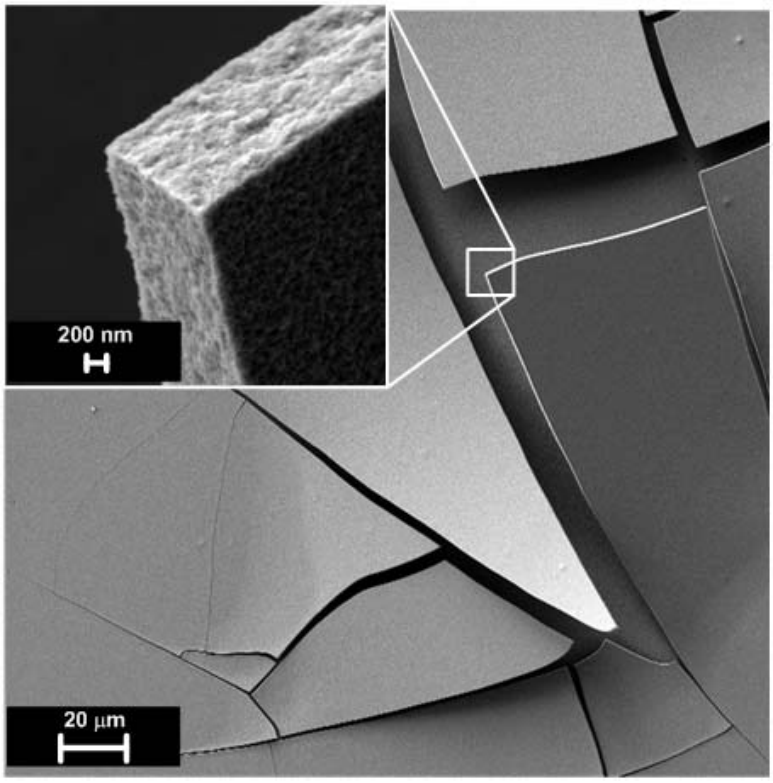

Figure 4.22 SEM picture of a printed *a*-WO3 film (Device no. 25); Inset: Magnified area showing layer cross-section

X-ray diffraction patterns realized on the film showed in Figure 4.26 allowed confirming that these WO_3 films are totally amorphous.

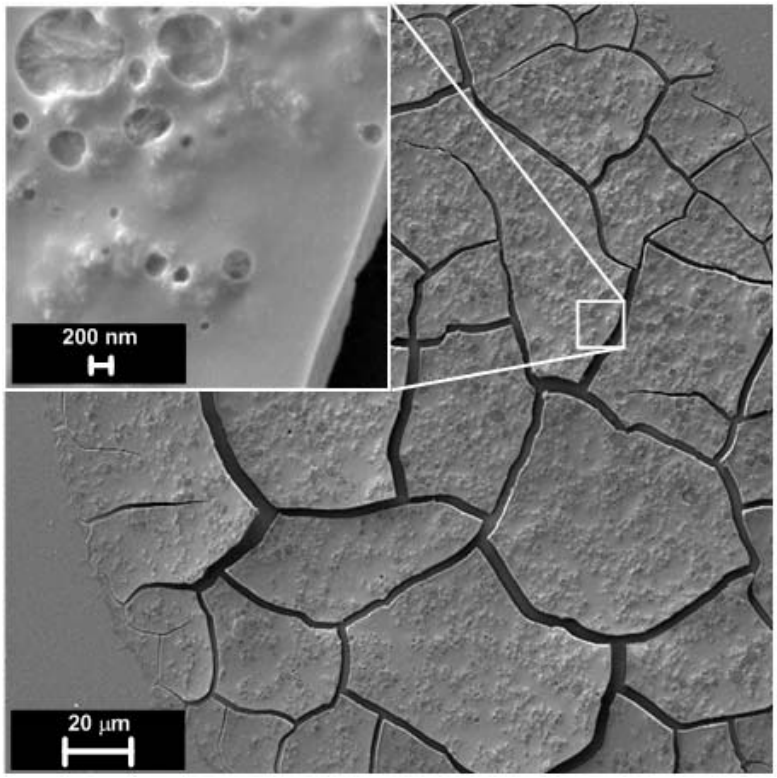

Figure 4.23 SEM picture of a printed *a*-$WO_3/TiO_2/WO_X$ (Device no. 19); Inset: Magnified area showing *chocolate with nuts* like structure

Structure shown in Figure 4.23, represents amorphous material combined with a porous nanocrystalline microstructure, which is favorable for a fast electrochromic response and high optical contrast. Nanocrystallites or their aggregates embedded in an amorphous matrix are clearly seen in the *a*-$WO_3/TiO_2/WO_X$ film. All across this film, a regular and a uniform distribution of these grains is observed making the layer structure similar to *chocolate with nuts* counterpart. Highly porous networks, as in this film, tend to reduce the diffusion path length in the film and improve kinetics as switching speeds are predominantly governed by the solid-state diffusion of lithium in WO_X. Such a microstructure aids in amplifying also the optical response. This conclusion is supported by the evidence of faster coloration and bleaching rates observed for the film containing nanoparticles in comparison with the amorphous layer.

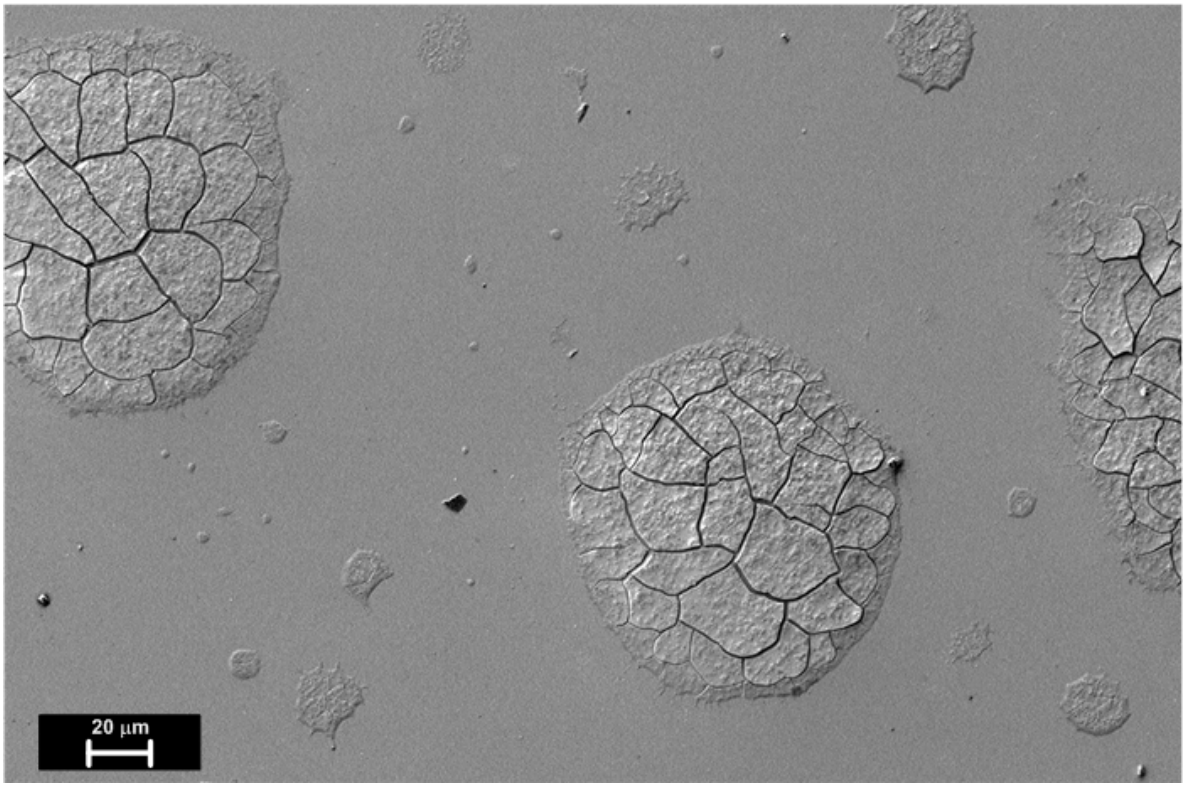

Figure 4.24 SEM picture of *a*-WO_3/TiO_2/WO_X printed film (Device no. 19). Visible islands of different sizes indicate that the layer is not continuous.

Wide view SEM picture shown in Figure 4.24 indicates that printed *a*-WO_3/TiO_2/WO_X layer does not form a continuous film. So, it is rather a pattern than a film, however in further considerations the term *film* will be applied in all cases of printed as well as spin-coated layers.

The addition of OAD to precursor solution based on PTA has been used in the state of the art for films deposited by spin coating [33]. The use of this organic compound clearly brings out the advantage to get crackles films of higher thickness annealed in temperature of 250 deg C. According to these studies, a small amount of OAD in the precursor brings more significant changes in the bleaching kinetics than in the coloration kinetics. The bleaching kinetics is faster when OAD was added, while the coloration seems to not be influenced by this component.

Studies on OAD influence performed by other groups [61] indicates that upon subliming out of the film (spin/dip-coated) OAD catalyzes the formation of a crystalline phase at elevated temperature (starting form 182 deg C) shows that a crystalline phase appears. Bellow this temperature no significant influence have been observed.

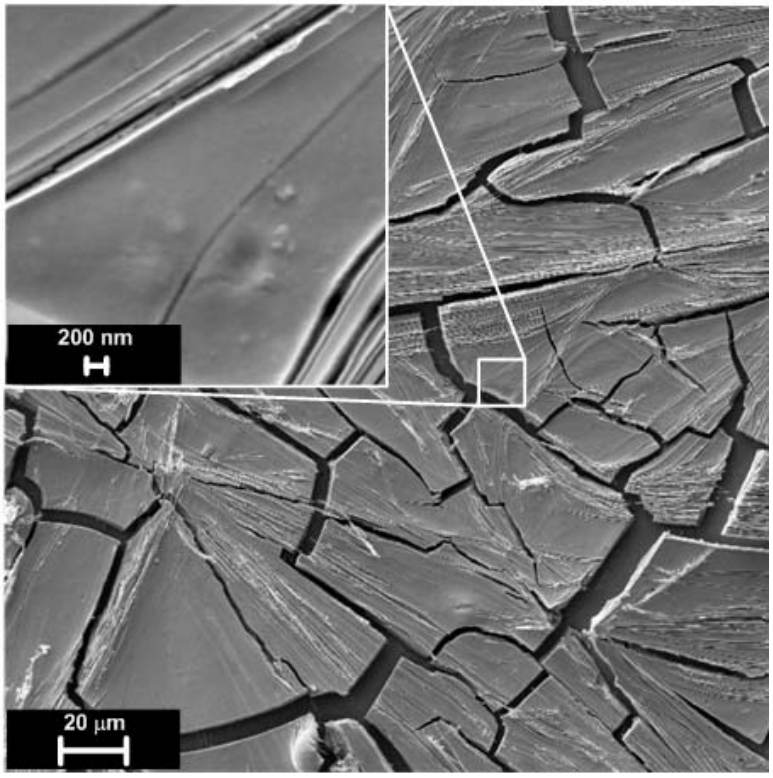

Figure 4.25 SEM picture of *a*-WO_3/TiO_2/WO_X printed film (Device no. 21) with addition of Oxalic Acid; Inset: Magnified area shows grooves formed on the surface due to acid crystallization.

Shown in Figure 4.25 micrograph of *a*-WO_3/TiO_2/WO_X with addition of OAD printed film varies considerably from the films that do not contain this organic compound. The film contains cracks, and its surface is patterned by grooves. The influence of OAD on electrochromic performance of the films is negligible and will not be study in details.

The X-ray diffraction of WO_X nanopowders shown in Figure 4.26a and 4.26b and films with different loadings of WO_3 and TiO_2 dispersions shown on Figure 4.26c, 4.26d and 4.26e were recorded using Bruker D8 Focus Advance diffractometer and a XPert PRO, PANalytical difractometer.

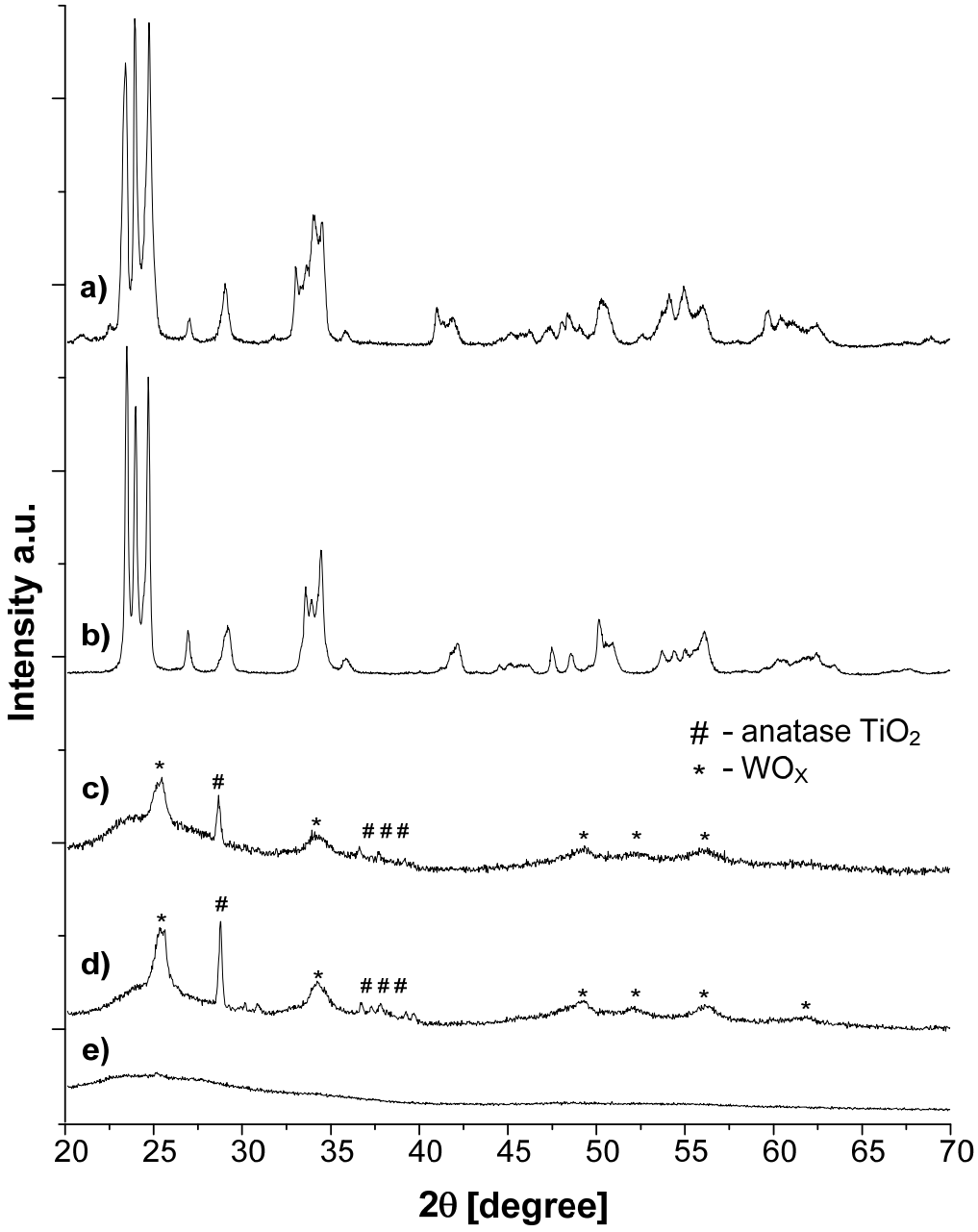

Figure 4.26 XRD patterns of a) $WO_{2.9}$ *blue* nanopowder, b) WO_3 *yellow* nanopowder, c) *ink 9* (w_{PTA}=0.01;w_{TiO2}=0.5;$w_{WO2.9}$=0.49), d) *ink 21* (w_{PTA}=0.08;w_{OAD}=0.02;w_{TiO2}=0.45;w_{WO3}=0.45), e) *ink 19* ($w_{iso/water}$=0.87;w_{PTA}=0.1;w_{OAD}=0.03)

Diffractograms in Figure 4.26a and 4.26b of the *blue* and *yellow* nanopowder respectively are characteristic of nanocrystalline WO_X. Material called *blue* match well with the monoclinic crystalline phase of $WO_{2.9991}$ (lattice constants: a=0.73 nm, b=0.75, c=1.05; space group: P21/c) with reference 04-008-1962 (C) from the ICDD PDF 4+ (2009) library, while the material called *yellow* match well with the monoclinic

crystalline phase of WO_3 (lattice constants: a=0.72 nm, b=0.75, c=0.76; space group: P21/n) with reference 04-005-4272 (I) from the same library.

Figure 4.26e shows an amorphous PTA film spectrum which exhibits a broad halo observed at *2θ~26* degrees which is characteristic of the amorphous nature of WO_3 films.

The XRD findings are augmented by SEM results. XRD patterns of films presented in Figure 4.26c and 4.26d clearly indicate the presence of TiO_2 and WO_X nanocrystals in a film.

Subsequent measurements relate to the optical properties of printed *a*-WO_3/TiO_2/WO_X films measured *in situ* as a working electrode in encapsulated device filled with a gel electrolyte.

The quantity of the optical density indicates how much the transmittance of the electrochromic layer reduces during the coloring process. The *a*-WO_X films (upper corner of ternary plots in Figure 4.28) are known to modulate their transmission primarily by absorption while crystalline films (bottom part of ternary plots in Figure 4.28) exhibit a pronounced reflection in the NIR region [55]. Figure 4.27 shows that the transmission modulation for the films *a*-WO_3/TiO_2/WO_X.

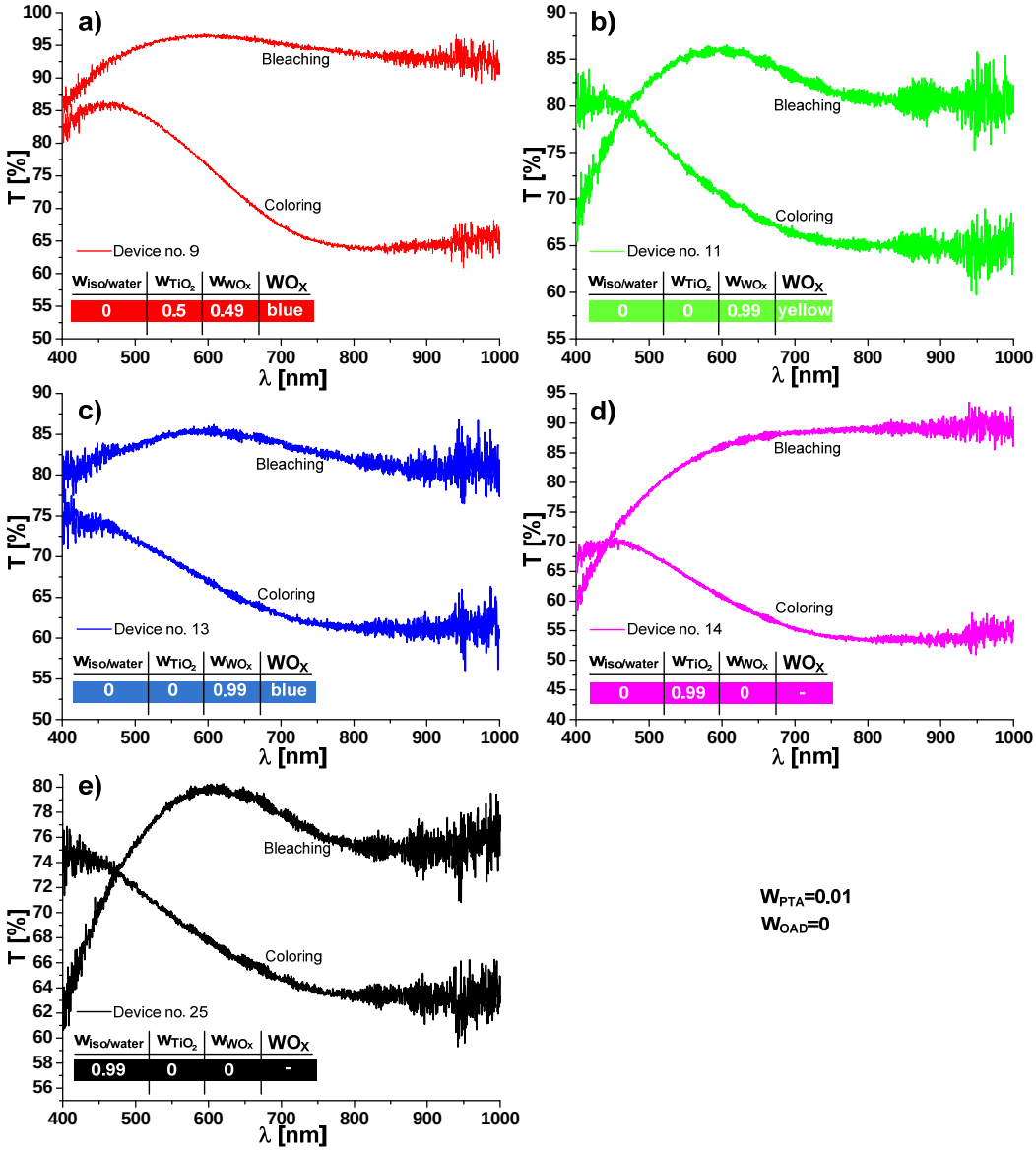

Figure 4.27 Transmission modulation of EC windows based on printed films containing a) *a*-WO_3 with TiO_2 and $WO_{2.9}$ nanoparticles, b) *a*-WO_3 with WO_3 nanoparticles, c) *a*-WO_3 with $WO_{2.9}$ nanoparticles, d) *a*-WO_3 with TiO_2 nanoparticles and e) pure *a*-WO_3. Annealing: 120 deg C, 1h.

The sharp reduction of the transmittance spectra at the wavelength of ~400 nm shown in plots above is due to the fundamental WO_3 absorption edge [10].

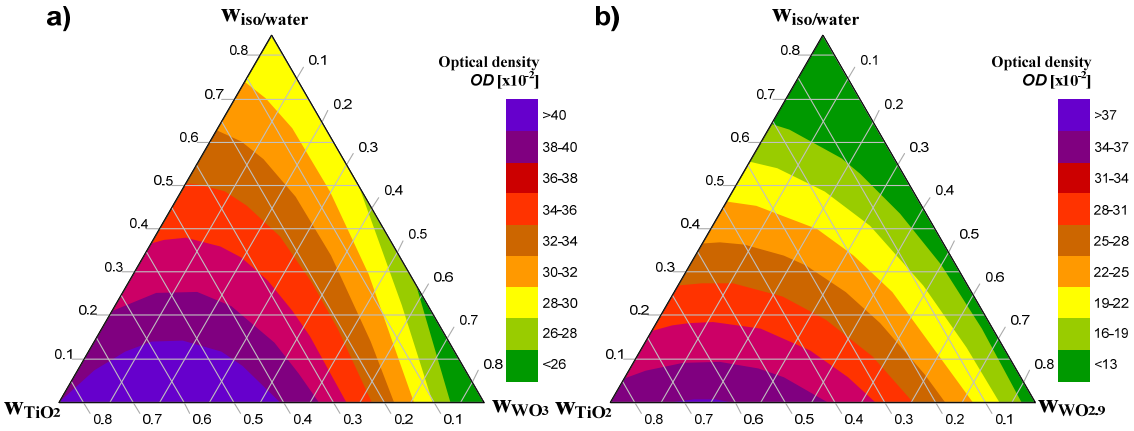

Figure 4.28 Surface response prediction of *ΔOD* for a) *a*-$WO_3/TiO_2/WO_3$ and b) *a*-$WO_3/TiO_2/WO_{2.9}$ printed layers

The optical behavior of printed coatings is distinctly different for *a*-WO_3 and *a*-$WO_3/TiO_2/WO_X$ materials. As displayed by the *ΔOD* surface response shown in Figure 4.28, films containing large amount of TiO_2 solid content with a smaller share of WO_X nanocrystals in amorphous matrix exhibit the highest transmission modulation. It is absolutely unexpected that, the *a*-$WO_3/TiO_2/WO_X$ coatings are characterized by a small charge inserted to the device and high optical transmittance change which leads to high relative coloration efficiency values. This leads to the conclusion that lithium ions easily diffuse into *a*-$WO_3/TiO_2/WO_X$ layers. Greater differences resulting from the presence of different WO_X particles stoichiometry haven't been observed.

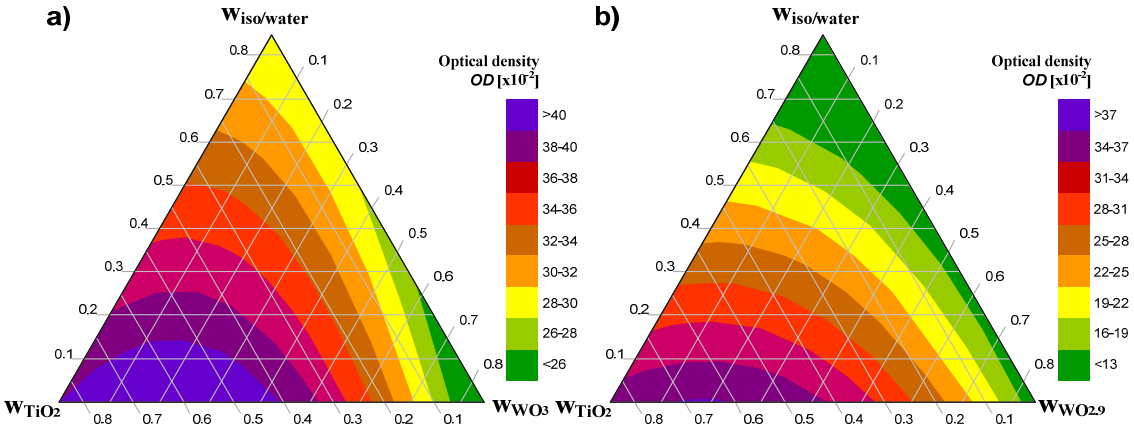

Figure 4.29 Surface response prediction of T_{bl} for a) a-$WO_3/TiO_2/WO_3$ and b) *a*-$WO_3/TiO_2/WO_{2.9}$ printed layers

As it is known, the optical transmission of the WO_X films strongly depends on the oxygen content in the structure (X value). In fact, nonstoichiometric

a-$WO_3/TiO_2/WO_X$ films with X=2.9 (*blue*) shown in Figure 4.29b, exhibit lower transmittance in bleaching state when comparing to *a*-$WO_3/TiO_2/WO_X$ films with X=3 shown in Figure 4.29a.

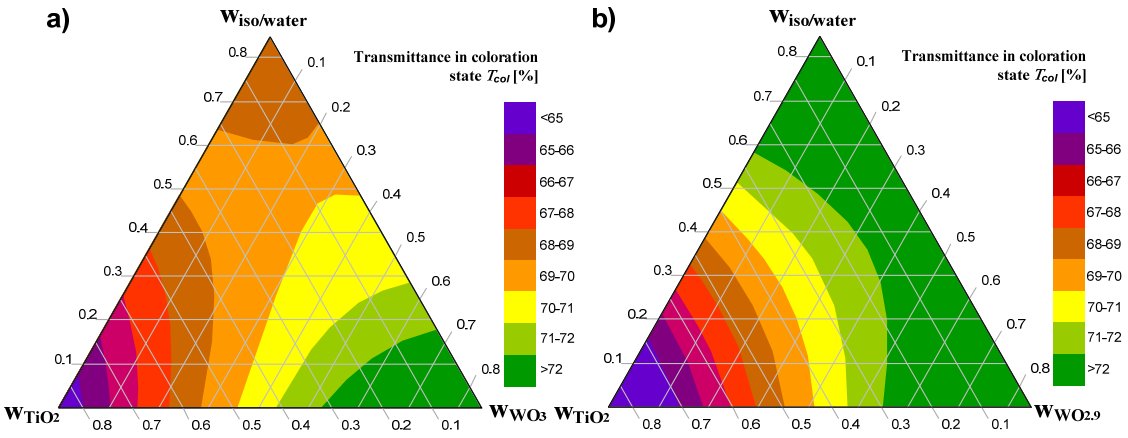

Figure 4.30 Surface response prediction of T_{col} for a) *a*-$WO_3/TiO_2/WO_3$ and b) *a*-$WO_3/TiO_2/WO_{2.9}$ printed layers

All the samples were almost colorless before cathodic polarization, whereas they turned colored after the polarization. One of the theories say that when a negative bias is applied, some W^V ions are produced, due to the electron transfer from the electrode to W^{VI} ions, and cations are inserted into the film simultaneously so as to maintain electroneutrality. Tungsten bronze ($Li_YW^{VI}{}_{1-Y}W_Y{}^VO_X$) is thus produced and a color appeared due to the optical intervalence charge transfer between tungsten atoms having different valence. The degree of coloration depends on the value of Y, which changes from grey to gold by increasing the Y in tungsten bronze. But, only for small values of Y ($Y \leq 0.5$) it leads to blue color and the coloration reactions are reversible. [62]

On the other hand, the preparative conditions of the *a*-$WO_3/TiO_2/WO_X$ electrochromic thin films influence on the intensity of color. As it is known form the state of the art, low crystallinity [63] and high porosity [64] of WO_X based films and addition of conducting materials to it [65] facilitate the diffusion of Li^+ to the layer. Thus, more penetrative ions cause stronger change in the color of the film, during coloration process. Moreover, other properties of the tungsten oxide layer such as its stoichiometry [66] and thickness can also affect its electrochromic performance. In fact, transmittance in colored state of printed *a*-$WO_3/TiO_2/WO_X$ films (Figure 4.30) varies

for different WO_X nanoparticles stoichiometry. However, these differences decrease when the layer is dominated by TiO_2 nanoparticles.

For electrochromic applications, the ability of a material to switch rapidly and to exhibit a striking color change is the most important. It is essential to decrease the time interval needed for coloration and bleaching processes, in practical applications. Electrochromic switching studies can monitor these types of properties via kinetic experiments, allowing the measurement of switching time between its redox states. A square-wave potential step method coupled with optical spectroscopy known as chronoabsorptometry is used to probe switching times and contrast of these composite films. The electrochromic layer photo-response versus time transients at 900 nm when the potential of the working electrode (area of $1cm^2$) was switched between -4V and 4V are shown in Figure 4.31.

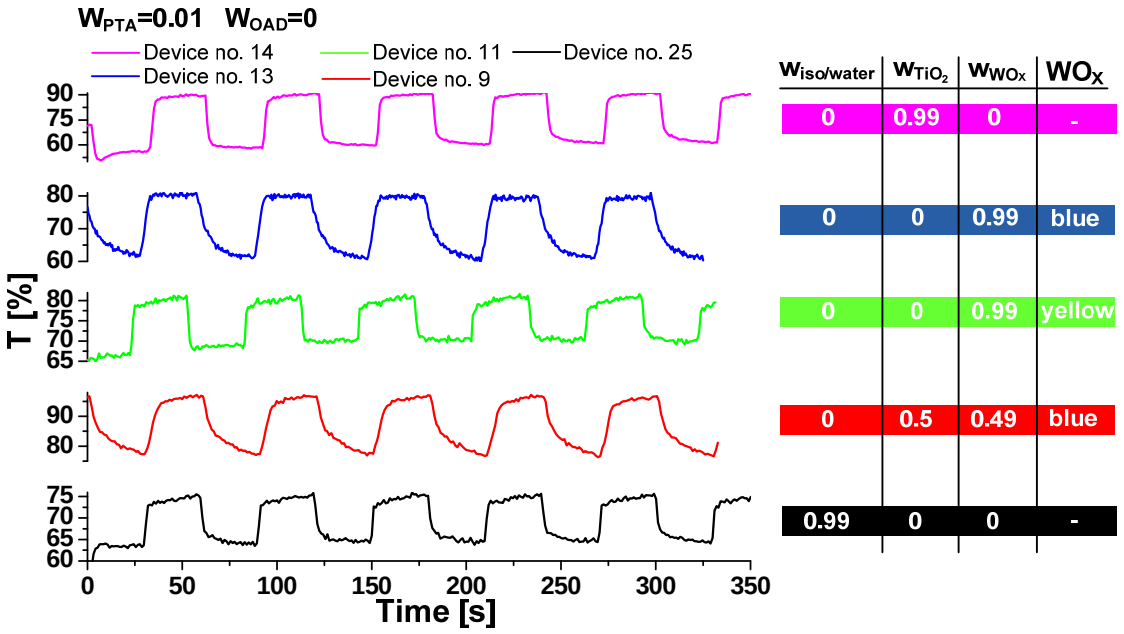

Figure 4.31 Color-bleached characteristics for *a*-$WO_3/TiO_2/WO_X$ printed films recorded at 900 nm under a square wave potential of ±4V at a frequency of 0.016 Hz in a first 5 cycles.

The coloration time (τ_{col}) is defined in these studies as the requisite time for reduction of the device's transmittance to 80% of the final reduction.

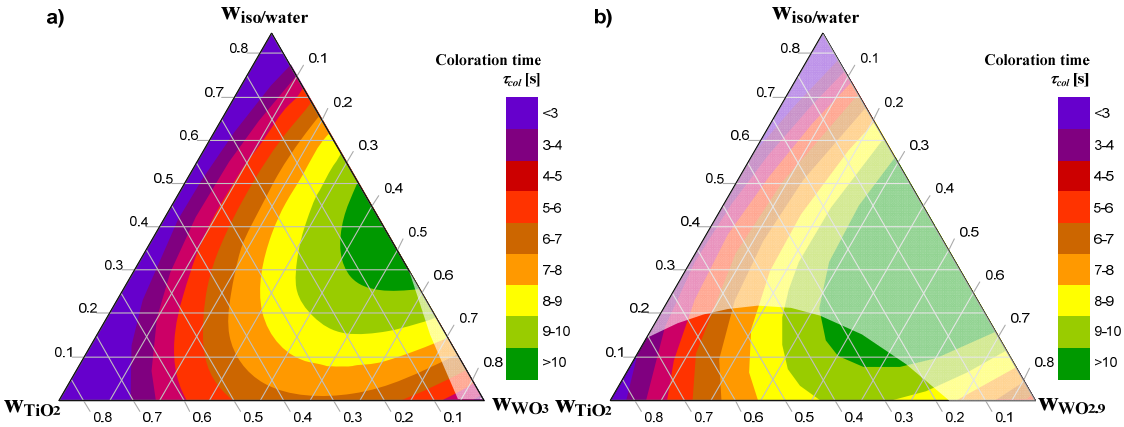

Figure 4.32 Surface response prediction of τ_{col} for a) *a*-$WO_3/TiO_2/WO_3$ and b) *a*-$WO_3/TiO_2/WO_{2.9}$ printed layers

The bleaching time (τ_{bl}) is defined in these studies as the requisite time for change of the device's transmittance to 80% of the final bleach level.

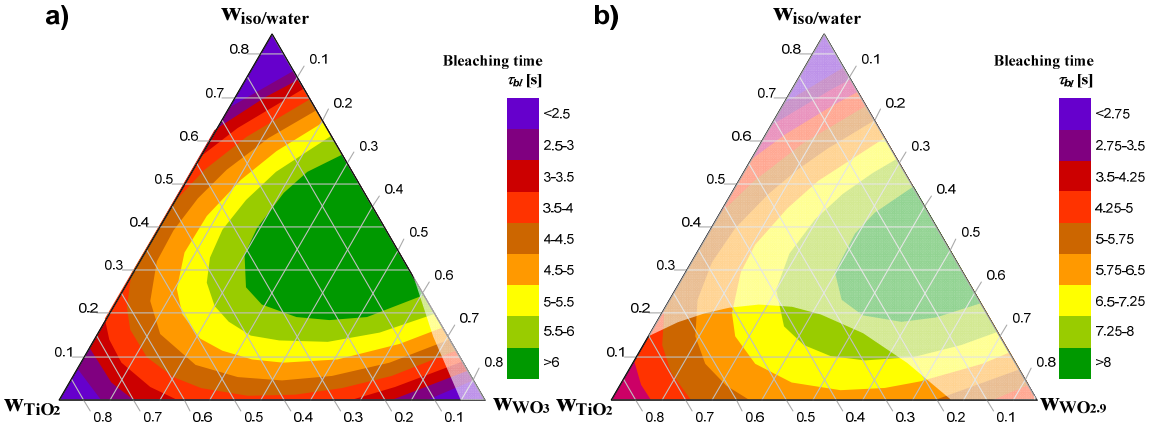

Figure 4.33 Surface response prediction of τ_{bl} for a) *a*-$WO_3/TiO_2/WO_3$ and b) *a*-$WO_3/TiO_2/WO_{2.9}$ printed layers

Due to the accuracy of determining τ_{col} and τ_{bl} values, the result analysis is restricted to those devices which exhibit change in transmittance during coloration process higher that 20%. The area with low measurement accuracy in Figures 4.32 and 4.33 has been brightened.

Coloration kinetics is observed to be slower than bleaching kinetics for all the films under investigation regardless of their compositions. This is in agreement with the well-defined but different mechanisms governing the two processes. While the exchange of current density at the WO_X electrode–electrolyte interface controls coloration kinetics, the space charge-limited lithium ion diffusion current governs the bleaching process.

Among all films under consideration, the films containing TiO_2/WO_X exhibit the fastest switching kinetics owing to the presence of nanocrystals. The improved coloration speed observed for these films is a direct repercussion of the high surface area of nanocrystallites embedded in an amorphous matrix and their morphology. The films containing *yellow* WO_3 nanoparticles (Figure 4.32a and 4.33a) have improved coloration and bleaching time what indicate their higher stability towards proton insertion when compared to films containing *blue* $WO_{2.9}$ nanoparticles (Figure 4.33b and 4.33b).

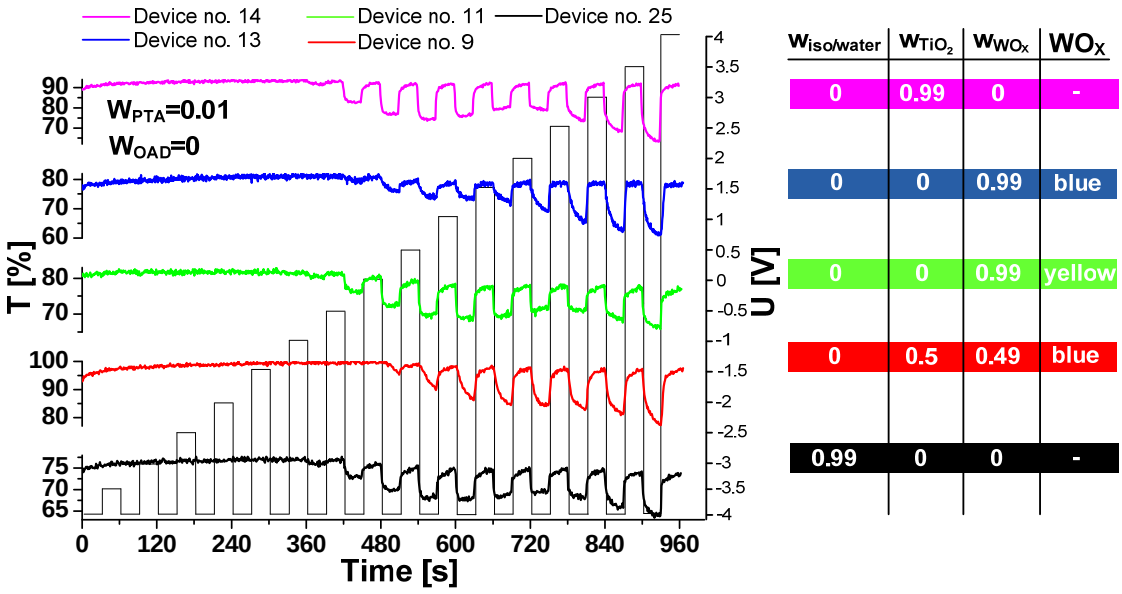

Figure 4.34 Step wave voltage transmittance for 900 nm

An important distinguishing factor of any electrochromic film is its reversibility. Reversibility of films is usually found out from the difference in the cathodic and anodic peak potentials. However in the absence of a cathodic peak or an anodic peak, reversibility of the film can be found out from the chronocoulometry studies or by measuring change in transmittance when *linear stair pulse wave* voltage is applied.

It is clear from Figure 4.34 that by increasing the coloring voltage, the transmittance of the colored films decreased and the rate of the coloration increased. When the coloring voltage exceeds a certain value, the transmission of the bleached films is markedly lower than its value before coloration. Those specific values of coloring voltage called optimum voltage (V_{opt}) was determined for the amorphous *a*-WO_3 and dual-phase *a*-$WO_3/TiO_2/WO_X$ films, under our experimental conditions and plotted in a ternary plot shown Figure 4.35.

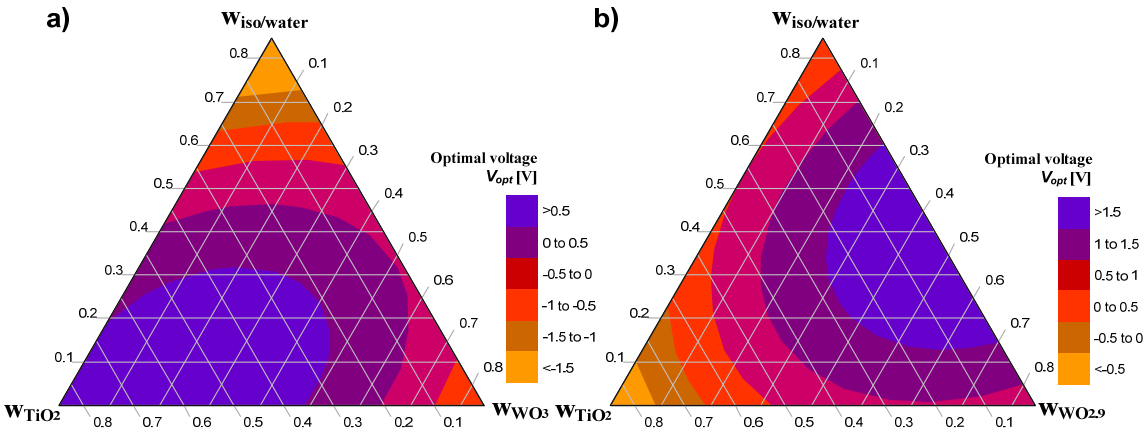

Figure 4.35 Surface response prediction of V_{opt} for a) *a*-$WO_3/TiO_2/WO_3$ and b) *a*-$WO_3/TiO_2/WO_{2.9}$ printed layers

In addition, due to measuring equal transmittance for the films, before coloration and after bleaching, it was found that the electrochromic reaction was reversible for voltages lower than the optimum value. But after applying a higher voltage, the transmittance of the bleached films further decreased and the process was irreversible (Figure 4.36 and 4.37). This is due to an effect called "site saturation" in which reversibility of optical effects at high Li^+ intercalations in the Li_YWO_X is not occurring [1]. This effect is widely explained in the state of the art [10] based on analysis of bleaching and coloring charges in a function of applied voltage. For the higher voltages, the bleaching charges are lower than the amount of the corresponding coloring charges what cause in reversibility decreasing.

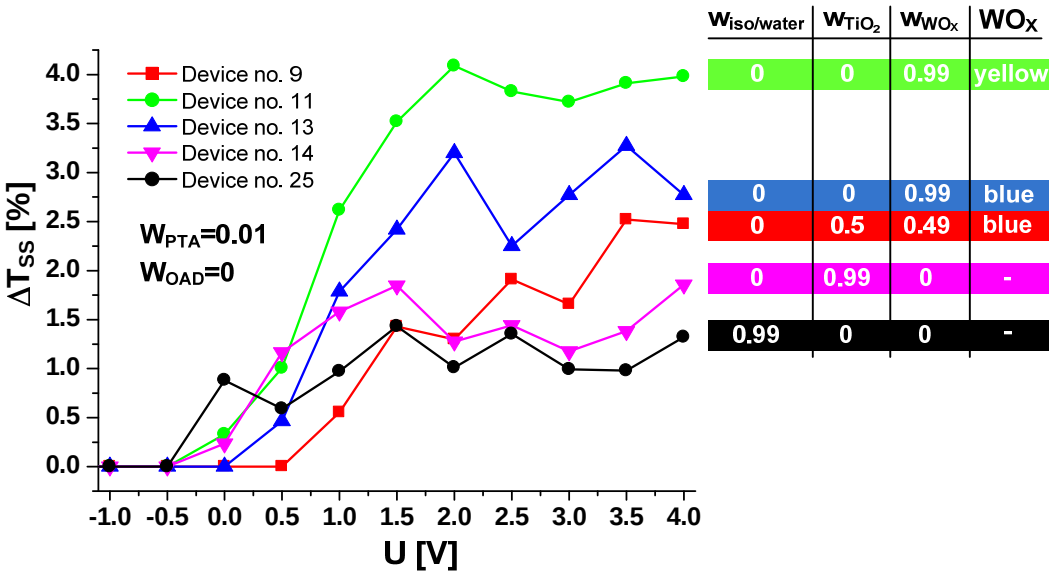

Figure 4.36 Change in transmittance due to site saturation effect (ΔT_{SS}) as a function of applied voltage (U) for different a-WO_3/TiO_2/WO_X film composition

The results shown in Figure 4.35 indicate that value of V_{opt} is the highest for amorphous films. The V_{opt} value decreases in films with high WO_X and TiO_2 nanocrystals concentration.

The observed differences in the optical and electrical reversibility is attributed to the change in microstructure of a-WO_3/TiO_2/WO_X thin films in comparison with a-WO_3 as it was observed also in other studies [67]. Such a high reversibility is due to the low density, open porous structure formation facilitated by presence of crystalline phase.

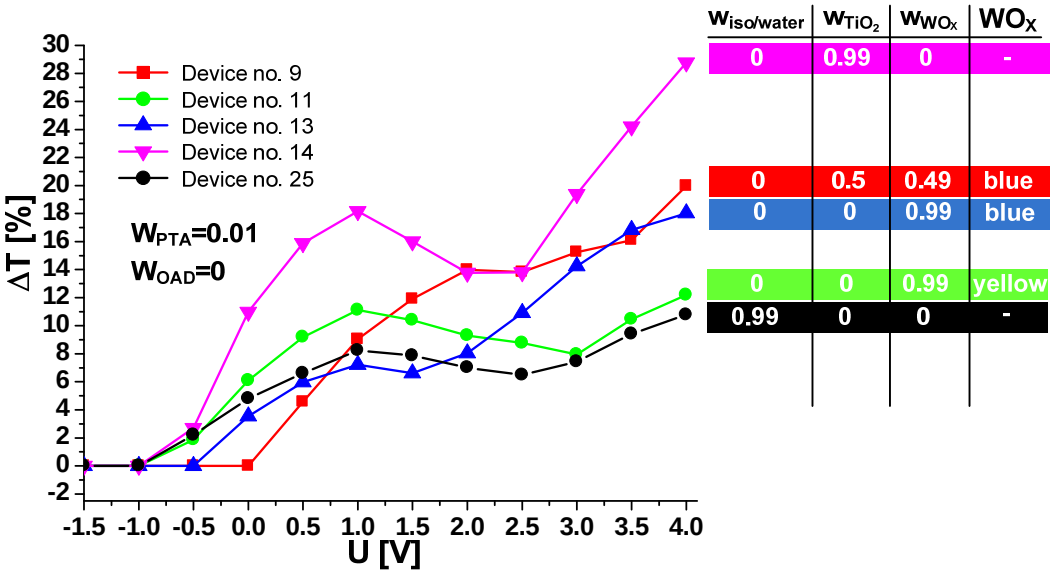

Figure 4.37 Change in transmittance ($\Delta T=T_{bl}-T_{col}$) as a function of applied voltage (U) for different a-$WO_3/TiO_2/WO_X$ film composition

The map of optical absorption coefficient in visible range for different layer compositions is shown in Figure 4.38. The higher values of absorption coefficient observed for the films containing nanoparticles, is attributed to disorder effects such as grain boundary scattering prevalent in the films and therefore related to the superposition of several bands corresponding to a higher spread of values [2].

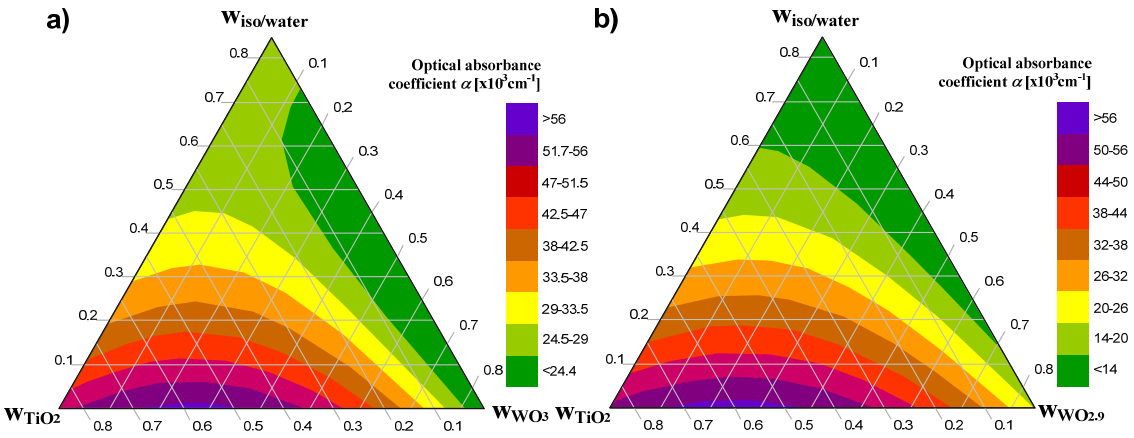

Figure 4.38 - Surface response prediction of α for a) a-$WO_3/TiO_2/WO_3$ and b) a-$WO_3/TiO_2/WO_{2.9}$ printed layers

Another group of electrochromic measurements starts with cyclic voltammograms obtained at a scan rate of 50 mV/s measuring *in situ* cycle life of the EC devices (Figure 4.39).

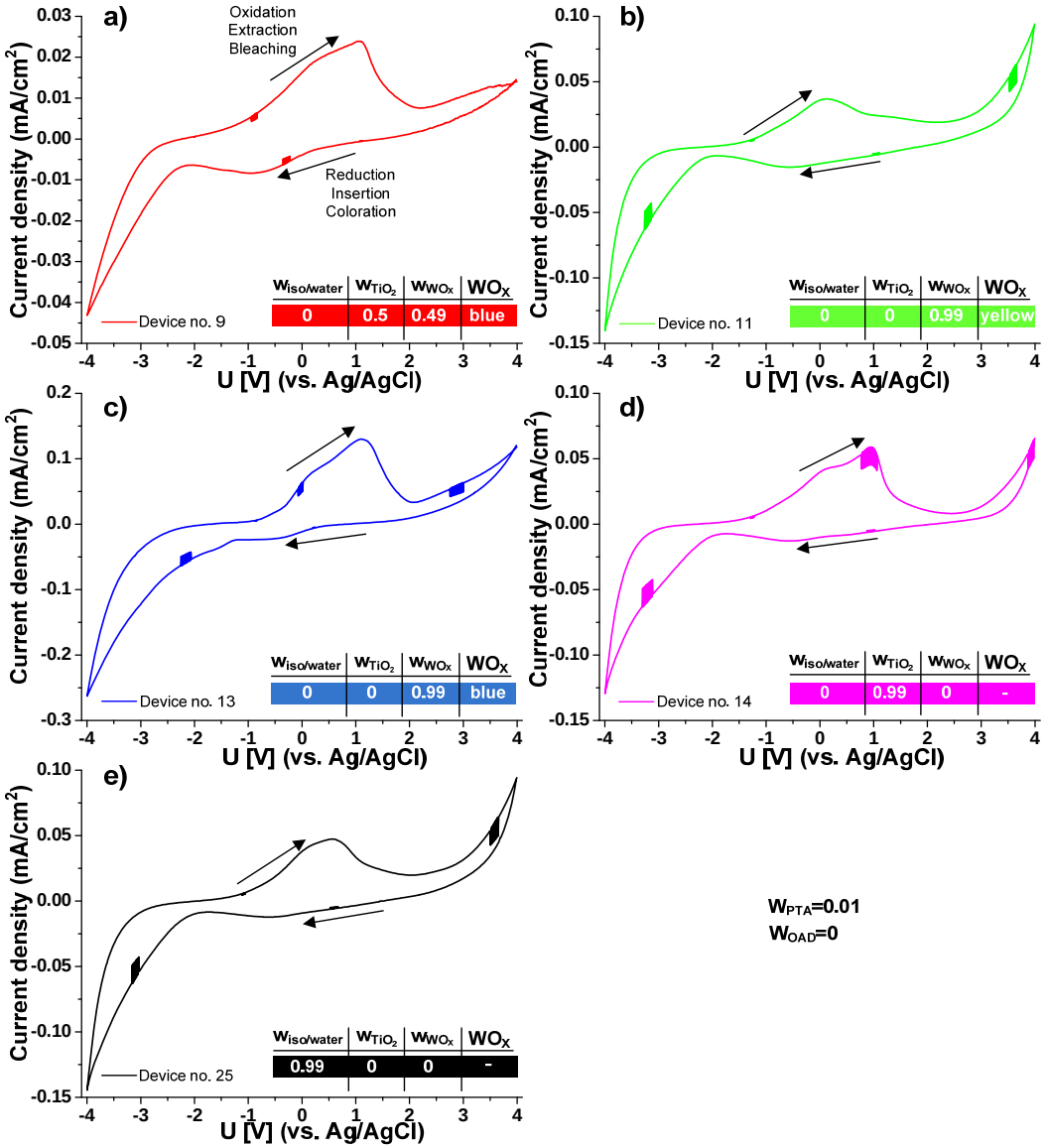

Figure 4.39 Cyclic voltammograms of EC windows based on printed films containing a) *a*-WO_3 with TiO_2 and $WO_{2.9}$ nanoparticles, b) *a*-WO_3 with WO_3 nanoparticles, c) *a*-WO_3 with $WO_{2.9}$ nanoparticles, d) *a*-WO_3 with TiO_2 nanoparticles and e) pure *a*-WO_3. The scan rate is 50 mV/s. Annealing: 120 deg C, 1h.

Figure 4.39 shows a typical cyclic voltammogram obtained for a printed EC films measured *in situ*, a few hours after refilling the device with lithium salt based electrolyte. By cycling between −4 and +4 V, oxidation and reduction charges were well

balanced after about 3 cycles. The asymmetry in the current curve is due to the difference in kinetics of ion insertion and extraction.

Figures 4.39b and 4.39c shows cyclic response of films containing dual phase tungsten oxide, containing WO_3 and $WO_{2.9}$ nanocrystals, respectively. Figure 4.39a shows dual phase *a*-WO_3/$WO_{2.9}$ film with addition of TiO_2 nanoparticles. Cyclic response of the film based on *a*-WO_3 and TiO_2 nanoparticles is plotted in Figure 4.39d. Figure 4.39e presents classical characteristics of *a*-WO_3. The sharp current peaks do not appear for either reduction (intercalation) or oxidation (deintercalation) since amorphous films have a broad distribution of energetically different intercalation sites.

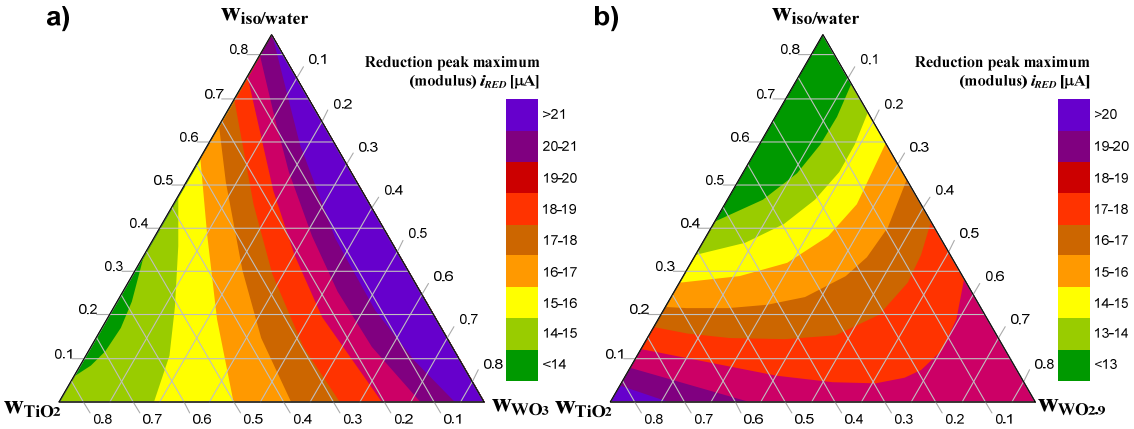

Figure 4.40 Surface response prediction of i_{RED} for a) *a*-WO_3/TiO_2/WO_3 and b) *a*-WO_3/TiO_2/$WO_{2.9}$ printed layers

The cathodic current has the highest modulus value for films containing WO_3 *yellow* nanocrystals rather than $WO_{2.9}$ *blue* (Figure 4.40). For the *a*-WO_3/TiO_2/WO_3 it is clear that the highest positive value is obtained for films with no TiO_2.

The anodic current has the highest value for films containing WO_X nanocrystals and decrease with increasing TiO_2 nanocrystals content (Figure 4.41).

The anodic current for the nanoparticle electrode is more positive compared with crystalline and amorphous films. Such a high value of anodic current may indicate that the presence of WO_X nanocrystals reduces interfacial charge-transfer resistance, providing another reason for the improved electrochemical response.

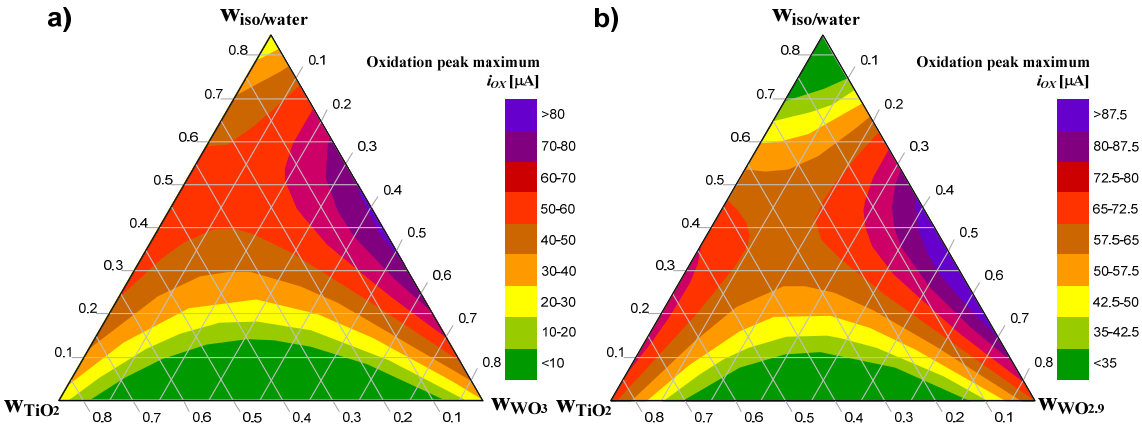

Figure 4.41 Surface response prediction of i_{OX} for a) a-$WO_3/TiO_2/WO_3$ and b) a-$WO_3/TiO_2/WO_{2.9}$ printed layers

The operation of conventional EC devices depends on the reversible electro-chemical double injection of positive ions and electrons into the host lattice of multivalent transition metal oxide materials, with positive ion insertion required to satisfy charge neutrality. However, diffusion of positive ions into the oxide layer is often slow, taking minutes to complete.

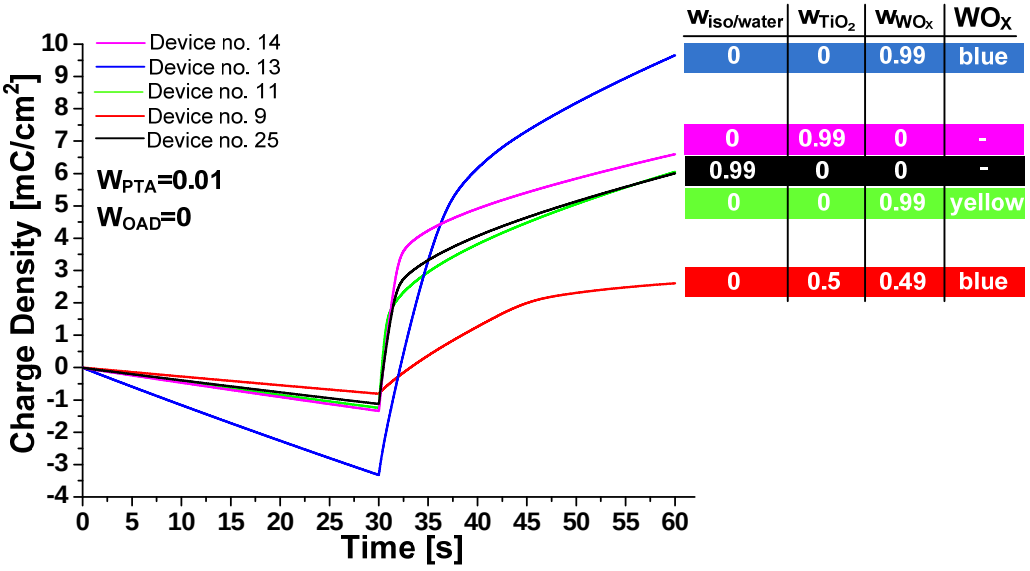

Figure 4.42 Chronocoulometric curves for films

As it is shown in Figure 4.42, the a-WO_3/WO_X and a-WO_3/TiO_2 films consume the highest (in modulus) amount of charges during coloration and bleaching process.

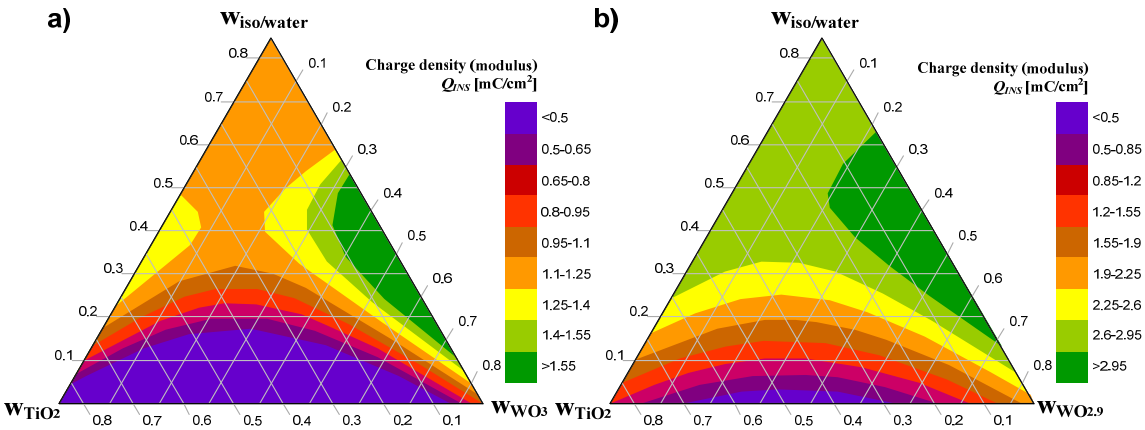

Figure 4.43 Surface response prediction of Q_{ISN} for a) *a*-WO_3/TiO_2/WO_3 and b) *a*-WO_3/TiO_2/$WO_{2.9}$ printed layers

Figure 4.43 presents the map of electrochromic charge passed through the devices with *a*-WO_3 and *a*-WO_3/TiO_2/WO_X coatings for applied voltage of -4V in coloring state. These results show similar values of charge density inserted into device for *a*-WO_3 and *a*-WO_3/TiO_2/WO_X coatings. High values of charge density inserted are observed for films with low TiO_2 solid content. The *a*-WO_3/TiO_2/WO_X coatings with higher solid content are characterized by the smallest charge values inserted to the device.

It is interesting to consider why films containing *blue* $WO_{2.9}$ nanoparticles displayed in Figure 4.43b have a higher charge transfer than films containing *yellow* WO_3 one, displayed in Figure 4.43a. One immediate observation is that the *blue* nanoparticles are smaller in diameter (~70 nm) leading to a higher surface area than *yellow* (~85 nm) nanoparticles.

Relative coloration efficiency (*CE)* at a particular wavelength correlates the optical contrast i.e. the change in optical density with charges inserted to the device per unit active electrode area [1]. In order to obtain relative coloration efficiencies, *in situ* transmittance and chronocoulometry measurements were performed on the devices filled with gel electrolyte. A high (*CE)* provides large optical modulation with a small charge insertion or extraction. This is a crucial parameter for EC devices, since a lower charge-insertion or charge-extraction rate enhances the long term cycling stability. As it was already reported elsewhere, the coloration efficiency is closely related to the water content left in the *a*-WO_3 material [68].

Most of the literature data for *CE* lie in the visible range of the spectrum. At the same time, stress has been laid on the fact that preparation techniques as well as post-annealing effects play a vital role in the tuning of the electrochemical properties [69]. According to the state of the art, *CE* of sol-gel deposited films increases after application of heat treatment [12,43]. However this rule does not apply for films deposited by dip-coating wherein *CE* reduces during heating because of densification of the film [69].

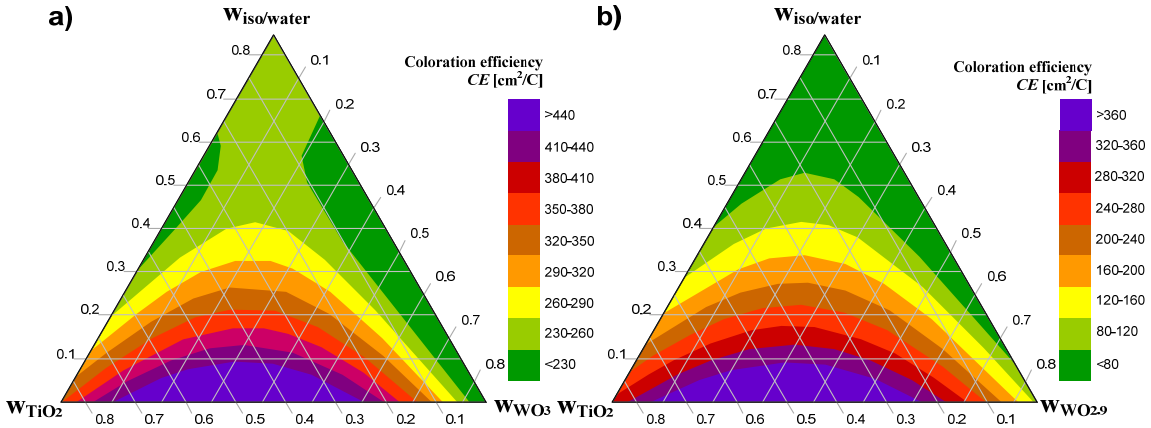

Figure 4.44 Surface response prediction of *CE* for a) *a*-$WO_3/TiO_2/WO_3$ and b) *a*-$WO_3/TiO_2/WO_{2.9}$ printed layers

Observed electrochromic devices based on TiO_2/WO_X nanocrystals interconnected by amorphous phase leads to higher values of coloration efficiency over the visible and region as compared to the poor electrochromic performance of amorphous and non-porous layers.

The TiO_2 and WO_X solid content impact on *CE* value illustrated in Figure 4.44 indicates that the highest values of *CE* above 400 cm^2/C can be obtained using those two nanocrystalline components in conjunction with amorphous PTA phase. The *CE* values retrieved from plot presented on Figure 4.44 are the highest for a layer deposited using a mixture containing equal amount of both TiO_2 and WO_X while w_{PTA}~*0.01*, w_{OAD} is negligible and no additional base solution is added.

However, such a high values of *CE* obtained in present studies cannot be directly compared with results of films deposited by other solution processed techniques. This differences arise from the fact that Inkjet printed films are not continuous, what was confirmed by SEM measurements. This means that the value of surface area taken to calculate the *CE* value is significantly underestimated.

One important part of Inkjet printing technology is the ink and its physical properties (viscosity, surface tension, contact angle to the substrate and density). The viscosity resists the necking motion of the liquid filament whereas surface tension is responsible for the spherical shape of the liquid drop emerging from the nozzles. Controlling droplet formation and in particular, the break up and corresponding tail or ligament is highly dependent on the rheology of ink as it flows through the nozzle. Those parameters (expect contact angle) describe general term called *printability* which should be as equal as possible for all ink in a series of test.

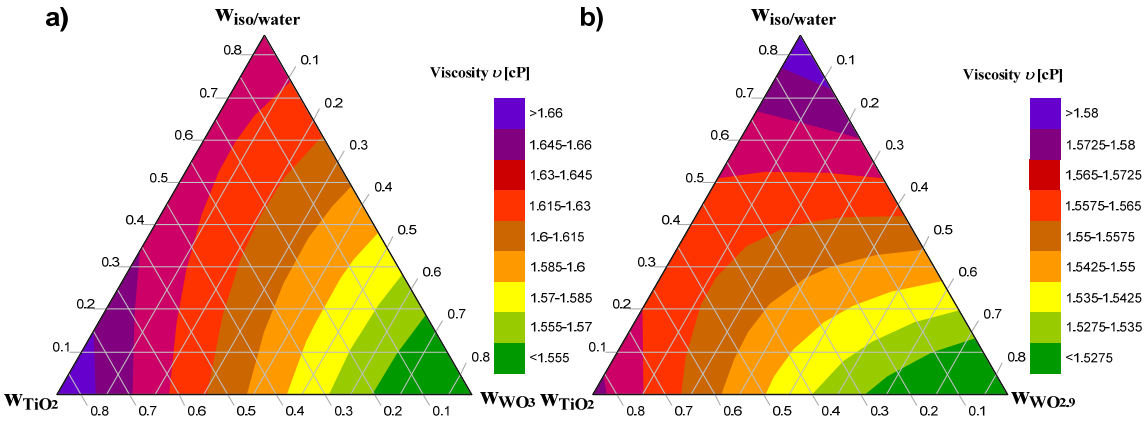

Figure 4.45 Surface response prediction of viscosity (ν) for precursor solution based on PTA, OAD, TiO_2 nanocrystals and a) WO_3 or b) $WO_{2.9}$ nanoparticles

Shown in Figure 4.45 response surfaces for viscosity indicate that there is no significant variation of this parameter for different ink compositions. All values are in the range acceptable for thermal inkjet printing. The same happens in case of surface tension (Figure 4.46) and density (Figure 4.47) response surface. Such small variation in those parameters is due to optimal selection of the base solution which consists of aqueous isopropyl alcohol mixture in proportion 0.3/0.7 by weight. Concluding, all devices were printed in a very similar deposition conditions defined by narrow range of ink *printability*.

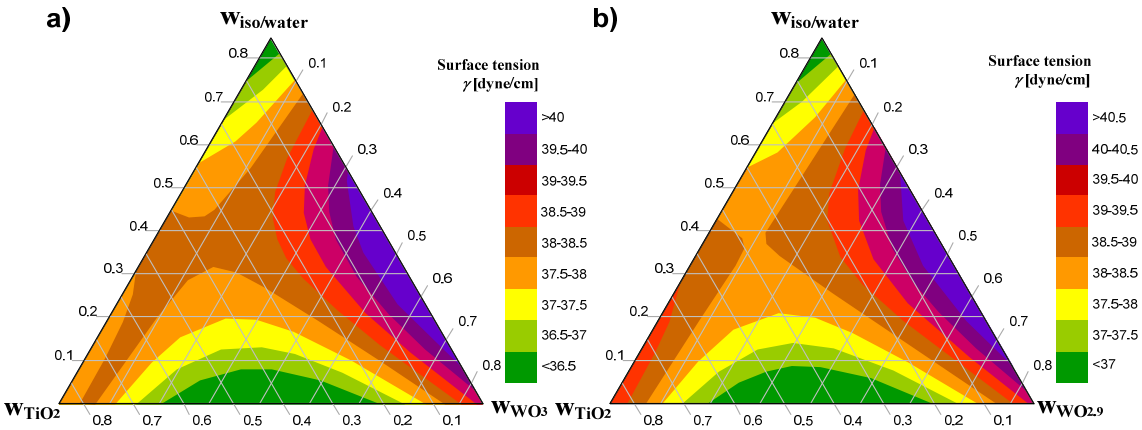

Figure 4.46 Surface response prediction of surface tension (γ) for precursor solution based on PTA, OAD, TiO_2 nanocrystals and a) WO_3 or b) $WO_{2.9}$ nanoparticles

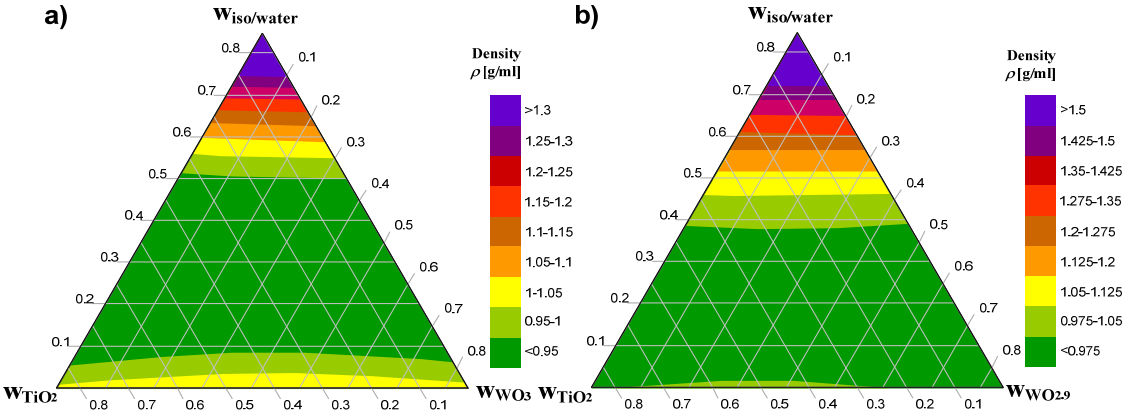

Figure 4.47 Surface response prediction of density (ρ) for precursor solution based on PTA, OAD, TiO_2 nanocrystals and a) WO_3 or b) $WO_{2.9}$ nanoparticles

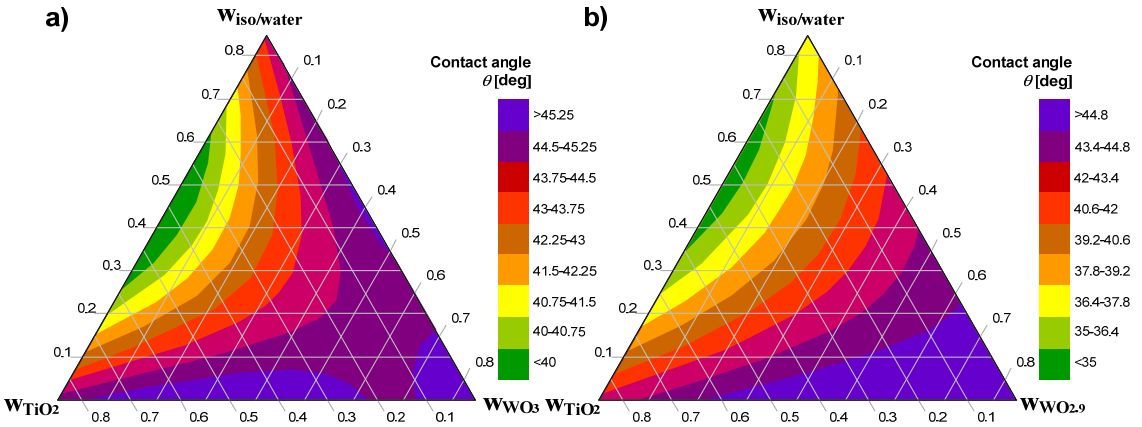

Figure 4.48 Surface response prediction of contact angle (θ) for precursor solution based on PTA, OAD, TiO_2 nanocrystals and a) WO_3 or b) $WO_{2.9}$ nanoparticles

The smooth distribution of contact angle shown in Figure 4.48, indicate that the spreading conditions are very similar for all ink compositions. Small but still significant impact on contact angle value has PTA and TiO_2 concentration.

4.4 Impact of deposition method on electrochromic properties

The transition from standard deposition techniques such as spin-coating, dip-coating or electrodeposition to Inkjet printing is instigated by the need to deposit films on large surfaces, as size poses a major limitation in the former methods. However, as it was observed by *Deepa et al.* [61] the spin and dip coated films based on PTA exhibits dramatic differences, which is indicative of the major role played by the deposition technique.

Since in these studies, the use of Inkjet Printing technique for inorganic EC windows development is pioneering, the impact of deposition method on electrochromic properties has been studied choosing spin-coating as a reference deposition technique.

It was surprising to observe that when the same sol–gel precursors and nanoparticles materials were employed for thin film deposited either by spin or inkjet methodologies, the mechanical, optical and electrical properties of the resulting films exhibit only small differences (Table 4.7), which is indicative of the compatibility between those two deposition techniques. However, it should be noted that the thickness and roughness of the Inkjet printed film is twice smaller when comparing with spin-coated one.

Table 4.7 Comparison of EC films parameters deposited via spin-coating and inkjet printing (device no. 21) for $w_{iso/water}=0$; $w_{PTA}=0.08$; $w_{OAD}=0.025$; $w_{TiO2}=0.44$; $w_{WOX}=0.45$; WO_X: *yellow*

Parameter	Deposition technique	
	Spin-coating	**Inkjet printing**
Thickness (d)	478 [nm]	220 [nm]
Roughness (R_q)	547 [nm]	204 [nm]
Coloration time (τ_{col})	13.96 [s]	14 [s]
Bleaching time (τ_{bl})	11.8 [s]	12 [s]
Change in optical density ($\Delta OD(\lambda)$)	95 [10^{-2}]	82 [10^{-2}]
Coloration efficiency ($CE(\lambda)$)	444 [cm^2/C]	454 [cm^2/C]
Oxidation peak max (i_{OX})	86 [μA]	114 [μA]
Reduction peak max (i_{RED})	-18.4 [μA]	-32 [μA]
Bleaching transmittance (T_{bl})	91.89 [%]	84 [%]
Coloring transmittance (T_{col})	35.33 [%]	36 [%]
Charge inserted density (Q_{ins})	2.15 [mC/cm^2]	1.82 [mC/cm^2]
Optical absorption coeff. (α)	16.65 [10^3 cm^{-1}]	40 [10^3 cm^{-1}]

The profiles of spin-coated and printed films (annealed at 120 deg C) exhibit much different thicknesses and topographies. The printed film which is 50% thinner is highly homogeneous in all deposition area, while spin-coated one includes spots uncoated by material (that is the reason of roughness being higher than the thickness). However, the differences in homogeneity might have been offset by optimizing the spin-coating process parameters.

Figure 4.49, 4.50 and 4.51 shows an electrochemical and optical response of both printed and spin-coated films measured *in situ*, a few hours after refilling the device with gel lithium salt based electrolyte.

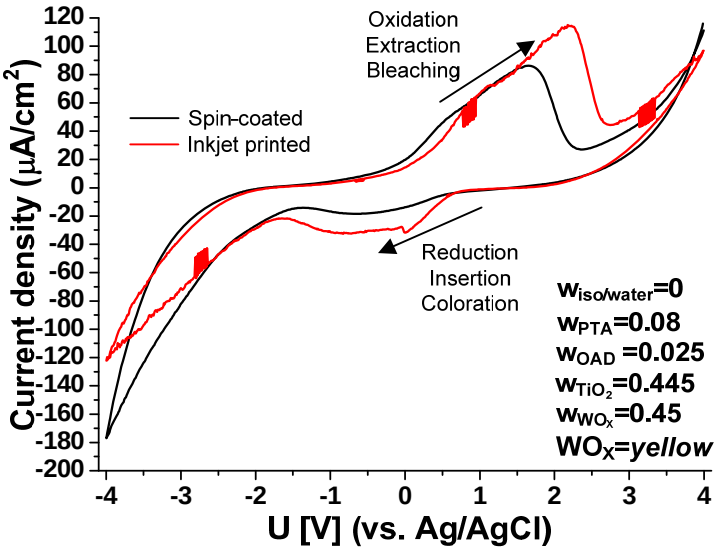

Figure 4.49 Cyclic voltammograms recorded at scan speed of 50 mV/s for spin-coated and Inkjet printed *a*-$WO_3/TiO_2/WO_X$ films

To assess the endurance of spin printed coated films, cyclic voltammograms were recorded at a scan speed of 50 mV/s under similar conditions and are illustrated in Figure 4.49. The values of reduction and oxidation peak currents gives a rough estimate of the electrochemical activity of the working electrode. The cathodic and anodic current is higher for printed films what means that the interfacial charge transfer resistance is lower due to the layer density.

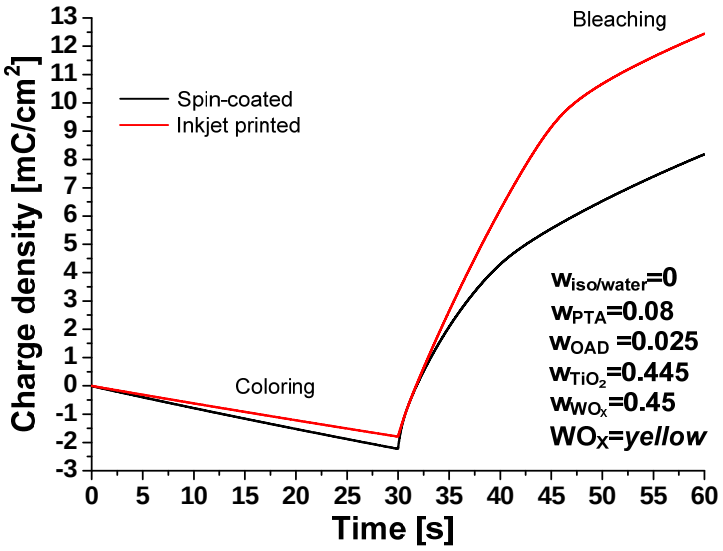

Figure 4.50 Charge density vs. time for spin-coated and inkjet printed *a*-$WO_3/TiO_2/WO_X$ films

As it is shown in Figure 4.50 both, spin-coated and printed films consume almost the same amount of charge during coloration process but printed layer consume more charge to bleach.

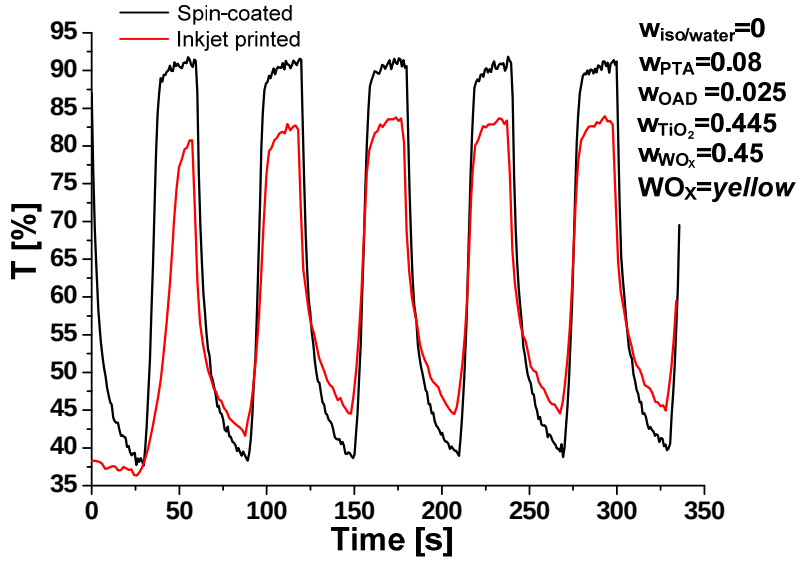

Figure 4.51 Coloration-bleaching characteristic of spin-coated and inkjet printed *a*-$WO_3/TiO_2/WO_X$ films

The coloration–bleaching kinetics for spin coated and printed films as a function of cycling were obtained from a repetitive potential step experiment (Figure 4.51). The difference in response time is negligible for both deposition techniques, while the $\Delta OD(\lambda)$ is 13% smaller for printed layer what can be explained by difference in film thickness.

The *a*-$WO_3/TiO_2/WO_X$ films prepared in this study irrespective of the coating method (Spin or Inkjet) outperform their state-of-the-art analogues owing to their superior chemical and physical properties.

5. Conclusions and future prospects

The main purpose of this work was to develop a complete solution processed and low temperature dual-phase electrochromic system based on WO_3 precursor and metal oxide nanocrystals deposited via Inkjet Printing Technology. This study aimed to develop an amorphous *a*-WO_3 matrix with TiO_2/WO_X nanocrystals embedded for electrochromic applications. The invented method consist of a combination of a set of materials (inks) and Inkjet Printing as a deposition technique which makes the system compatible with temperature sensitive substrates such as PET, PEN and paper.

The scope of this work was find the best combination of factors (components of the mixture) to obtain the EC window with the best performance. The Inkjet printing of the electrochromic inks with different composition on top of flexible ITO-PET substrates was obtained using a Canon PIXMA IP4500 desktop printer. This solution processed method is a low temperature, non-contact, digital, no mask and no vacuum patterning, eco friendly, cost efficient in mass production and allows the coexistence of amorphous and nanocrystalline phases. Briefly, the invented system is an innovative method for electrochromic device manufacturing based on inorganic nanomaterials.

The use of Inkjet Printing technique for inorganic EC devices development presented in this thesis is pioneering and the electrochromic performance of the printed films demonstrates the potential it has for electrochromic applications.

All experimental work and data analysis performed in these studies have been supported by JMP® Statistical Discovery Software. This statistical design of mixture experiments and response surface methodologies proved to be a powerful tool for planning and analyzing experiments to ascertain the influence of electrochromic ink components like PTA, Oxalic acid, TiO_2 and WO_X nanoparticles, on the performance of Inkjet printed electrochromic devices, in particular electrochromic windows.

One of the partial objectives of this research was to find optimum *number of passes* which defines layer thickness and roughness and makes it the main Inkjet deposition parameter. The results obtained lead to the conclusion that the device based on layer printed 3 times shows the best electrochromic performance. Consequently, this value was considered as optimum for a set of used materials.

Based on measurements performed on 30 test devices the analysis of significance have been performed in order to know which factors (mixture components) are significant and how those factors influence the most important electrochromic parameters (τ_{col}, τ_{bl}, *ΔOD*, *CE)*. The significance analysis leads to the conclusion that the coloration time (τ_{col}) depends mainly on the quantity of WO_X nanocrystals in electrochromic layer. The bleaching time (τ_{bl}) is influenced by the quantity of WO_X and TiO_2 nanocrystals and also depends of WO_3 amorphous content formed from PTA precursor. The change in optical density (*ΔOD)* which describes the optical contrast between colored and bleached states mainly depends on quantity of TiO_2 nanocrystals and WO_3 amorphous content. Finally, the coloration efficiency (*CE*) which describes overall device performance depends to a greater or lesser extent on all the mixture components, but the most significant are TiO_2 and WO_X crystalline nanoparticles.

The main task of desirability optimization was to maximize *CE* and *ΔOD* while the response time values of τ_{col} and τ_{bl} should be as small as possible. The result of optimization calculated for maximum desirability indicates that EC device with the best performance would have the following concentration: $w_{iso/water}=0$; $w_{PTA}=0.01$; $w_{OAD}=0$; $w_{TiO2}=0.83$; $w_{WOX}=0.16$; WO_X *stoichiometry: yellow*.

SEM analysis of a few representative devices indicates that:

- the film based on pure *a*-WO_3 is continuous and has a smooth surface; no grains were observed even at a magnification;
- the *a*-WO_3/TiO_2/WO_X films are favorable for a fast electrochromic response and high optical contrast;
- the *a*-WO_3/TiO_2/WO_X films have a regular and a uniform distribution of metal oxide nanocrystalls or their aggregates what makes the structure similar to *chocolate with nuts* counterpart;
- The wide view SEM picture indicates that printed *a*-WO_3/TiO_2/WO_X layer does not form a continuous film; this is rather a pattern than a film;
- the presence of OAD in *a*-WO_3/TiO_2/WO_X film leads to the appearance of grooves is the film but do not affect the electrochromic properties significantly.

The XRD diffractograms confirmed that the WO_X *blue* nanopowder match well with the monoclinic crystalline phase of $WO_{2.9991,}$ while the material called *yellow* matched well with the monoclinic crystalline phase of WO_3. The film based only on PTA precursor exhibits a broad halo observed at 2θ~*26* degrees which is characteristic of the amorphous nature of WO_3 films.

Subsequent measurements related to the optical properties of printed *a*-$WO_3/TiO_2/WO_X$ films measured *in situ* as a working electrode in encapsulated device filled with a gel electrolyte provided the following conclusions:

- films containing large amount of TiO_2 solid content with a smaller share of WO_X nanocrystals in amorphous matrix exhibit the highest transmission modulation due to increased surface area;
- transmittance in colored state of printed *a*-$WO_3/TiO_2/WO_X$ films varies for different WO_X nanoparticles stoichiometry, however, these differences disappear when the layer is dominated by TiO_2 nanoparticles;
- coloration kinetics is observed to be slower than bleaching kinetics for all the films under investigation regardless of their compositions;
- among all films under consideration, the films containing TiO_2/WO_X exhibit the fastest switching kinetics owing to the presence of nanocrystals;
- V_{opt} value is the highest for amorphous films.

The electrochromic measurements lead to the following conclusions:

- the cathodic current has the highest modulus value for films containing WO_3 *yellow* nanocrystals rather than $WO_{2.9}$ *blue*;
- The anodic current has the highest value for films containing WO_X nanocrystals and decrease with increasing TiO_2 nanocrystals content;
- *a*-WO_3/WO_X and *a*-WO_3/TiO_2 films consume the highest amount of charges during coloration and bleaching process;
- high values of charge density inserted are observed for films with low TiO_2 solid content;
- the *a*-$WO_3/TiO_2/WO_X$ coatings with higher solid content are characterized by the smallest charge values inserted to the devices what indicates low power consumption of those devices.
- films containing *blue* $WO_{2.9}$ nanoparticles have a higher charge transfer than films containing *yellow* WO_3 nanopowder.

The coloration efficiency which is a parameter that gives the overall performance of the devices has a value above 400 cm^2/C for *a*-$WO_3/TiO_2/WO_X$ films. However, such a high values of *CE* shown in present studies cannot be directly compared with results of films deposited by other solution processed techniques. These differences arise from the fact that Inkjet printed films are not continuous, what was confirmed by SEM measurements. This means that the value of surface area taken to calculate the *CE* value is significantly underestimated.

One important part of Inkjet Printing technology is the ink and its physical properties (viscosity, surface tension, contact angle to the substrate and density). Based on rheological measurements, it was concluded that there is no significant variation of viscosity for different ink compositions and all values are in the range acceptable for thermal Inkjet printing. The same happens in case of surface tension and density. Such small variation in those parameters is due to optimal selection of the base solution which consists of aqueous isopropyl alcohol mixture in proportion 0.3/0.7 by weight. Concluding, all devices were printed in a very similar deposition conditions defined by narrow range of ink *printability*. Regarding the contact angle, it was shown that the spreading conditions were very similar for all ink compositions. Small but still significant impact on contact angle value has PTA and TiO_2 concentration.

The optimization process performed using statistical software indicated that device with the highest performance have been deposited from the ink with following composition: $w_{iso/water}=0;\ w_{PTA}=0.08;\ w_{OAD}=0.025;\ w_{TiO2}=0.44;\ w_{WOX}=0.45;$ *WO_X: yellow*. Such an ideal electrochromic performance, which is a result of the several competing mechanisms, demonstrates the potential it has for electrochromic window applications.

Since in these studies, the use of Inkjet Printing technique for inorganic EC windows development is pioneering, the impact of deposition method on electrochromic properties has been studied choosing spin-coating as a reference deposition technique.

Therefore when the same sol–gel precursors and nanoparticles materials were employed for thin film deposited either by spin or inkjet methodologies, the mechanical, optical and electrical properties of the resulting films exhibit only small differences, which is indicative of the compatibility between those two deposition techniques. However there are some differences that should be noted:

- the thickness and roughness of the Inkjet printed film is twice smaller when comparing with spin-coated one;
- the cathodic and anodic current is higher for printed films what means that the interfacial charge transfer resistance is lower due to the layer density;
- both, spin-coated and printed films consume almost the same amount of charge during coloration process but printed layer consume more charge to bleach;
- the difference in response time is negligible for both deposition techniques, while the $\Delta OD(\lambda)$ is 13% smaller for printed layer what can be explained by difference in film thickness;
- the *a*-$WO_3/TiO_2/WO_X$ films prepared in this study irrespective of the coating method (spin or inkjet) outperform their state-of-the-art analogues owing to their superior chemical and physical properties.

The electrochromic properties of the printed *a*-$WO_3/TiO_2/WO_X$ films annealed at 120 deg C are a balance among good electrochemical activity, fast switching kinetics, high electrochromic efficiency, and ion storage capacity and these are attributable to the layer density and high surface area of nanocrystals in the printed films which facilitate fast coloration. The ease processing via Inkjet Printing is evidenced from the fact that dual-phase films can be fabricated at room-temperature. These properties render them to be promising candidates for electrochromic windows manufacturing.

The developed method of electrochromic windows manufacturing meets all the assumptions posed on the beginning of the study. The results obtained during all the analysis will significantly impact current EC technologies and have promising implications for the development of electrochromic devices.

Following this study there's the possibility of producing devices via inkjet printing, based on WO_X nanoparticles synthesized e.g. via hydrothermal process from the same WO_3 sol. As future prospects, this work had open a wide window of opportunities with this innovative EC deposition technique which allows a great development in the area, with the cost efficient, mass production of flexible electrochromic windows. The EC windows developed by inkjet printing on flexible substrates makes the possibility of the window to adapt to different shapes, like greenhouses, roofs and walls of buildings, canopies, top of convertible cars, tents, curtains, and so on.

References

[1] P. Patil, S. Mujawar, A. Inamdar, and S. Sadale, "Electrochromic properties of spray deposited TiO2-doped WO3 thin films," *Applied Surface Science*, vol. 250, Aug. 2005, pp. 117-123.

[2] Z. Wang and X. Hu, "Electrochromic properties of TiO 2 -doped WO 3 films spin-coated from Ti-stabilized peroxotungstic acid," *Electrochimica Acta*, vol. 46, 2001, pp. 1951- 1956.

[3] C.G. Granqvist, P.C. Lansaker, N.R. Mlyuka, G.A. Niklasson, and E. Avendano, "Progress in chromogenics : New results for electrochromic and thermochromic materials and devices," *Solar Energy Materials*, vol. 93, 2009, pp. 2032-2039.

[4] "http://host.nigde.edu.tr/sahmetlioglu/research%20areas/Chromism.pdf." accessed in 10/05/2010

[5] C.G. Granqvist, "Oxide electrochromics : Why , how , and whither," *Solar Energy Materials*, vol. 92, 2008, pp. 203-208.

[6] "http://chemistry.about.com/od/chemistryfaqs/f/moodring.htm.", accessed in 10/05/2010

[7] "http://blog.everydayscientist.com/?cat=26.", accessed in 15/09/2010

[8] "http://www.flickr.com/photos/zack_mensinger/247225099/.", accessed in 10/05/2010

[9] G. Campet, J. Portier, S.J. Wen, B. Morel, M. Bourrel, and J.M. Chabagno, "Electrochromism and electrochromic windows," *Active and Passive Elec. Comp.*, vol. 14, 1992, pp. 225-231.

[10] P.R. Somani and S. Radhakrishnan, "Electrochromic materials and devices: present and future," *Materials Chemistry and Physics*, vol. 77, 2002, pp. 117-133.

[11] T. Yang, Z. Lin, and M. Wong, "Structures and electrochromic properties of tungsten oxide films prepared by magnetron sputtering," *Applied Surface Science*, vol. 252, 2005, pp. 2029-2037.

[12] P.M.S. Monk, R.J. Mortimer, and D.R. Rosseinsk, *Electrochromism and Electrochromic Devices*, Cambridge University Press, 2007.

[13] C.G. Granqvist, *Handbook of inorganic Electrochromic Materials*, Elsevier, 2002.

[14] E. Avendano, L. Berggren, G.A. Niklasson, C.G. Granqvist, and A. Azens, "Electrochromic materials and devices : Brief survey and new data on optical absorption in tungsten oxide and nickel oxide films," *Thin Solid Films*, vol. 496, 2006, pp. 30 - 36.

[15] Y. Takahashi, "Radical-Bearing Redox Polymers and Their Application to Electrochromic Cell," 2008.

[16] S.K. Deb, "Opportunities and challenges in science and technology of WO 3 for electrochromic and related applications," *Solar Energy Materials and Solar Cells*, vol. 92, 2008, pp. 245-258.

[17] D.R. Rosseinsky and R.J. Mortimer, "Electrochromic Systems and the Prospects for Devices **," *Advanced Materials*, vol. 13, 2001, pp. 783-793.

[18] "http://casa.hsw.uol.com.br/janelas-inteligentes4.htm.", accessed in 15/06/2010

[19] "http://eetdnews.lbl.gov/nl05/eetd-nl05-1-window.html.", 14/06/2010

[20] R.J. Mortimer, A.L. Dyer, and J.R. Reynolds, "Electrochromic organic and polymeric materials for display applications," *Displays*, vol. 27, 2006, pp. 2-18.

[21] R. Baetens, B. Petter, and A. Gustavsen, "Properties , requirements and possibilities of smart windows for dynamic daylight and solar energy control in buildings : A state-of-the-art review," *Solar Energy Materials and Solar Cells*, vol. 94, 2010, pp. 87-105.

[22] F. Carpi and D.D. Rossi, "Colours from electroactive polymers : Electrochromic , electroluminescent and laser devices based on organic materials," *Optics & Laser Technology*, vol. 38, 2006, pp. 292-305.

[23] L. Su, Z. Xiao, and Z. Lu, "All Solid-state electrochromic device with PMMA gel electrolyte," *Materials Chemistry and Physics*, vol. 52, 1998, pp. 180-183.

[24] A. Goswami, *Thin Film Fundamentals*, New Delhi: New Age International Publishers, 1996.

[25] A. Elshabini-Riad and F.D. Barlow III, *Thin Film Technology Handbook*, New-York: McGraw-Hill, 1997.

[26] J.B. Bates, ed., *Proceedings of the Symposium on Thin Film Solid Ionic Devices and Materials*, Pennington: The Electrochemical Society, 1996.

[27] P.J. Smith, "Introduction to Inkjet," . Dutch Polymer Institute, Netherlands

[28] P.J. Wojcik, A. Gonçalves, S. Pereira, G. Gonçalves, I. Ferreira, R. Martins, and E. Fortunato, "Functional Materials For Inkjet Printing Technology - Chemical And Physicochemical Requirements For Novel Applications," .

[29] "http://www.dimatix.com/markets/index.asp.", accessed in 01/07/2010

[30] P.J. Wojcik, “An Introduction to Ink Jet Technology,” , 2009.

[31] A. Bessiere, J.-C. Badot, M.-C. Certiat, J. Livafe, and V. Lucas, “Sol – gel deposition of electrochromic WO 3 thin film on flexible ITO / PET substrate,” *Electrochimica Acta*, vol. 46, 2001, pp. 2251- 2256.

[32] A.C. Pierre, *Introduction to Sol-Gel Processing*, Boston: Kluwer Academic Publishers, 1998.

[33] M. Deepa, T.K. Saxena, D.P. Singh, K.N. Sood, and S.A. Agnihotry, “Spin coated versus dip coated electrochromic tungsten oxide films : Structure , morphology , optical and electrochemical properties,” *Electrochimica Acta*, vol. 51, 2006, pp. 1974-1989.

[34] P.K. Biswas, N.C. Pramanik, M.K. Mahapatra, D. Ganguli, and J. Livage, “Optical and electrochromic properties of sol – gel WO 3 films on conducting glass,” *Materials Letters*, vol. 57, 2003, pp. 4429 - 4432.

[35] J. Livage and D. Ganguli, “Sol - gel electrochromic coatings and devices : A review,” *Solar Energy Materials*, vol. 68, 2001, pp. 365-381.

[36] M. Sharbatdaran, A. Novinrooz, and H. Noorkojouri, “Preparation and Characterization of WO3 Electrochromic Films Obtained by the Sol-Gel Process,” *Iran. J. Chem. Chem. Eng.*, vol. 25, 2006, pp. 25-29.

[37] H. Okamoto, A. Ishikawa, and T. Kudo, “Amorphous and Crystalline Peroxopolytungstic Acids Formed from Tungsten and Hydrogen Peroxide,” *The Chemical Society of Japan*, vol. 62, 1989, pp. 2723-2724.

[38] M.A. Aegerter and M. Menning, *Sol-Gel Technologies for Glass Producers and Users*, Saarbrucken: Kluwer Academic Publishers, 2004.

[39] A. Novinrooz, M. Sharbatdaran, and H. Noorkojouri, “Structural and optical properties of WO3 electrochromic layers prepared by the sol-gel method,” *Central European Journal of Physics*, vol. 3, Sep. 2005, pp. 456-466.

[40] C.M. White, D.T. Gillaspie, E. Whitney, S.-H. Lee, and A.C. Dillon, “Flexible electrochromic devices based on crystalline WO3 nanostructures produced with hot-wire chemical vapor deposition,” *Thin Solid Films*, vol. 517, Apr. 2009, pp. 3596-3599.

[41] G. Leftheriotis and P. Yianoulis, “Development of electrodeposited WO3 films with modified surface morphology and improved electrochromic properties,” *Solid State Ionics*, vol. 179, Nov. 2008, pp. 2192-2197.

[42] M. Geiger, “Making Smart Windows Smarter: Improving Optical Efficiency and Intercalation Rates in Sol-Gel Derived Tungsten Trioxide,” Literature Seminar, 2007.

[43] M. Deepa, R. Sharma, A. Basu, and S. Agnihotry, “Effect of oxalic acid dihydrate on optical and electrochemical properties of sol–gel derived amorphous electrochromic WO3 films,” *Electrochimica Acta*, vol. 50, May. 2005, pp. 3545-3555.

[44] “JMP Design of Experiments, Release 6,” 2005.

[45] P.J. Wojcik, A.S. Cruz, L. Santos, A.M. Ramos, L. Pereira, R. Martins, and E. Fortunato, *Ink Jet Printed Nanostructured Materials - Applications of Titanium Dioxide and Tungsten Trioxide Nanocrystals for Photovoltaic and Eelectrochromic Window*, Poster presented in ANM 2010.

[46] DataPhysics, “Operating manual OCA,” 1998.

[47] “http://www.attension.com/contact-angle.aspx.”, accessed in 24/08/2010

[48] “http://www.gsishop.com/webmagzine/20020925/contact.htm.”, accessed in 24/08/2010

[49] P. Valente, “Desenvolvimento de um Electrólito Polimérico para Mostradores Electrocrómicos,” 2007.

[50] “http://miam2.physics.mcgill.ca/?q=content/ambios-xp200-profiler.”, accessed in 25/08/2010

[51] L. Pereira, “Produção e caracterização de silício policristalino e a sua aplicação a TFTs,”PHD Thesis, FCT-UNL 2008.

[52] B. Brás, “Produção e Caracterização de Baterias de Filme Fino de Papel,”, Master thesis, FCT-UNL 2009.

[53] P.J. Wojcik and L. Santos, “Electrochromic Measurement Protocol,” 2010.

[54] Y. Shen, Z. Lu, S. Spiers, H.A. Mackenzie, H.S. Ashton, J. Hannigan, S.S. Freeborn, and J. Lindberg, “Measurement of the optical absorption coefficient of a liquid by use of a time-resolved photoacoustic technique,” *Applied Optics*, vol. 39, 2000, pp. 4007-4012.

[55] N. Naseri, R. Azimirad, O. Akhavan, and A.Z. Moshfegh, “Improved electrochromical properties of sol–gel WO3 thin films by doping gold nanocrystals,” *Thin Solid Films*, vol. 518, Feb. 2010, pp. 2250-2257.

[56] a Vanderkooij, J. Meulman, and W. Heiser, “Local minima in categorical multiple regression,” *Computational Statistics & Data Analysis*, vol. 50, Jan. 2006, pp. 446-462.

[57] “JMP Introductory Guide, Release 8,” *Addiction*, vol. 99, Nov. 2009.

[58] “http://www.surveysystem.com/signif.htm.”, accessed in 23/09/2010

[59] J. Sall, “Leverage Plots for General Linear Hypotheses,” *The American Statistician*, vol. 44, Nov. 1990, p. 308.

[60] N. Sharma, M. Deepa, P. Varshney, and S.A. Agnihotry, “Influence of Organic Additive on the Morphological , Electrical and Electrochromic Properties of Sol-Gel Derived WO 3 Coatings,” *Journal of Sol-Gel Science and Technology*, vol. 18, 2000, pp. 167-173.

[61] M. Deepa, “Electrodeposited tungsten oxide films: annealing effects on structure and electrochromic performance,” *Thin Solid Films*, vol. 468, Dec. 2004, pp. 32-42.

[62] a Cremonesi, Y. Djaoued, D. Bersani, and P. Lottici, “Micro-Raman spectroscopy on polyethylene-glycol assisted sol–gel meso and macroporous WO3 thin films for electrochromic applications,” *Thin Solid Films*, vol. 516, Oct. 2007, pp. 4128 - 4132.

[63] Y. Nah, a Ghicov, D. Kim, and P. Schmuki, “Enhanced electrochromic properties of self-organized nanoporous WO3,” *Electrochemistry Communications*, vol. 10, Nov. 2008, pp. 1777-1780.

[64] O. Lavi, G. Frey, a Siegmann, and Y. Eineli, “Enhanced tungstate electrochromism via formation of transparent conductive networks,” *Electrochemistry Communications*, vol. 10, Aug. 2008, pp. 1210-1213.

[65] R. Sato, N. Kawamura, and H. Tokumaru, “The coloration of tungsten-oxide film by oxygen deficiency and its mechanism,” *Applied Surface Science*, vol. 254, Sep. 2008, pp. 7676-7678.

[66] C.G. Granqvist, “Transparent conductors as solar energy materials: A panoramic review,” *Solar Energy Materials and Solar Cells*, vol. 91, Oct. 2007, pp. 1529-1598.

[67] M. Deepa, P. Singh, S. Sharma, and S. Agnihotry, “Effect of humidity on structure and electrochromic properties of sol–gel-derived tungsten oxide films,” *Solar Energy Materials and Solar Cells*, vol. 90, Oct. 2006, pp. 2665-2682.

[68] S.S. Kalagi, D.S. Dalavi, R.C. Pawar, N.L. Tarwal, S.S. Mali, and P.S. Patil, “Polymer assisted deposition of electrochromic tungsten oxide thin films,” *Journal of Alloys and Compounds*, vol. 493, Mar. 2010, pp. 335-339.

[69] V.V. Abramova, A.S. Sinitskii, E. a Goodilin, and Y.D. Tretyakov, “Preparation and properties of electrochromic coatings based on nanoparticle tungsten oxide,” *Mendeleev Communications*, vol. 15, 2005, pp. 178-180.